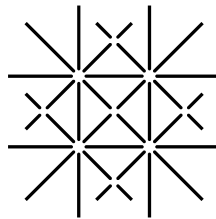


# **The Influence of GABAergic signaling on dendritic processing**



UNI  
BASEL

## **Inauguraldissertation**

zur  
Erlangung der Würde eines Doktors der Philosophie  
vorgelegt der  
Philosophisch-Naturwissenschaftlichen Fakultät  
der Universität Basel  
von

**Silvia Willadt**

aus Augsburg, Deutschland

Basel, 2013



Genehmigt von der Philosophisch-Naturwissenschaftlichen Fakultät  
auf Antrag von  
(Mitglieder des Dissertationskomitees)

**Prof. Dr. Heinrich Reichert (Fakultätsverantwortlicher)**

**Prof. Dr. Kaspar Vogt (Leitung der Dissertation)**

**Prof. Dr. Hans Rudolf Brenner (Koreferent)**

Basel, den 13.12.2011

Prof. Dr. Martin Spiess  
(Dekan)



**Für meine “Mom”, auf die ich unglaublich stolz bin  
und  
Für meinen “Dad”, den ich sehr vermisse.**



## **Summary**

GABAergic ( $\gamma$ -aminobutyric acid-releasing) signaling plays a crucial role in integration processes of pyramidal neurons. Specific subtypes of GABA releasing interneurons innervate different compartments of pyramidal neurons; thereby modulating the summation of excitatory synaptic input in space and time to generate neuronal output. The intrinsic signaling capabilities of neuronal compartments have been extensively studied and many results about the local processes have been elucidated. However, the functional role of the specific GABAergic innervation in dependence of the location is largely unknown.

At the beginning of my thesis we studied the effects of GABAergic signals on dendritic excitability of layer V pyramidal cells. While hyperpolarization through activation of dendritic GABA<sub>A</sub> receptors lowered the threshold for dendritic sodium-calcium spikes, somatic hyperpolarization increased the threshold to initiate dendritic spikes. Blockade of low-voltage activated calcium channels abolished the excitatory effect of dendritic GABA<sub>A</sub> receptors. The results show that specific pattern of GABAergic pyramidal cell innervation can lead to distinct effects on neuronal function, highly dependent on the site of innervation and local intrinsic signaling mechanisms.

Measurements of this study were restricted to somatic whole-cell patch-clamp recordings and its spatial information had to be obtained indirectly. To overcome these limitations we developed a novel approach to record inhibitory postsynaptic potentials by voltage-sensitive dye imaging. Using an improved voltage-imaging technique, the origin and the spread of physiological GABAergic signals as small as 1 mV could be optically resolved from multiple sites in neuronal dendrites. Hence, recordings of specific dendritic GABAergic innervation patterns are able to be performed locally and the GABAergic impact on neuronal integration processes can be evaluated.

Finally, we designed experiments that reveal clearly the shaping effects of GABA<sub>A</sub> receptor activation of different interneuron classes on subcellular dendritic excitatory postsynaptic potentials. Using voltage-sensitive dye imaging we studied the transmembrane voltage patterns in CA1 pyramidal neurons after Schaffer collateral stimulation. The observed

excitation/inhibition ratio showed a high variability degree between different branches of the apical-basal dendritic tree, tending to more inhibitory innervation in the apical dendrite close to the soma. Application of the GABA<sub>A</sub> receptor antagonist bicuculline revealed an excitatory signal in all dendritic segments studied, indicating that the original patterns were indeed due to inhibitory synaptic transmission. We show that GABAergic inhibition shapes synaptic integration in a dendrite-specific manner, with a large fraction of the dendritic arborization receiving predominantly or exclusively inhibitory signals after stimulation of CA1 inputs.

In summary, my thesis demonstrates that the location of specific GABAergic innervation is of fundamental relevance for neuronal integration processes.



## Zusammenfassung

GABAerge (durch  $\gamma$ -Aminobuttersäure ausgelöste) Signalinduktion spielt eine entscheidende Rolle in den Integrationsprozessen der Pyramidenzellen. Spezifische Subtypen von GABA freisetzenden Interneuronen innervieren verschiedene Kompartimente der Neurone; dabei wird die Aufsummierung exzitatorischer synaptischer Potentiale zur Generierung neuronaler Ausgangssignale räumlich und zeitlich moduliert. Da die intrinsischen Fähigkeiten der Signalverarbeitung in neuronalen Kompartimenten bereits reichlich untersucht wurden, konnten viele Ergebnisse über lokale Prozesse erhalten werden. Allerdings ist die funktionelle Rolle spezifischer GABAerger Innervation in Abhängigkeit des Ortes weitgehend noch unbekannt.

Zu Beginn meiner Doktorarbeit untersuchten wir die Effekte GABAerger Signale auf die dendritische Erregbarkeit von Schicht-V Pyramidenzellen. Während durch dendritische GABA<sub>A</sub> Rezeptor aktivierte Hyperpolarisierung den Schwellenwert für die Auslösung von dendritischen Natrium-Kalzium Potentialen herabgesetzt wurde, erhöhte eine somatische Hyperpolarisierung den Schwellenwert. Eine Hemmung niedrig spannungsabhängiger Kalzium-Kanäle unterdrückte den anregenden Effekt dendritischer GABA<sub>A</sub> Rezeptoren. Die Ergebnisse zeigen, dass spezifische Muster der GABAergen Innervierung von Pyramidenzellen zu unterschiedlichen Effekten in der neuronalen Funktion führen können, welche hoch abhängig vom Ort der Innervierung und der lokalen intrinsischen Signalverarbeitung sind.

Aufgrund der durchgeführten somatischen Aufnahmen waren die erhaltenen räumlichen Informationen der dendritischen GABAergen Effekte begrenzt. Zur Lösung dieser Begrenzung wurde von uns ein neuer Ansatz entwickelt inhibitorische postsynaptische Potentiale durch eine bildgebende Technik mit einem spannungsabhängigen Farbstoff zu messen. Bei Verwendung dieser verbesserten Technik konnten wir die Herkunft und die physiologische GABAerge Signalausbreitung selbst mit Werten kleiner als 1 mV optisch von mehreren Orten im neuronalen Dendriten auflösen. Auf diese Art und Weise können nun Aufnahmen von Mustern spezifischer dendritischer GABAerger Innervierung räumlich durchgeführt werden und die GABAerge Auswirkung auf neuronale Integrationsprozesse bestimmt werden.

Die Schlussstudie zeigte die beeinflussenden Effekte der GABA<sub>A</sub> Rezeptor Aktivierung durch unterschiedliche Interneuronen Klassen auf sub-zelluläre dendritische exzitatorische postsynaptische Potentiale. Mit der Verwendung des bildgebenden Verfahrens durch einen spannungsabhängigen Farbstoff konnten wir transmembrane Spannungsmuster in CA1 Pyramidenzellen nach Aktivierung der Schaffer Kollateralen studieren. Das beobachtete exzitatorisch/inhibitorische-Verhältnis zeigte eine hohe Variabilität zwischen unterschiedlichen dendritischen Ästen des apikalen-basalen Dendritenbaumes, mit einer hohen Tendenz zu überwiegend inhibitorischer Innervierung in der Nähe des Somas im apikalem Dendriten. Zugabe des GABA<sub>A</sub> Rezeptor Antagonisten Bicucullin zeigte ein exzitatorisches Signal in allen untersuchten dendritischen Abschnitten, was auf eine inhibitorische synaptische Transmission der Originalmuster hindeutet. Wir zeigen, dass GABAerge Inhibition synaptische Integration in einer Dendriten-abhängigen Weise beeinflusst, wobei ein hoher Anteil des Dendritenbaumes überwiegend oder ausschliesslich inhibitorische Signal durch CA1 Stimulation erhält. Zusammengefasst zeigt meine Doktorarbeit, dass der Ort GABAerger Innervierung von entscheidender Bedeutung für neuronale Integrationsprozesse ist.

# **Table of Contents**

<b>1</b>	<b>Introduction</b>	<b>5</b>
1.1	GABA	5
1.2	GABA <sub>A</sub> receptor and its signaling	7
1.3	GABA-mediated signals during the development of the animal brain	9
1.4	Excitatory effects of GABA in mature neurons	11
1.5	Interneurons	13
1.6	Spatial aspects of inhibition in neuronal computation	17
1.7	Overview	22
<b>2</b>	<b>Manuscript I: GABAergic Hyperpolarization Facilitates Dendritic Spike Firing in Cortical Pyramidal Cells</b>	<b>25</b>
2.1	Abstract	26
2.2	Introduction	27
2.3	Materials and Methods	29
2.3.1	Slice preparation	29
2.3.2	Electrophysiology	30
2.3.3	Calcium Imaging	31
2.3.4	Iontophoresis	31
2.3.5	Data Analysis	32
2.3.6	Immunohistochemistry	32
2.3.7	Drugs	32
2.4	Results	33
2.5	Discussion	42
2.6	References	45
<b>3</b>	<b>Manuscript II: Imaging Inhibitory Synaptic Potentials Using Voltage Sensitive Dyes</b>	<b>49</b>
3.1	Abstract	50
3.2	Introduction	51
3.3	Materials and Methods	52
3.3.1	Slice preparation and electrophysiology	52

3.3.2	Neuronal loading	52
3.3.3	Optical recording	53
3.3.4	Anatomical reconstruction and data analysis	55
<b>3.4</b>	<b>Results</b>	<b>56</b>
3.4.1	Staining procedure and IPSP optical recordings	56
3.4.2	Estimate of intracellular Cl <sup>-</sup> concentration ([Cl <sup>-</sup> ] <sub>i</sub> ) without use of electrodes	59
3.4.3	Resolution of optical IPSP measurements	63
3.4.4	Spatial distribution of IPSPs from different classes of interneurons	65
3.4.5	IPSP recordings from axons and basal dendrites	68
<b>3.5</b>	<b>Discussion</b>	<b>71</b>
<b>3.6</b>	<b>Supplementary material</b>	<b>73</b>
<b>3.7</b>	<b>References</b>	<b>74</b>
<b>4</b>	<b>Manuscript III: Feedforward Inhibition Controls The Spread Of Excitation Within The Dendritic Tree Of CA1 Pyramidal Neurons</b>	<b>77</b>
<b>4.1</b>	<b>Abstract</b>	<b>78</b>
<b>4.2</b>	<b>Introduction</b>	<b>79</b>
<b>4.3</b>	<b>Materials and methods</b>	<b>81</b>
4.3.1	Brain slice preparation	81
4.3.2	Neuronal loading	81
4.3.3	Electrophysiology	82
4.3.4	Optical recordings	82
4.3.5	Stimulation and Pharmacology	83
4.3.6	Anatomical reconstruction and analysis	84
<b>4.4</b>	<b>Results</b>	<b>85</b>
<b>4.5</b>	<b>Discussion</b>	<b>96</b>
<b>4.6</b>	<b>Supplementary material</b>	<b>99</b>
<b>4.7</b>	<b>References</b>	<b>100</b>
<b>5</b>	<b>Discussion</b>	<b>103</b>
<b>6</b>	<b>References</b>	<b>110</b>
<b>7</b>	<b>Supplementary Material</b>	<b>116</b>
<b>8</b>	<b>List of Abbreviations</b>	<b>117</b>

<b>9 Acknowledgements</b>	<b>118</b>
<b>10 Curriculum vitae</b>	<b>119</b>



# 1 Introduction

## 1.1 GABA

The central nervous system (CNS) is a high complex system of connected neurons exchanging information with each other. Neuron interaction occurs between a presynaptic and a postsynaptic cell at structures that are called synapses (Sherrington, 1947). There exist two fundamental types of synapses, the chemical and the electrical one. In electrical synapses the neurons are connected by channels, passing electrical currents whereby voltage changes in the presynaptic element causes a voltage changes in the postsynaptic one. Chemical synapses are separated by a small space, the synaptic cleft, in which endogenous chemicals, so-called neurotransmitters are released from the presynaptic neuron. The release is triggered by the arrival of a nerve impulse in the presynaptic side. Freely diffusing neurotransmitters bind to receptors in the membrane on the postsynaptic part of the synapse and open ion channels either directly next to the receptors or indirectly via signal cascades. Ions are conducted through the channels along their electrochemical gradient from one side of the membrane to the other and induce postsynaptic potentials (PSPs) across the membrane of the neuron.

The effect of the PSP – whether it is excitatory or inhibitory – is determined not by the type of transmitter released from the presynaptic side but by the type of ion channels that were opened by transmitter binding their receptors (Kandel et al., 2000). However, most transmitters are recognized by types of receptors that mediate either excitatory or inhibitory potentials (EPSPs, IPSPs). For this reason, most of the time neurotransmitters are referred to as excitatory or inhibitory.

The key excitatory neurotransmitters are glutamate, acetylcholine, noradrenalin, dopamine and serine.

The main inhibitory neurotransmitter in the CNS, aside from Glycine in the spinal cord, is  $\gamma$ -aminobutyric acid (GABA; Figure 1.1) that binds to several types of GABA-gated chloride ( $\text{Cl}^-$ )-channels (GABA receptors).

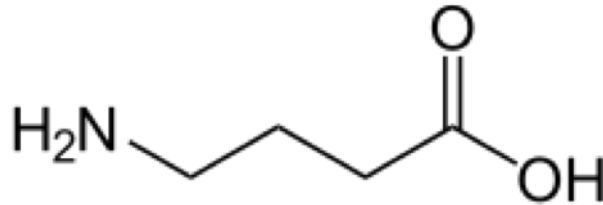


**Figure 1.1 . Structure of  $\gamma$ -aminobutyric acid.**

In the 1950, GABA was found for the first time in large quantities as an unidentified ninhydrin-reactive compound in extracts of fresh mouse, rat, rabbit, guinea pig, human and frog brains. Chromatographically analysis conclusively characterized the compound (Roberts and Frankel, 1950).

GABA is synthesized by decarboxylation of L-glutamic acid. The chemical reaction is catalyzed by two L-glutamic acid decarboxylases (GAD65 or GAD67), which are found in specific neurons of the CNS.

At the same time GABA was discovered, an inhibitory brain substitute called Factor I was found. It was demonstrated that the brain extract possessed anti-acetylcholine effects by preventing the stimulating action of acetylcholine on the crayfish stretch receptor neuron, the crayfish heart and crayfish intestine (Florey, 1954). Shortly afterwards, the inhibitory Factor I was identified as  $\gamma$ -aminobutyric acid (Bazemore et al., 1956). In the following years, numerous studies confirmed that GABA has a function specifically related to inhibitory neurons (Kravitz et al., 1963 a+b; Florey, 1991). Shortly afterwards, the hypothesis that GABA acts as an inhibitory neurotransmitter was proven by Krnjevic und Schwartz. They applied extracellular GABA on cat brains while intracellular recordings measured inhibitory postsynaptic potentials (Krnjevic and Schwartz, 1966). Conclusively, little doubt remained about the role of GABA as an inhibitory neurotransmitter in the CNS.



## 1.2 GABA<sub>A</sub> receptor and its signaling

Depending on the specific brain region, GABA is estimated to be present in 20-50 % of several thousand synaptic contacts found on a neuron (Halasy and Somogyi, 1993; Hevers and Lüddens, 1998). The neurotransmitter mediates changes in membrane currents by activating GABA receptors. Two main classes of GABA receptors exist: the fast ionotropic GABA<sub>A</sub> receptor (GABA<sub>A</sub>R; Figure 1.2) and the slower metabotropic GABA<sub>B</sub> receptor (GABA<sub>B</sub>R).

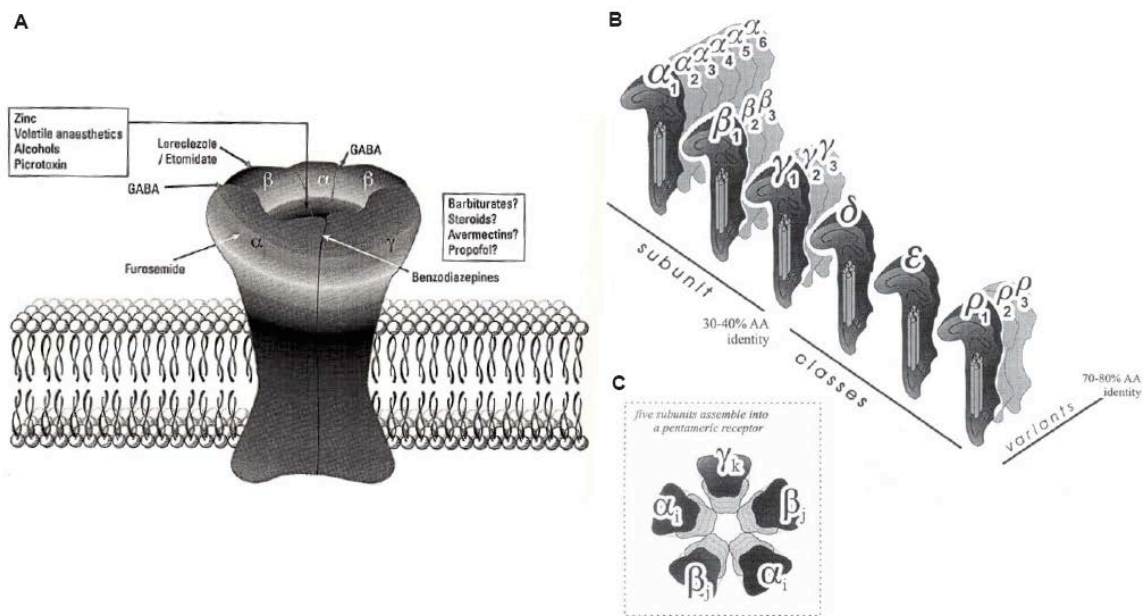


**Figure 1.2 . GABA<sub>A</sub>-receptor. (A)** Diagram showing sites of action of various classes of anti-epileptic drugs. Modified from Möhler (Möhler, 2001). **(B, C)** Schematic representations of GABA<sub>A</sub> receptor subunits. **(B)** Grouping of six classes ( $\alpha$ ,  $\beta$ ,  $\gamma$ ,  $\delta$ ,  $\epsilon$  and  $\rho$ ) based on sequence identity of 30-40 %. Within each class between one and six variants exist that share 70-80 % amino acid identity. **(C)** Five of such subunits assemble into a heteropentameric receptor with the most commonly combination of two  $\alpha_i$  (i:1-6), two  $\beta_j$  (j:1-3), and one  $\gamma_k$  (k:1-3) subunits, but other combinations are possible. Modified from Hevers and Lüddens (1998).

This work focuses on potentials mediated by GABA<sub>A</sub> receptors. The receptors consist of five transmembrane subunits. 19 such homologous subunits are known (Figure 1.2, B). The most typical arrangement consists of two  $\alpha$ , two  $\beta$  and one  $\gamma$  subunit (Figure 1.2, C). Although, the subunits are encoded by different genes, they share at least 20-40 % homologous sequences with each other and

10-20 % with nicotinic acetylcholine receptors and strychnine-sensitive glycine receptors, strongly confirming their evolutionary relationship (Olsen and Tobin, 1990).

Structurally, subunits are composed of a putative large N-terminal extracellular domain, thought to be responsible for ligand-channel interactions, and four putative transmembrane domains (TM) with a large intracellular loop containing sites for regulation, for example, phosphorylation, between TM3 and TM4 (Smith and Olsen, 1995; Galzi and Changeux, 1994).

The receptor-forming subunits are arranged in a pentameric form in which in the center the ion channel is located. In case of the GABA<sub>A</sub>R, it selectively conducts Cl<sup>-</sup> ions and hydrogen carbonate (HCO<sub>3</sub><sup>-</sup>). The open probability of the channel can be modulated by various drugs through distinct binding sites on the GABA<sub>A</sub>R subunits. Whereas GABA attaches to its recognition site on a specific amino acid sequence in the  $\alpha$  subunits, other positive modulatory drugs, like barbiturates, benzodiazepines, alcohol, neurosteroids and other anesthetics, bind to other components of the receptor complex (Enna and Möhler, 2007; Figure 1.2, A). The most clinically relevant modulators are the benzodiazepines, with their most commonly used representative, diazepam. It has been shown that this positive allosteric drug binds at the histidine positions of benzodiazepine-sensitive subtypes ( $\alpha$ 1,  $\alpha$ 2,  $\alpha$ 3, and  $\alpha$ 5) and also at  $\alpha$ 4 and  $\alpha$ 6 subunits when arginine is replaced a histidine amino acid (Rudolph et al., 1999). Binding of diazepam enhances the open probability of the channel after GABA attaching to its recognition sites. Some negative ligands of the GABA<sub>A</sub>R, which completely block GABA mediated currents are also known. The best known are the competitive and non-competitive antagonists, bicuculline and picrotoxinin, respectively.

After GABA binds to the receptor, channel opening evokes an increase in membrane conductance for Cl<sup>-</sup>. The Cl<sup>-</sup> flux across the membrane is determined by the electrochemical gradient of the ion. No net flow occurs when the gradient is in equilibrium, the so-called electrochemical equilibrium potential ( $E_{Cl^-}$ ), which is under physiological conditions in adult animals between -60 and -70 mV. In adult mammalian brains, the internal chloride concentration ( $[Cl^-]_i$ ) is typically

around 4 mM and the external concentration ( $[Cl^-]_o$ ) around 116 mM (Lodish and Harvay, 1999).  $E_{Cl^-}$  can be determined by the equation of Walther Nernst ( $E = -RT/zF \cdot \ln([Cl^-]_i/[Cl^-]_o)$ ). As GABA<sub>A</sub>-receptor signaling is mediated by Cl<sup>-</sup>-channels, the concentration gradient for Cl<sup>-</sup> across the cell membrane determines the nature of the signaling effect (Alger and Nicoll, 1979). Under physiological conditions  $E_{Cl^-}$  is below the resting membrane potential ( $V_m$ ) and channel opening drives Cl<sup>-</sup>-ions into the cell, hyperpolarizing the membrane. Synchronous excitatory synaptic input is limited by the hyperpolarization to depolarize  $V_m$  to spike threshold (Owens and Kriegstein, 2002). GABA<sub>A</sub> receptor activation can also induce 'shunting' effects on the membrane, occurring when the activation is opening a large number of Cl<sup>-</sup>-channels while hyperpolarizing the cell membrane. A special case of shunting inhibition occurs when  $E_{Cl^-}$  is almost equals then  $V_m$  and below the threshold for action potential (AP) generation. Here, the net driving force is zero (Driving force =  $V_m - E_{Cl^-}$ ) and channel opening would not induce any change in the membrane potential. In a shunting process the inhibitory conductance change is similar to a transient reduction in the membrane resistivity ( $R_m$ ), which 'shunts' the EPSP without an obvious change in membrane potential (Rall, 1964; Staley and Mody, 1992; Mann and Paulsen, 2007; Stuart et al., 2008).

### **1.3 GABA-mediated signals during the development of the animal brain**

It has been shown in work of Yehezkel Ben-Ari and co-workers that GABA might also depolarize the membrane. They discovered giant depolarizing potentials (GDPs) in young (postnatal day (P) 0 – 18) hippocampal CA3 neurons (Ben-Ari et al., 1989). The reason was an increased internal Cl<sup>-</sup>-concentration inducing a more depolarized  $E_{Cl^-}$  than AP threshold. Accordingly, an inward directed net flow forces Cl<sup>-</sup>-ions out of the cell when the channels are open (Ben-Ari, 2002). During mammalian brain development, the excitatory effects of GABA change to inhibitory ones due to progressive shift in  $E_{Cl^-}$  (-30-(-40) mV to -50-(-60) mV)

which is evoked by a reduction in  $[Cl^-]_i$  from high values of  $\sim 40$  mM to  $\sim 5$  mM (Ben-Ari et al., 2007; Figure 1.3).

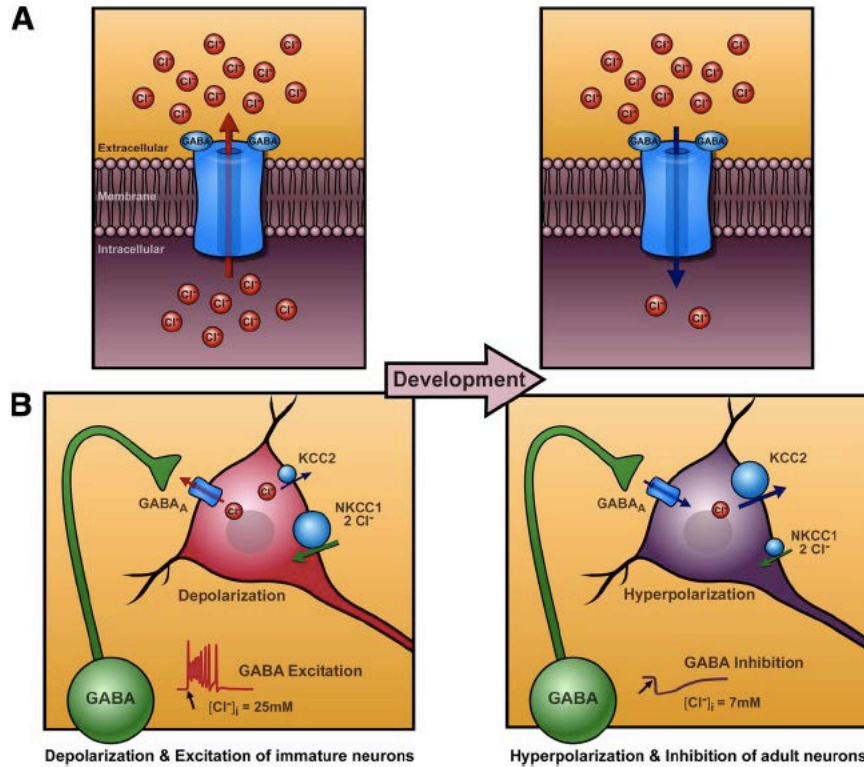


**Figure 1.3 . Developmental changes in  $Cl^-$  homeostasis during development. (A)** Decrease of intracellular  $Cl^-$ -concentration during development. Immature neurons (left): efflux of  $Cl^-$ -ions produces inward electric current and depolarization (insert (B) left). Mature neurons (right):  $Cl^-$  enters cells and produces outward electric current and hyperpolarization (insert (B) right). **(B)** Changes in  $Cl^-$ -concentration is due to changes in expression of two major chloride cotransporters, KCC2 and NKCC1. KCC2 is expressed late in development, whereas NKCC1, which accumulates  $Cl^-$  in the cell, is more expressed in the immature neurons. Modified from Ben-Ari (Ben-Ari et al., 2007).

Members of the cation-chloride cotransporters (CCC) are responsible for the regulation of the  $Cl^-$ -homeostasis (Blaesse et al., 2009); the Na-K-2Cl cotransporter (NKCC1) and the K-Cl cotransporter (KCC2) enhance and reduce  $[Cl^-]_i$ , respectively (Cherubini and Ben-Ari, 2011). At birth, there is an enhanced expression of NKCC1, which accumulates  $Cl^-$  inside the cell. The shift from GABA<sub>A</sub>-mediated depolarization to hyperpolarization, is coupled to a developmental increase in the expression of KCC2 (Rivera et al., 1999), which reduces  $[Cl^-]_i$  by active outwards cotransport of  $Cl^-$  and  $K^+$ . As a consequence,

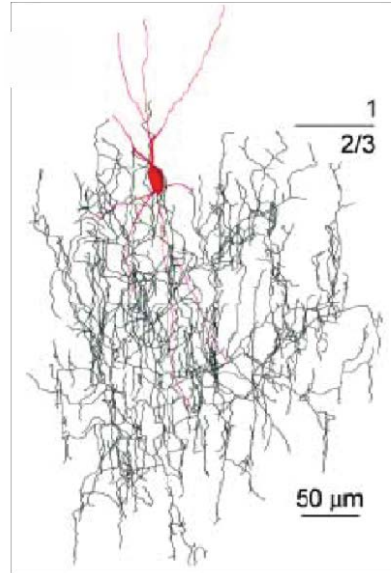
$E_{Cl^-}$  is reduced to below  $V_m$  and GABA-mediated currents become hyperpolarizing.

In contrast to the explanations for the described excitatory effects of GABA in development, recent literature suggests, that early GABA-mediated depolarization may also be determined by the availability and age-dependent concentration change of energy substrates like ketone bodies, pyruvate and lactate (Rheims et al., 2009; Holmgren et al., 2009). While application of adequately supplied energy substrates to postnatal mice brain slices (P3-P19) maintained  $V_m$  and  $E_{Cl^-}$  at negative levels of -53 mV and -80 mV, respectively, a decrease in the level of ketone bodies in the extracellular solution caused a significant increase in  $V_m$  as well as  $E_{Cl^-}$ . The occurrence of GDPs in early developmental stages was also significantly inhibited. Rheims and Holmgren suggested that use of an artificial cerebrospinal fluid (ACSF) with lacking developmentally adequate energy substrates, has caused the depolarizing effects of GABA-mediated currents seen in postnatal in vitro experiments. These results have started a debate on GABA-mediated effects in early developmental stages and the hypothesis of Ben-Ari was revised lately by Tyzio and co-workers (Tyzio et al., 2011).

#### **1.4 Excitatory effects of GABA in mature neurons**

Depolarizing GABA effects have not only been shown during development, there is also a discussion about possible excitatory effects of GABA<sub>A</sub>R in the axon-initial segment of neurons. Receptor activating cells in this area are the chandelier cells or also called axo-axonic cells (AACs; Figure 1.4).

**Figure 1.4 . Reconstruction of Axo-axonic-cell in layer 2/3 of somatosensory cortex.** Soma and dendrite are in red, and axon in black. Layer 1 and layer 2/3. Modified from Szabadics (Szabadics et al., 2006).



This type of neuron has been found in nearly all layered cortical areas, the amygdala, some unlaminated cortical structures and the hippocampus. Anatomical studies of neocortical AACs normally revealed fusiform somata and bitufted dendrites parallel to pyramidal cell apical dendrites (Howard et al., 2005). In the CA1 area of the hippocampus, the AAC dendrites are positioned more horizontally along the stratum oriens and their axons with radially aligned rows of boutons synapse exclusively onto axon initial segments of pyramidal cells (Ganter et al., 2004). Neocortical and hippocampal AACs display fast APs curtailed by a prominent long-duration afterhyperpolarization. Responses of AACs to afferent pathway stimulation are in higher spiking frequency ranges and also show accommodation in the amplitudes of AP bursts (Buhl et al., 1994; Howard et al., 2005). The main role of AACs in the network is to control and shape the signal threshold, and thus the firing behavior of pyramidal cells (Douglas and Martin, 1990). In 2006, Szabadics and co-workers found that AACs were able to depolarize pyramidal cells and to initiate stereotyped series of synaptic events in rats and human cortical networks (Szabadics et al., 2006). In this study, responsible for the excitatory effect in pyramidal cells was a low density of KCC2 transporters in the axon initial segment and hence, a decreased efflux of  $\text{Cl}^-$  ions. The increase in  $[\text{Cl}^-]_i$  forced a depolarization of the cell membrane after  $\text{GABA}_A\text{R}$

activation. More recently, the group of Massimo Scanziani showed that the excitatory effects of GABA<sub>A</sub>-mediated currents are due to invasive techniques used (Glickfeld et al., 2009). Field recordings performed with simultaneous whole-cell recordings of AAC neurons in the CA1 area of the hippocampus clearly indicated the hyperpolarizing action of AACs on their targets.

## 1.5 Interneurons

GABA-releasing inhibitory neurons are commonly known as interneurons. In the 19<sup>th</sup> century Ramon y Cajal already described a large diversity of different looking cells types lying in between homogenously shaped neuron networks (Figure 1.5; (y Cajal, 1911). Later, those cell types were identified as GABAergic interneurons. Already at the first description of interneuron no reliable coincidence between the neurons could be detected and it was getting even more difficult when new developed methods gained more data about the cells.

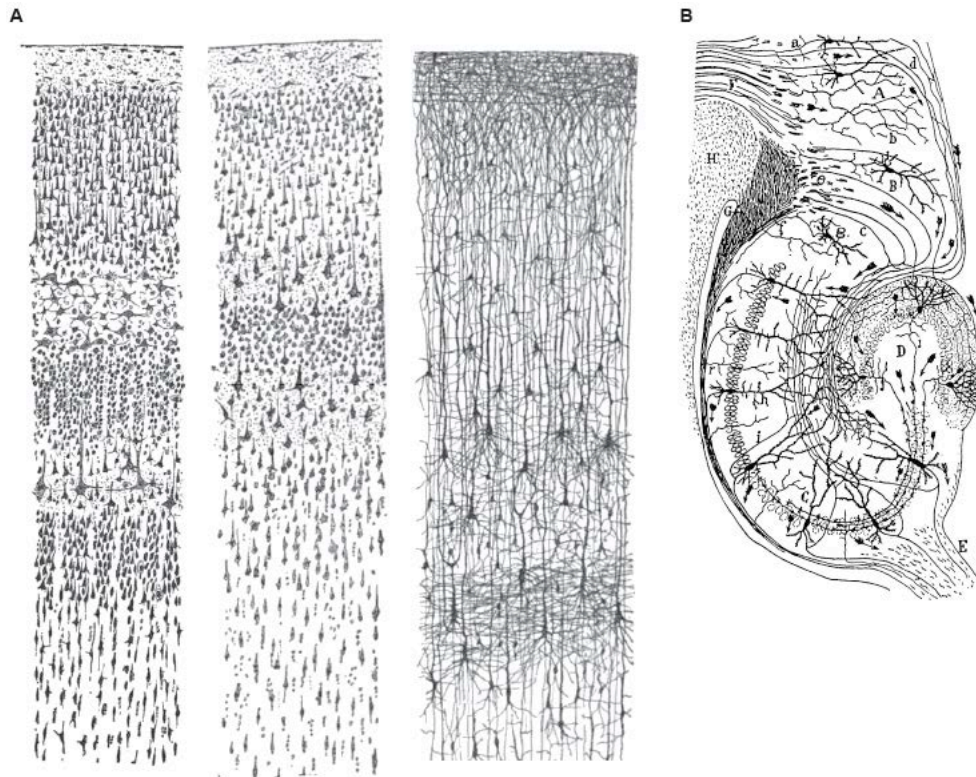


**Figure 1.5 . Drawings by Santiago Ramon y Cajal. (A)** Three drawings of cortical lamination, vertical cross-sections with the surface of the cortex at the top. Left: visual cortex of a human adult. Middle: motor cortex of a human adult. Right: cortex of a 1 ½ month old infant. **(B)** Drawing of the neural circuitry of the rodent hippocampus, transversal section. Taken from S. Ramon y Cajal (1911).

Accordingly, it was necessary to develop a comprehensive system to classify and to organize interneurons on their relevant features. Recently, the Petilla Interneuron Nomenclature Group created a newly revised classification system of neocortical interneurons (Petilla Interneuron Nomenclature Group, 2008). Interneurons were organized according to the anatomical (e.g. the shape of the soma, morphological feature of the axon), physiological (e.g. firing patterns) and molecular features of the cells. In terms of the molecular features, many molecules and gene expression profiles were taken into account. Thus, they grouped the molecules into categories: transcription factors, neurotransmitters or their synthesizing enzymes, neuropeptides,  $\text{Ca}^{2+}$ -binding proteins, neurotransmitter receptors, structural proteins, ion channels, connexins, pannexins and membrane transporters (Petilla Interneuron Nomenclature Group,



2008). Another aspect that should be considered in the grouping is the developmental ontogeny.

The Petilla terminology of neocortical interneurons in specific types and subtypes of neurons was a stepping stone towards a future classification of these complex and heterogeneous cells. Newly identified GABAergic neurons might be able to be characterized more easily and their physiological relevance might be detected more rapidly. The Petilla terminology of neocortical interneurons in specific types and subtypes of neurons was a stepping stone towards a future classification of these complex and heterogeneous cells.

In the hippocampus a similar classification could be developed and at least 21 different interneuron types were described.

On one side, it was found that during a given behavior-contingent network oscillations, interneurons of a given type exhibit similar firing patterns. On the other, also a characterization due to the spatial connectivity to CA1 pyramidal cells was possible (Somogyi and Klausberger, 2005; Klausberger and Somogyi, 2008). Interestingly, interneurons with the same molecular feature are also innervating different dendritic domains, e.g. the following types of parvalbumin- (PV-; a calcium-binding albumin protein) expressing neurons: the previously mentioned AAC (Figure 1.4) exclusively innervate the axon initial segment (Figure 1.6; type 1 cell); basket cells contact the soma and proximal dendritic regions (Figure 1.6; type 2-4 cells); bistratified cells target basal and oblique dendrites (Figure 1.6; type 5, 6 cell); and the oriens-lacunosum moleculare (O-LM) interneurons have synaptic contacts at the distal tuft of pyramidal cells (Figure 1.6; type 7 cell).

It was suggested that specific hippocampal interneuron types play their roles in structuring the activity of pyramidal cells via their respective target domains, and accurately timing and synchronizing pyramidal cell discharge, rather than providing generalized inhibition. Furthermore it was demonstrated that interneurons of the same class show different firing patterns during different network oscillations representing two distinct brain states; and contrary, interneurons belonging to different classes may fire preferentially at distinct time

points during a given oscillation. Thus, a dynamic, spatio-temporal, GABAergic control is given to evolves distinct patterns during different brain states (Somogyi and Klausberger, 2005).

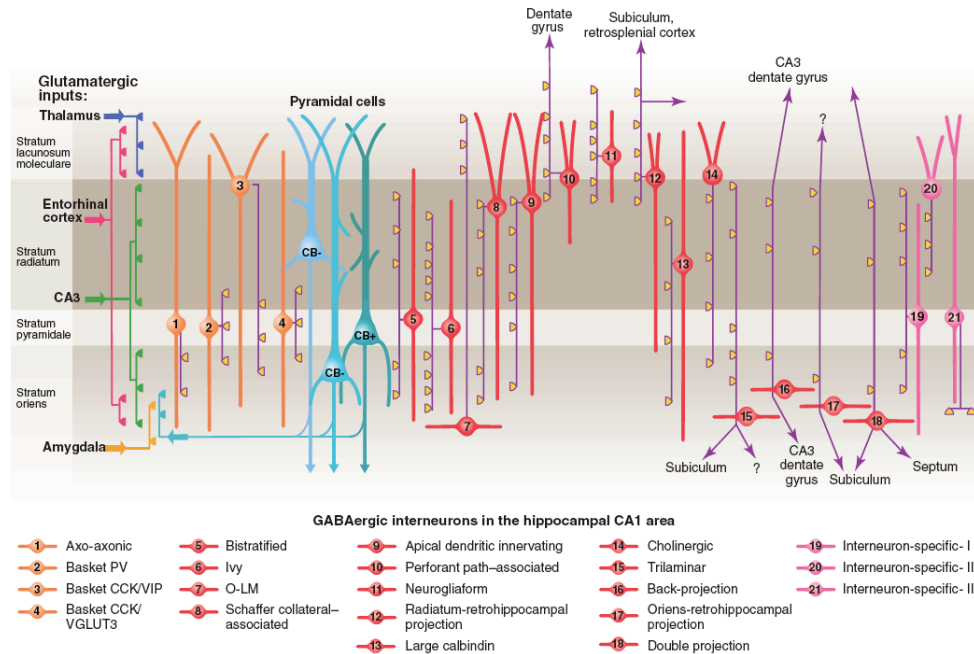


**Figure 1.6 . Overview of different types of GABAergic interneurons in the hippocampal CA1 area.** Main terminations of five glutamatergic inputs to the hippocampus are on the left. Somata and dendrites of interneurons innervating pyramidal cells (blue) are orange, and those innervating mainly other interneurons are pink. Axons are purple; the main synaptic terminations are yellow. Modified from Klausberger and Somogyi (2008).

A variety of interneurons contact pyramidal cells over the entire basal-apical dendrite, partitioned into the soma, the axo-initial segment and several dendritic domains. Ultimately, the almost 12'000  $\mu\text{m}$  of dendrites of CA1 principle cells receive approximately 1'700 inhibitory inputs in addition to about 30'000 excitatory inputs (Megías et al., 2001). This synaptic diversity is crucial to secure the dynamic range of neuronal activity and to correlate the imbalance between excitatory and inhibitory input supporting optimal information processing (Markram et al., 2004).

## 1.6 Spatial aspects of inhibition in neuronal computation

The targeting of distinct interneurons at cellular domains on pyramidal neurons almost certainly plays an essential role in generating and modulating specific brain functions (McBain and Fisahn, 2001). Hence, it is important to understand how each of these interneurons influences synaptic integration.

Synaptic integration describes the process of generating neuronal outputs, usually in form of APs in response to synaptic inputs in the dendrites. The generation of APs depends on the summation of potentials propagating in dendrites towards the soma until the threshold for AP firing is reached in the axon initial segment. Both the generation of AP and the frequency rate of neuron AP firing are determined by inhibitory sculpting of these excitatory input-output patterns.

In a simple integration model, inhibition counteracts depolarization. Thus, the number of active excitatory inputs required to reach the threshold has to be increased for AP initiation (Eccles, 1994; Stuart et al., 1997 b). However, under physiological conditions neuronal integration is thought to be far more complex.

The propagation of postsynaptic potentials from their site of generation towards their summation region in the AP initial zone is affected by passive cable properties of dendrites and their active voltage-gated conductances.

The electrical behavior of the dendrite is determined by three passive electrical properties: the specific membrane resistivity ( $R_m$ ), the specific membrane capacitance ( $C_m$ ), and the intracellular resistivity ( $R_i$ ). Passively propagating PSPs in the dendrites are more attenuated by high values of  $R_i$  and low values of  $R_m$  (Stuart et al., 2008). Wilfrid Rall, a pioneer in the theoretical framework of neuronal computation, demonstrated that distal excitatory synapses are contributing to the depolarizing charge that reaches the cell body. His predicted cable theory states that the time course of the intrasomatically measured potential changes as a function of input location due to filtering of high

frequencies by the distributed capacitance along the dendritic membrane. Conclusively, while PSPs generated in the soma are broader and faster, the more distal initiated PSPs are smaller and have slower rise times. Beyond that, the summation of two or more excitatory inputs in the soma is dependent on the distance of the two synapses from each other. Theoretically, the shorter the distances are, the smaller the response to simultaneous activation is compared to the sum of the individual responses. This is due to the membrane depolarization and hence, a reduced driving force (Rall, 1967; Rall et al., 1967). Additionally, the summation of PSPs in the axon initial segment is dependent on the duration of a defined time window. This window is determined by the membrane time constant ( $\tau_m$ ), given by the product of  $R_m$  and  $C_m$ . Rall demonstrated that theoretically, many small time constants governing the rapid equalization of membrane potential over the dendritic length (Rall, 1969), strongly indicating a non-uniform signal integration in neuronal dendrites. It was subsequently argued that, under physiological conditions, dendrites are divided into numerous functional subunits, each processing synaptic information quasi-independently and consequently, enormously expanding the computational power of each neuron (Segev, 2006; London and Häusser, 2005; Spruston, 2008; Spruston et al., 1995; Koch and Segev, 2000). We can therefore conclude that a strong location dependence of synaptic integration results in specific AP output patterns. These theoretical predictions have been tested in various cell types, especially in hippocampal CA1 and neocortical pyramidal cells, as well as in spinal motor neurons strongly indicating for all areas that synaptic integration may show minimal location dependence of the synaptic input (Cash and Yuste, 1999).

In addition to the cable theory is the fact that active conductance influences integration processes through a large variety of distributed voltage-gated channels along the dendrites. These dendritic channels contribute to synaptic integration, but further experiments are required to completely understand the process. Voltage-gated channels support the propagation of dendritic AP even in reverse direction (Stuart et al., 1997 a+b). In dendrites, backpropagating

potentials interact with a second initiation site for APs in the distal part of the dendrite where sodium-calcium spikes are evoked (Schiller et al., 1997; Larkum et al., 1999 a). A more detailed explanation of this phenomenon, as well an analysis of inhibitory influences on active dendritic voltage-gated conductance is in Manuscript I.

GABA-mediated inhibition plays another central role in the complex integration process.

Inhibition does not merely counteract excitation as suggested in the first simple integration models; rather, it spatially and temporally modulates the summation of excitatory synaptic inputs during synaptic integration (Stuart et al., 2008).

A critical factor in temporal summation is whether interneurons are activated in a feedforward or a feedback manner. In a feedforward circuit, interneurons are activated by the same synapses that excite the principle cells whereas, in a feedback circuit, by the firing of the principle cells themselves. In case of feedforward inhibition, summation of excitatory potentials to reach threshold for AP generation has to occur within less than 2 ms, which was demonstrated in hippocampale CA1 pyramidal cells (Pouille and Scanziani, 2001). In contrast, the effect of feedback inhibition limits sustained pyramidal neuron firing and prevents the cells from overexcitation. Different innervation locations of feedback-activated interneurons are combined with different temporal dynamics in the integration processes. Soma and proximal dendrite targeting interneurons deliver onset-transient inhibition. They respond quickly to firing of the CA1 neuron but ceases rapidly. Distal dendrite targeting interneurons convey late-persistent inhibition, which takes longer to develop but is sustained (Pouille and Scanziani, 2004; Spruston, 2008).

The process of inhibitory and excitatory potential is governed by similar principles; indicating that the time course and the duration of inhibitory potentials propagating towards the soma are also determined by the location of innervation as it is valid for excitatory potentials. Hence, the wide variety of synaptic contacts

made by numerous different interneurons might be crucial to coordinate the balance between excitatory and inhibitory integration.

In 1964, Rall showed that the effectiveness of excitatory and inhibitory interaction has a strong spatial component. A wide synaptic separation between two different inputs, perhaps even located on different branches, will tend to sum, whereas adjacent positions can produce a highly nonlinear “shunting” of the excitatory input (Rall, 1964; London and Häusser, 2005). The summation effects on excitatory currents by the spatial arrangement of excitatory and inhibitory synaptic location is illustrated in Figure 1.7 (Stuart et al., 2008). Inhibition at the soma has a similar effect on EPSPs arriving from all dendritic locations, whereas inhibition on dendrites in some distance to the soma can be specific for the particular input.

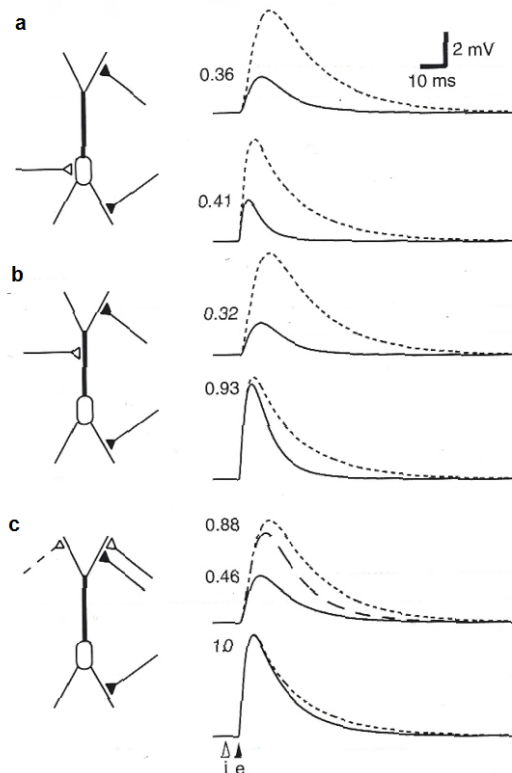


**Figure 1.7 . The spatial relationship between inhibition and excitation influences dendritic integration.**

Left: Schematic diagram with excitatory and inhibitory synapses positioned as shown. Right: Inhibitory synapse (i) is activated 5 ms before excitatory synapse (e) and has  $E_{rev} = V_{rest}$ , meaning that no hyperpolarization is caused by activation of the inhibitory synapse. Numbers by each pair of traces represent the peak of the EPSP with inhibition (solid trace) relative to the EPSP without inhibition (dashed trace) summated in the soma. **a)** Separate responses to activation of the excitatory synapse on the apical dendrite (top traces) or basal dendrite (bottom traces) with and without somatic inhibition. **b)** Responses to activation of the same synapses as in a) with and without apical dendritic inhibition. **c)** Responses to activation of the same excitatory synapses as in a) and b) with and without distal apical inhibition. Long-dashed trace indicates simultaneous activation of excitatory and inhibitory synapses on a different branch. Modified from Dendrites by Stuart et al (2008).

Specific effects of dendritic located inhibition on EPSPs very likely influence the propagation of excitatory potential towards the soma. Due to methodological

limitations, the propagation of the potentials has not been observed thus far. However, we developed a novel approach to investigate the inhibitory effects on the propagation of EPSPs in a highly spatial manner by using voltage-sensitive dye imaging (Manuscript II, III).

## 1.7 Overview

Summarized, the goal of my thesis was to investigate the functional role of GABAergic innervation on dendritic integration in different subcompartments of pyramidal cells.

- ❖ **Manuscript I:** GABAergic hyperpolarization facilitates dendritic spike firing in cortical pyramidal cells

*Prenosil G., Willadt S., Canepari M., Rudolph U. and Vogt K.E.*

*Ready to submit.*

- ❖ **Manuscript II:** Imaging inhibitory synaptic potentials using voltage sensitive dyes

*Willadt S. \*, Canepari M. \*, Zecevic D. and Vogt K.E.*

*Published in Biophysical Journal, 2010, 98(9), p 2032-2040.*

- ❖ **Manuscript III:** Feedforward inhibition controls the spread of excitation within the dendritic tree in CA1 pyramidal neurons

*Willadt S., Nenniger M. and Vogt K.E.*

*Submitted PlosOne.*

Initially, we investigated the effects of GABAergic signals on the dendritic excitability of cortical layer V pyramidal cells (Manuscript I). Dendritic excitability was determined by the frequency of somatic APs we applied to evoke dendritic sodium-calcium spikes. GABA<sub>A</sub> receptor activation was limited to different compartments of the neuron by focal iontophoresis of GABA to either the soma or the distal dendrite. In further experiments, specific subtypes of GABA<sub>A</sub> receptors were blocked by application of the positive allosteric modulator Diazepam. Surprisingly, we observed that hyperpolarization of the dendritic compartment caused an increase in dendritic excitability, in contrast to somatic hyperpolarization which reduced excitability. GABAergic innervation in the distal dendrite activates specific intrinsic activity distinct from other parts in the neuron dendrite. As a possible explanation, we demonstrated that Nickel-sensitive



Calcium-channels were responsible for translating GABA<sub>A</sub>-mediated inhibition into increased dendritic excitability.

The specific effects of GABAergic innervation in distinctive subcompartments of pyramidal cells caught our interest. However, performing further experiments required a technique to investigate GABAergic innervation with a high spatial distribution to measure on different locations simultaneously.

We developed a novel approach using voltage-sensitive dye imaging (Manuscript II). We loaded CA1 pyramidal neurons with the dye JPW1114 from a somatic patch electrode in whole-cell configuration. Interestingly, these neurons could recover their physiological intracellular chloride concentration after removal of the patch electrodes. In a non-patched configuration, we monitored the origin and spread of GABAergic signals propagating from different areas of the apical dendrite. We were able to optically resolve dendritic IPSPs as small as 1 mV from multiple sites. After all, we had a technique to study GABAergic signals with a high spatial-temporal distribution.

Lastly, we were investigating how feedforward inhibition affects the integration of synaptic signals in distinctive subcompartments of pyramidal cell dendrites using voltage-sensitive dye imaging (Manuscript III). Feedforward inhibition was activated by Schaffer collateral stimulation. We observed a high variability in the excitation/inhibition ratio between different compartments of the dendritic tree. Most interestingly, apical dendritic regions close to the soma and the basal dendrites, in particular, predominately received inhibition only. Application of the GABA<sub>A</sub> receptor antagonist bicuculline erased the excitation/inhibition pattern and in all dendritic segments studied only excitatory signals could be detected. Subsequently, we showed that GABAergic inhibition shapes synaptic integration in a dendrite-specific manner. The site of specific GABAergic innervation is of fundamental relevance for neuronal integration processes.



## **2 Manuscript I: GABAergic Hyperpolarization Facilitates Dendritic Spike Firing in Cortical Pyramidal Cells**

Running title: Hyperpolarization-induced spike facilitation

**G. Prenosil<sup>1</sup> S. Willadt<sup>2</sup>, M.Canepari<sup>3</sup>, U. Rudolph<sup>4</sup> and K.E. Vogt<sup>2</sup>**

Status of publication: ready to submit

<sup>1</sup> Department of Pharmacology and Therapeutics; McIntyre Medical Sciences Building; 3655 Promenade Sir-William-Osler; Montréal, Québec, Canada H3G 1Y6

<sup>2</sup> Neurobiology/Pharmacology; Biozentrum; Klingelbergstrasse 50/70; 4056 Basel, Switzerland

<sup>3</sup> Grenoble Institute of Neuroscience; Inserm U 836 - Team 3; Bâtiment Edmond Safra ; Chemin Fortune Ferrini ; Site santé de la Tronche - BP 170 ; 38042 Grenoble cedex 9, France

<sup>4</sup> Laboratory of Genetic Neuropharmacology; McLean Hospital; Department of Psychiatry; Harvard Medical School; 115 Mill Street; Belmont, MA 02478, USA

Corresponding author:

Kaspar Vogt; Neurobiology/Pharmacology; Biozentrum; Klingelbergstrasse 50/70; 4056 Basel, Switzerland

[kaspar.vogt@unibas.ch](mailto:kaspar.vogt@unibas.ch)

My contribution to this manuscript refers generally to participation in experimental procedure and analysis. In particular, I performed research in parts for Figure 2.4 and for Figure 2.5.

## 2.1 Abstract

Different compartments of cortical pyramidal neurons receive input from specific subtypes of  $\gamma$ -aminobutyric acid (GABA) releasing interneurons. Many of the intrinsic signaling capabilities of these compartments have been elucidated; however, the functional role of the specific GABAergic innervation is largely unknown. We studied the effects of GABAergic signals on dendritic excitability of layer V pyramidal cells. Hyperpolarization through activation of dendritic GABA<sub>A</sub> receptors lowered the threshold for dendritic sodium-calcium spikes. In contrast, somatic GABA<sub>A</sub> receptor-mediated hyperpolarization increased the threshold for dendritic spikes. Blockade of low voltage-activated calcium channels abolished the excitatory effect of dendritic GABA<sub>A</sub> receptors. Pairing glutamatergic input with postsynaptic activation produced synaptic depression, if the activity was below dendritic spike threshold and a modest potentiation, if dendritic spikes were fired. Thus, the specific pattern of GABAergic pyramidal cell innervation can lead to distinct effects on neuronal function, depending on the site of innervation and local intrinsic signaling mechanisms.

## 2.2 Introduction

Layer V pyramidal cells are among the largest neurons in the neocortex and possess characteristically elaborate dendritic trees (Feldman, 1984). In adult rodents, long apical dendrites electrically isolate the apical dendritic tuft from the soma (Cauler and Connors, 1994; Williams and Stuart, 2002) and thus create a distinct apical signaling compartment (Yuste et al., 1994). Spurred by dendritic patch-clamp recording and the discovery of voltage-gated conductances in pyramidal cell dendrites (Huguenard et al., 1989; Stuart and Sakmann, 1994) the signaling-capabilities of different pyramidal cell compartments have been intensely studied (Yuste and Tank, 1996; Hausser et al., 2000; Spruston, 2008). The apical dendrites of layer V pyramidal neurons are characterized by their capacity to produce sodium-calcium spikes (Yuste et al., 1994; Schiller et al., 1997). Such spikes can be triggered by large excitatory input to the distal dendrite (Stuart and Sakmann, 1994), by concomitant excitatory input and postsynaptic sodium action potentials (Larkum et al., 1999 b) or by brief bursts of backpropagating action potentials above a certain 'critical' frequency (Larkum et al., 1999 a). The functional role of these spikes is not completely understood; however, several groups have shown an involvement in synaptic plasticity (Nevian and Sakmann, 2006) and in functionally linking the distal dendritic compartment with the soma (Larkum et al., 1999 b).

In addition to this intrinsic compartmentalization, pyramidal cells receive both excitatory and inhibitory synaptic inputs in a compartmentalized manner (Spruston, 2008). For cortical interneurons in particular, the subcellular target region of pyramidal cells is an important characteristic of the various subtypes (McBain and Fisahn, 2001; Petilla Interneuron Nomenclature Group, 2008). For example, axo-axonic cells form synapses specifically on the axon initial segment of pyramidal cells, basket cells target soma and proximal dendrites and Martinotti cells specifically innervate the apical dendrite (Markram and Sakmann, 1994). These interneurons activate a large variety of different GABA<sub>A</sub> receptor subtypes, with the different subtypes again distributed in a compartment-specific manner in

cortical pyramidal cells (Fritschy and Mohler, 1995; Loup et al., 1998; Sieghart and Sperk, 2002).

A wealth of data is available on the effects of GABA<sub>A</sub> receptor signaling on somatic excitability (McCormick, 1989; Pouille and Scanziani, 2001; Gullledge and Stuart, 2003), however, the picture is less clear for GABA<sub>A</sub>-receptor activation in other compartments (Szabadics et al., 2006; Khirug et al., 2008; Glickfeld et al., 2009). We studied GABAergic signaling in layer V pyramidal neurons to determine the effects of somatic and dendritic GABA<sub>A</sub> receptor activation on dendritic excitability. Dendritic sodium-calcium spikes were evoked through somatic action potential bursts above the critical frequency (Larkum et al., 1999 a). To limit the activation of GABA<sub>A</sub> receptors to somatic and dendritic compartments respectively we used focal iontophoresis of GABA and application of diazepam to brain slices from wild-type mice and from animals with a genetically controlled sensitivity of specific subtypes of GABA<sub>A</sub> receptors to this positive allosteric modulator (Löw et al., 2000).

We found that activation of dendritic, but not somatic GABA<sub>A</sub> receptors increased dendritic excitability and suggest a mechanism for this subtype- and compartment-specific action.

## 2.3 Materials and Methods

### 2.3.1 Slice preparation

All experiments and animal handling was approved by the veterinary office of the canton of Basel, Switzerland and in compliance with local and national rules. Slices were obtained from wild-type (WT) C57BL/6J mice and C57BL/6J- $\alpha 2$ (H101R) mice that carried diazepam-insensitive  $\alpha 2$ -containing GABA<sub>A</sub> receptors obtained by a histidine-to-arginine point-mutation in the  $\alpha 2$  subunit gene (L w et al., 2000). The mutation was originally created in 129P2/OlaHsd-derived embryonic stem cells by homologous recombination and bred onto the C57BL/6J background for >10 generations. Existence of the mutation was confirmed by PCR analysis. WT and  $\alpha 2$  mice (p18 to p35) from both sexes were deeply anesthetized with inhaled isoflurane and immediately decapitated thereafter. The brain was quickly removed and placed into ice chilled artificial cerebral spine fluid (ACSF, composition in mM: NaCl 87, NaHCO<sub>3</sub> 26, NaH<sub>2</sub>PO<sub>4</sub> 1.25, KCl 2.5, MgCl<sub>2</sub> 9, CaCl<sub>2</sub> 0.5, Sucrose 75, Glucose 25). The hemispheres were separated along the medial plane and glued to a stainless steel stage of a vibrating microtome (Microm HM 650 V, Germany) using cyanoacrylate glue. Orientation of the hemispheres was arranged, such that their dorsal cerebral cortex was facing the blade. Acute parasagittal cortical slices (250  $\mu$ m thick) were cut, while the stage holding the brain was tilted eleven degrees downwards versus the cutting plane. This allowed us to obtain slices from the somatosensory cortex with dendrites oriented parallel to the plane of cutting in one or two slices per hemisphere. Cut slices were incubated in 33°C ACSF for 45 min and stored afterwards at room temperature (25°C) prior to use. Throughout the experiments all ACSF solutions were constantly aerated with a mixture of 95% O<sub>2</sub> and 5% CO<sub>2</sub>.

### **2.3.2 Electrophysiology**

All experiments were performed on layer V pyramidal cells in the somatosensory cortex. Cells were visualized with a CCD camera (PCO VX 55; Till Photonics, Germany) mounted on an upright microscope (Olympus BX51WI, Switzerland), equipped with a long working-distance water-immersion objective (Olympus XlumplanFI 20x, 0.95 numerical aperture), a fourfold magnification changer, Nomarski-type differential interference contrast and infrared illumination. The recording chamber was perfused at 1 ml/min with 33°C ACSF solution. The ACSF solution contained additionally 10  $\mu$ M 2,3-Dioxo-6-nitro-1,2,3,4-tetrahydrobenzo[f]quinoxaline -7-sulfonamide disodium salt (NBQX) and 50  $\mu$ M D-(-)-2-Amino-5-phosphonopentanoic acid (D-AP5) to block excitatory synaptic transmission. GABA<sub>B</sub> receptor mediated activity was suppressed in all experiments by adding the selective antagonist CGP 55845 (1  $\mu$ M) to the ACSF. For whole cell electrophysiological recordings a Multiclamp 700A patch clamp amplifier (Axon Instruments, USA) was utilized. Data was filtered at 4 kHz, digitized at 20 kHz, stored and analyzed using IGOR Pro software (Wave Metrics, Lake Oswego, USA). Recording patch electrodes were pulled from borosilicate glass (GC150TC; Clark, UK) on a horizontal puller (Zeitz Instruments, Germany) and fire polished. The electrodes had an open tip resistance of 3-4 M $\Omega$ , when filled with the internal solution, containing (in mM): K-gluconate 130, EGTA 1, HEPES 10, Mg-ATP 5, Na-GTP 0.5, NaCl 5; pH adjusted with KOH to 7.3. For experiments with varying chloride concentrations we used a mixture of nominally chloride free and high chloride internal at the appropriate ratio. The nominally chloride free internal contained (in mM): K-gluconate 120, Tris phosphate 11, HEPES 10, Mg-ATP 4.5, Tris-GTP 0.3, pH adjusted with NaOH to 7.3. The high chloride internal contained (in mM): KCl 100, K-gluconate 30, Tris phosphate 11, HEPES 10, Mg-ATP 4.5, Tris-GTP 0.3, pH adjusted with NaOH to 7.3. If fluorescence visualization of the apical dendrite was required, these solutions were augmented with the fluophore Alexa-488 (Invitrogen AG, Switzerland). Individual action potentials (APs) were elicited with brief depolarizing somatic current injections (2 ms / AP, 2-3 nA). APs were



elicited in bursts at frequencies ranging from 20 to 180 Hz. To record a somatic afterdepolarisation potential (ADP) usually 3 to 4 APs had to be elicited above a critical frequency, whose value was established for each cell (Fig. 1 C and D). It was carefully monitored, that only the minimal number of APs required to reliably elicit an ADP were used in the experiments.

### **2.3.3 Calcium Imaging**

The  $\text{Ca}^{2+}$  indicator Bis-Fura-2 (Invitrogen AG, Switzerland) was added at a concentration of 500  $\mu\text{M}$  to the internal solutions described above, when imaging of dendritic  $\text{Ca}^{2+}$  transients was combined with whole cell electrophysiological recordings. In this case EGTA was omitted in the intracellular solution. The fluorescent indicator was excited at  $387 \pm 6$  nm (Semrock Inc., USA) with a 100 Watt Hg-lamp (Olympus, Switzerland) and the emitted light deflected with a dichroic mirror at 470 nm (Olympus, Switzerland) and filtered at  $510 \pm 42$  nm (Semrock Inc., USA) to detect the fluophore-bound  $\text{Ca}^{2+}$  with a CCD camera of 80 x 80 pixels (Neuro CCD-SM, RedShirt Imaging LLC, USA). The images of stained neurons were recorded at a frame rate of 500 Hz while the protocol to elicit and record ADPs was applied.

### **2.3.4 Iontophoresis**

Electrodes for iontophoresis were pulled from borosilicate glass to an open tip resistance of 5-6 M $\Omega$  and filled with a solution containing 3 mM GABA, buffered with 10 mM HEPES and adjusted with NaOH to a pH of 7.3. The electrodes were connected to a constant-current micro-iontophoresis unit (WPI, USA) and placed either close to the soma or near the apical dendrite of the recorded pyramidal cells. Dendrites were visualized by filling the cell with the fluorescent dye Alexa-488. GABA was ejected with rectangular current pulses (80 - 120 nA) of 80 to 100 ms duration. If GABA iontophoresis was required while recording ADPs, the onset of this rectangular current pulse preceded the last AP in a series usually by

100 to 120 ms, meaning that the current pulse was stopped 20 to 40 ms before recording the somatic ADP.

### **2.3.5 Data Analysis**

The ADP was usually detected online, while recording from a layer V pyramidal cell and a sigmoid curve fitted to the ADP versus AP burst frequency after one full set of frequencies was applied (Larkum et al., 1999 a).

All averaged results are presented as the mean  $\pm$  standard error of the mean (SEM). Statistical tests used were paired and unpaired Student's t-test. Their use is indicated at the appropriate position.

### **2.3.6 Immunohistochemistry**

Immunohistochemical visualization of the GABA<sub>A</sub> receptor  $\alpha 2$  subunit was performed as described previously (Fritschy et al., 1998).

### **2.3.7 Drugs**

NBQX, D-AP5 and CGP 55845 were purchased from Tocris Bioscience (USA). Salts for the extra- and intracellular solutions were purchased from Sigma-Aldrich Chemie GmbH (Switzerland). Diazepam was generously provided by Hoffmann-La Roche Inc.

## 2.4 Results

Dendritic sodium-calcium spikes in layer V pyramidal cells can be both elicited and detected using somatic patch clamp recordings (Larkum et al., 1999 a).

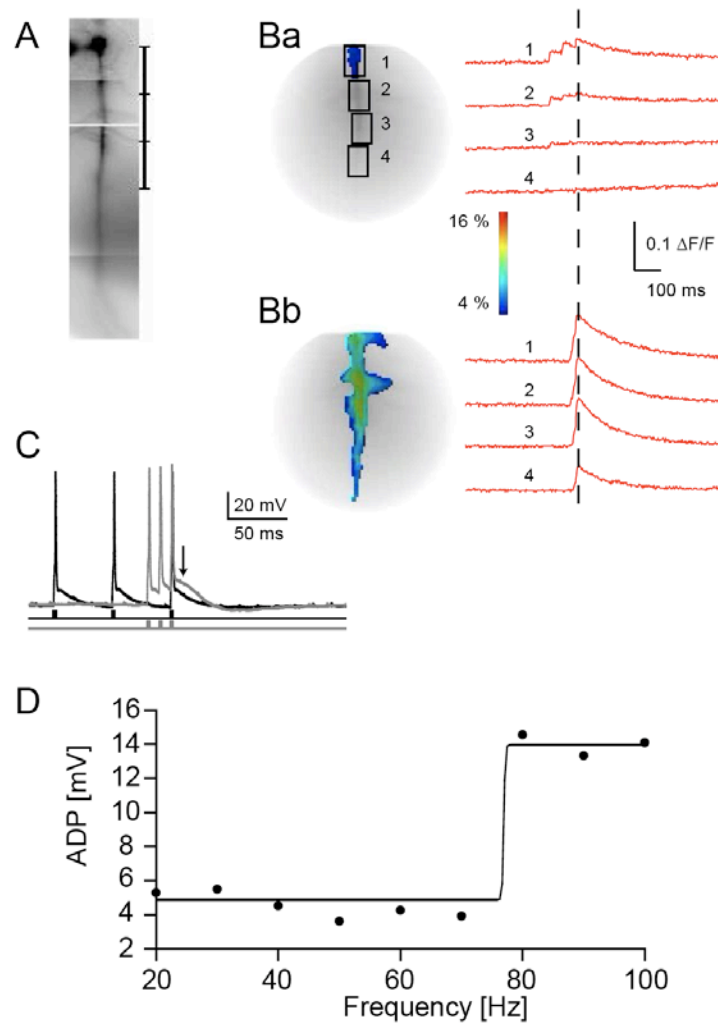


**Figure 2.1 . Bursts of somatic sodium action potentials trigger dendritic calcium spikes above a critical frequency.** **A)** Grey-scale picture of a layer V pyramidal cell filled with calcium dye. Soma and patch electrode are visible near the top, the apical dendrite extends downward. The bar indicates the area of interest. **B)** False color pictures of  $\text{Ca}^{2+}$  dye fluorescence at peak, indicated with the vertical dotted line, at stimulation frequencies below (Ba) and above (Bb) the critical frequency ( $F_c$ ). The traces at right show the fluorescence intensity at four different sites along the apical dendrite. **C)** Current-clamp recording at the soma. Action potentials are evoked by somatic injections indicated in the bottom traces. The top traces show the appearance of an afterdepolarisation (ADP) (arrow) with increasing stimulation frequency. **D)** ADP amplitude as a function of the burst stimulus frequency. Note the sharp appearance. The solid line is a sigmoid fit to the plot,  $F_c$  is at its inflection point.

Bursts of three to four action potentials were elicited in layer V pyramidal cells in the somatosensory cortex of mice. If applied above the critical frequency, the volley of backpropagating action potentials (*BPAP*), elicited dendritic sodium-calcium spikes (Figure 2.1 B) and caused a distinct afterdepolarisation (Figure 2.1 C arrow). Plotting the BPAP frequency against ADP amplitude revealed a typical, highly nonlinear relationship (Figure 2.1 D). The critical frequency ( $F_c$ ) was determined as the inflection point of a sigmoid curve fitted to this data (Larkum et al., 1999 a).

We were interested in the effect of GABA<sub>A</sub> receptor activation on the threshold of dendritic sodium-calcium spike generation. We bath-applied diazepam (1  $\mu$ M) a positive allosteric modulator of GABA<sub>A</sub> receptors, thereby increasing the activation of the receptors due to spontaneously released GABA.

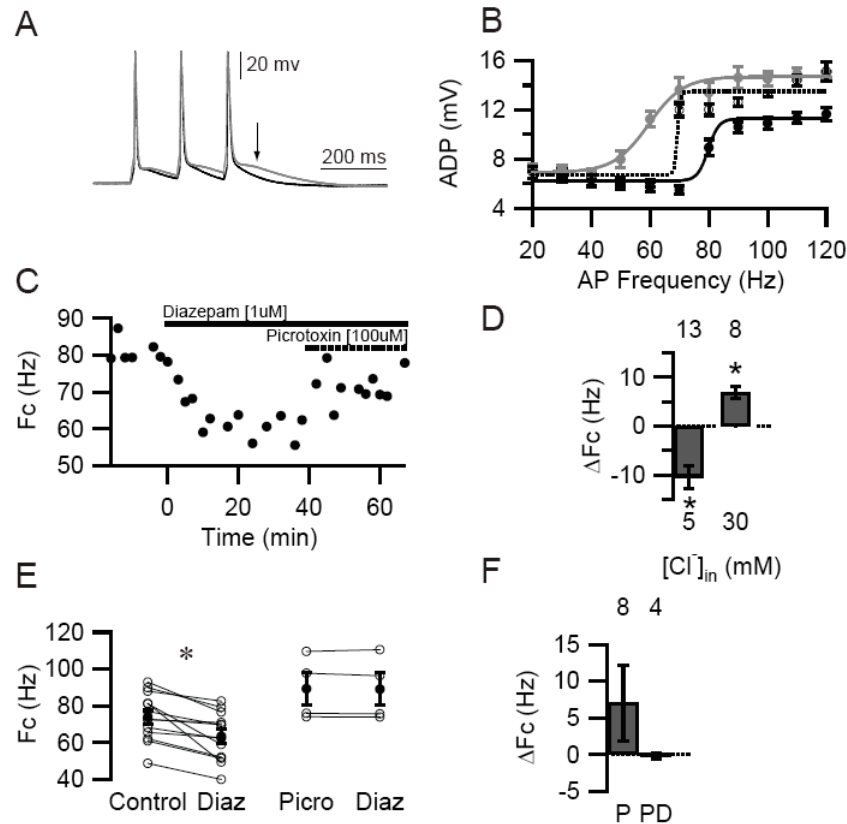


**Figure 2.2 . Increasing GABA<sub>A</sub> receptor function lowers the calcium spike threshold. A)** Action potential burst in a layer V pyramidal cell before (black) and after the application of diazepam (1  $\mu$ M) (grey). At this particular frequency the calcium spike is only visible in the presence of diazepam. **B)** ADP-versus-frequency plots for three conditions: baseline (black), diazepam (grey) and picrotoxin (100  $\mu$ M) (dotted). **C)** Development of  $F_c$  over time as first diazepam and then picrotoxin are applied to the bath (times indicated by the bars). **D)** Average change in  $F_c$  after diazepam application in 5 mM  $Cl^-$  and 30 mM  $Cl^-$ , respectively. The numbers above the bars indicate the number of experiments. **E)** Diazepam effect in individual experiments in 5 mM  $Cl^-$  under control conditions and in the presence of picrotoxin. **F)** Bar graph of the effect of picrotoxin alone and of diazepam in the presence of picrotoxin.

Application of diazepam caused a decrease in the sodium-calcium spike threshold, with an ADP (Figure 2.2 A&B) appearing at frequencies that were previously below threshold. The mean  $F_c$  was decreased from  $73.9 \pm 3.6$  Hz to  $63.4 \pm 3.7$  Hz ( $n=13$ ,  $p < 0.01$ , paired t-test) (Figure 2.2 D&E). Application of the GABA<sub>A</sub> receptor blocker picrotoxin (100  $\mu$ M) reversed the effect of diazepam, but the effect did not reach statistical significance (Figure 2.2 F). In the presence of picrotoxin the effect of diazepam was completely blocked with  $F_c$  at  $89.2 \pm 8.6$  Hz before and  $89.0 \pm 8.7$  Hz ( $n=4$ ,  $p > 0.1$ , paired t-test) after diazepam (Figure

2.2 E&F). We therefore concluded that increased GABA<sub>A</sub> receptor function enhanced dendritic excitability. Excitatory effects of dendritic GABA<sub>A</sub> receptors have been described previously and were shown to be due to depolarizing chloride reversal potentials (Gulledge and Stuart, 2003). We tested the effect of diazepam in cells that were recorded with internal solutions containing 30 mM chloride, forcing a depolarizing GABA<sub>A</sub> receptor reversal potential. Under these circumstances, diazepam increased the critical frequency from 81.7 +/- 5.2 Hz to 88.5 +/- 5.1 Hz (n=8, p<0.05, paired t-test; Figure 2.2 D). Depolarizing GABAergic responses thus decreased dendritic excitability.

To better understand the basis of the observed increase in dendritic excitability we wanted to identify the location and subtype of the involved receptors. Different GABA<sub>A</sub> receptor subtypes in the cortex show laminar preferences, with  $\alpha$ 2 subunit containing receptors found predominantly in the outer cortical layers (Figure 2.3 A; Paysan et al., 1997). To selectively block activation of these receptors, we used mice in which  $\alpha$ 2 subunit containing receptors were rendered diazepam insensitive (Löw et al., 2000). Application of diazepam in these mice resulted in a significant increase of  $F_c$  in layer V pyramidal cells from 98.5 +/- 9.4 Hz to 106.3 +/- 10.3 Hz (n=7, p<0.05, paired t-test; Figure 2.3 B). Thus,  $\alpha$ 2 subunit containing GABA<sub>A</sub> receptors mediated the excitatory effect of diazepam in layer V pyramidal neurons, while the remaining diazepam-sensitive subtypes (containing  $\alpha$ 1, 3 or  $\alpha$ 5 subunits) exerted a net inhibitory effect on distal dendritic sodium-calcium spike generation. To determine whether the spatial distribution of the receptors primarily influenced the direction of their effect, we directly applied GABA to dendrites and somata of layer V pyramidal neurons using focal iontophoresis (Figure 2.3 D).  $F_c$  was determined under control conditions and in the presence of GABA. Application of GABA at the soma resulted in an increase of  $F_c$  from 98 +/- 8.3 Hz to 109.2 +/- 9.9 Hz (n=7, p<0.01, paired t-test), while application of GABA to the distal dendrite reduced  $F_c$  from 91.4 +/- 8.2 Hz to 85.2 +/- 7.8 Hz (n=6, p<0.01, paired t-test; Figure 2.3 E&F). Thus the site of GABA<sub>A</sub> receptor activation determined their effect on dendritic excitability in line with the

previous finding that  $\alpha 2$  subunit containing receptors were responsible for the diazepam-mediated increase in dendritic excitability. We repeated these experiments forcing a depolarizing GABA<sub>A</sub> receptor reversal potential using 30 mM chloride in the recording pipette. Under these circumstances somatic GABA application did not significantly affect  $F_c$ , which decreased from 81.2 +/- 7.7 Hz to 79.4 +/- 8.8 Hz (n=5, p>0.1, paired t-test). Application of GABA to the dendrite under high chloride conditions produced a biphasic reaction. Immediately after establishing a whole-cell configuration, GABA iontophoresis decreased the  $F_c$  from 92.1 +/- 25 Hz to 80.8 +/- 23 Hz (n=4, p<0.05, paired t-test). After equilibration with the internal solution (>30 min), iontophoretic GABA application decreased dendritic excitability, with  $F_c$  increasing from 86.8 +/- 10.2 Hz to 95.5 +/- 10.9 (n=4, p<0.01, paired t-test; Figure 2.3 G). These findings further support the hypothesis that GABA<sub>A</sub> receptor-mediated dendritic hyperpolarization causes an increased propensity for dendritic sodium-calcium spike firing. Hyperpolarization-induced increases in calcium spiking are prominently observed in thalamic neurons and have been shown to depend on low-voltage activated calcium channels (Suzuki and Rogawski, 1989; Huguenard and McCormick, 1992). In a modeling study, the lowest threshold for action potential generation was found in a hyperpolarized region around membrane potentials of -80 to -70 mV (Destexhe and Sejnowski, 2002).

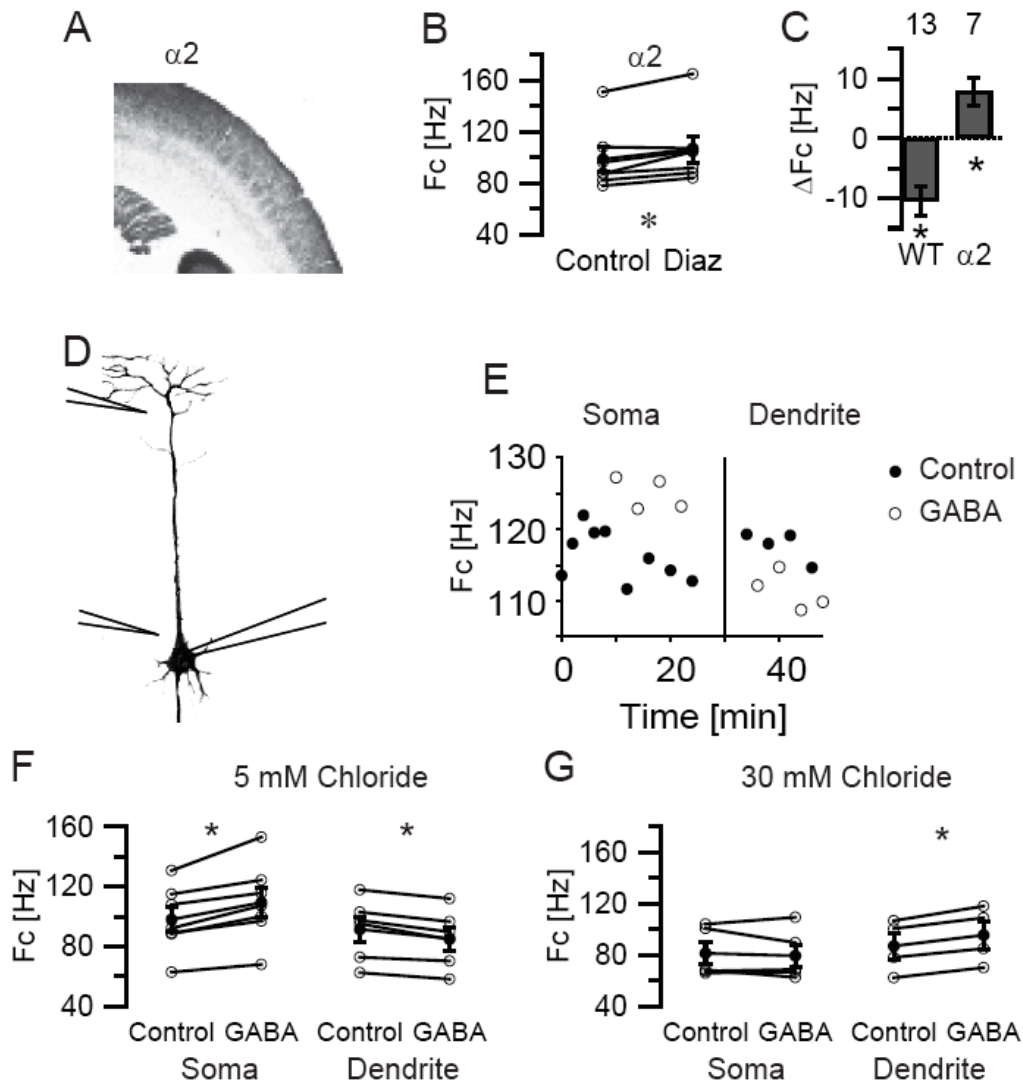


**Figure 2.3 . Dendritic, but not somatic GABA<sub>A</sub> receptor mediated hyperpolarization is responsible for the increased likelihood of dendritic calcium spikes. A)** Distribution of GABA<sub>A</sub> receptor  $\alpha 2$  subunits in the cortex revealed through antibody staining. Note the intense staining in the outer cortical layers. **B)**  $F_c$  in control conditions and in the presence of diazepam (1  $\mu$ M) in  $\alpha 2$  (H101R) point mutated mice in which alpha2 subunit containing GABA<sub>A</sub> receptors no longer react to diazepam. **C)** Comparison of the mean diazepam effect in wild-type and alpha2 subunit point mutated mice. **D)** Schematic drawing of the iontophoresis arrangement: layer V pyramidal cell with somatic patch electrode (right) and the two placement positions of the iontophoresis electrode (left). **E)**  $F_c$  over time during one iontophoresis experiment. Filled circles indicate control conditions open circles indicate the presence of iontophored GABA. The iontophoresis electrode was moved from the soma to the distal dendritic position at  $t=30$  min (vertical line). **F)** Summary for all the iontophoresis experiment in 5 mM Cl<sup>-</sup>. Open circles denote individual experiments filled circles show the mean values. Notice the opposite effect on  $F_c$  for somatic versus dendritic location in all experiments. **G)** The same data as in F, but with 30 mM Cl<sup>-</sup> in the patch pipette after >30 min equilibration. Note the reversal of the effects compared to 5 mM Cl<sup>-</sup>.



We applied nickel (Ni) at a concentration of 20  $\mu\text{M}$  selective for blocking low voltage-activated calcium channels of the CaV3.2 type (Kang et al., 2006).  $F_c$  was increased by the application of Ni from 80.5  $\pm$  6.8 Hz to 87.5  $\pm$  6.9 Hz ( $n=6$ ,  $p<0.01$ , paired t-test). Application of diazepam in the presence of Ni resulted in a further increase of  $F_c$  from 88.2  $\pm$  4.7 Hz to 91.7  $\pm$  4.5 Hz ( $n=5$ ,  $p<0.01$ , paired t-test; Figure 2.4 A&B). Thus Ni-sensitive channels were responsible for translating the hyperpolarizing action of GABA<sub>A</sub> receptors into increased dendritic excitability (Figure 2.4 C).

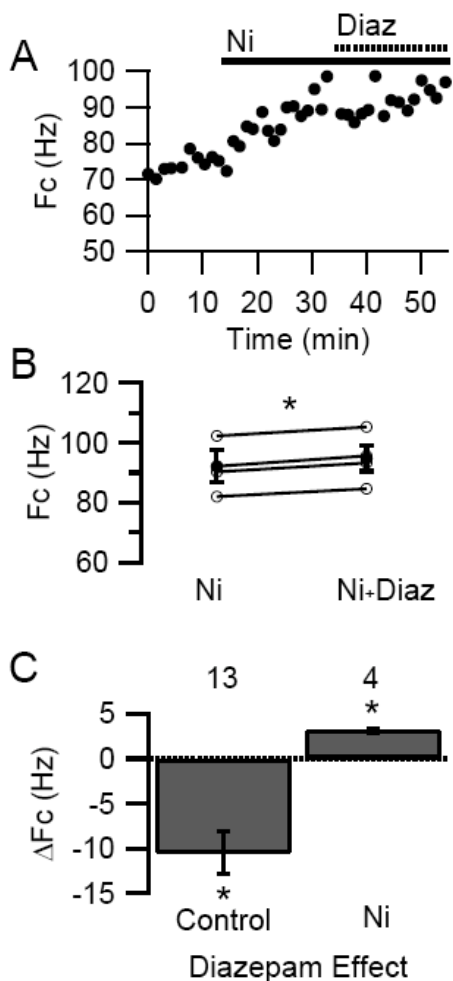


**Figure 2.4 . Nickel-sensitive (20  $\mu\text{M}$ ) calcium channels mediate the hyperpolarization-induced reduction in spike threshold. A)** Bath-application of Ni increases  $F_c$  and additional application of diazepam no longer causes a reduction of  $F_c$ . Plot of  $F_c$  over time with the application of the respective substances indicated by the horizontal bars. **B)**  $F_c$  in the presence of Ni and after application of diazepam, individual experiments (open circles) and average result (solid dots) are shown. **C)** Comparison of the average  $F_c$  reduction due to diazepam in control conditions and the diazepam-invoked increase of  $F_c$  in the presence of Ni.

What are the possible consequences of an increase in dendritic excitability? A number of groups have shown that pairing excitatory glutamatergic input with postsynaptic activity can lead to different outcomes, depending on the location of

the synaptic input and the amount of postsynaptic activation (Birtoli and Ulrich, 2004; Nevian and Sakmann, 2006). We paired excitatory postsynaptic potentials (EPSPs) evoked by extracellular stimulation of upper cortical layers with postsynaptic activity in layer V pyramidal neurons (Figure 2.5 A).  $F_c$  was determined for all cells; six cells were then paired with postsynaptic activity 20 Hz above  $F_c$  (Figure 2.5 C), seven cells with activity 20 Hz below  $F_c$  (Figure 2.5 D). Pairing protocols above threshold induced an increase in EPSP size, which did not reach significance. Pairing below the critical frequency induced a significant decrease in EPSP size 30 min after induction (Figure 2.5 D).

Taken together our results show an opposite effect of somatic and distal dendritic GABA<sub>A</sub> receptor activation on dendritic sodium-calcium spikes. A shift in the threshold for dendritic spikes had long-term consequences for neuronal signaling, due to their influence on synaptic plasticity.

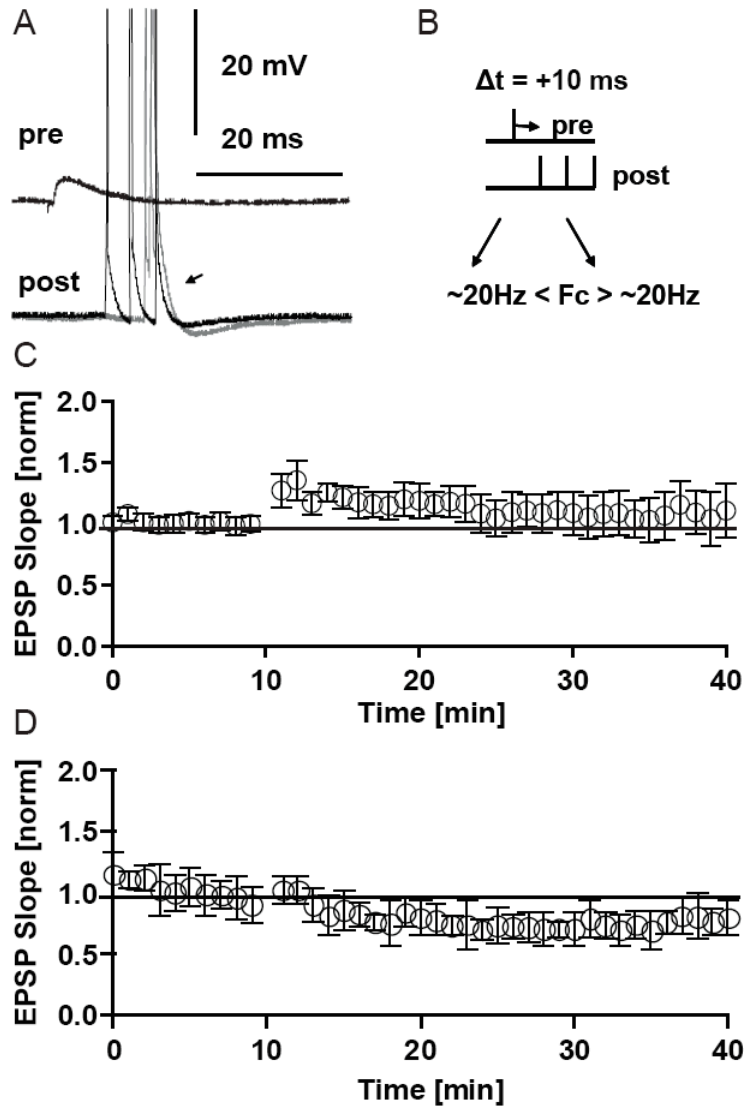


**Figure 2.5 . Dendritic calcium spike firing affects excitatory synaptic plasticity in a pairing protocol. A)** Pairing protocol: examples of an extracellularly evoked excitatory postsynaptic potential (EPSP) (top trace) and postsynaptic action potential (AP) burst (bottom traces). Subthreshold burst (black) and suprathreshold (grey) burst, with the calcium spike-induced afterdepolarisation (arrow). **B)** Schematic of the timing arrangement.  $F_c$  was determined individually for each neuron and the pairing burst then adjusted to 20 Hz above or below this value. **C)** Plot of EPSP initial slope versus time. Pairing was induced at  $t=10$  min. and the recoding continued for another 30 min. Pairing was done with a suprathreshold burst. **D)** Same plot as in C) but the pairing burst was subthreshold for distal dendritic calcium spikes.

## 2.5 Discussion

In this work we show a novel compartment-specific effect of GABA<sub>A</sub> receptor activation in cortical pyramidal neurons. The differential effect is not dependent on differences in chloride reversal potentials (Khirug et al., 2008), but rather on the presence of low-voltage activated calcium channels in dendrites (Johnston et al., 1996).

Morphological and functional compartmentalization of neurons greatly enhances their signaling repertoire. In cortical neurons, especially in layer V pyramidal neurons, apical distal dendrites are electrically remote from the soma. They perform local synaptic signal integration and produce distinctive sodium-calcium action potentials (Larkum et al., 1999 a). Both excitatory and inhibitory synaptic connections from different sources are targeted to different signaling compartments of layer V pyramidal neurons. The apical dendrite of layer V pyramidal cells is specifically targeted by GABAergic Martinotti and neurogliaform cells (Markram et al., 2004) and receives long-range associative input from other cortical areas and from the thalamus (Cauller et al., 1998).

We have found that the same GABAergic signal (Broser et al., 2008) can exert opposite effects on apical dendritic excitability, depending on the subcellular location of the involved GABA<sub>A</sub> receptors. This differential effect is due to the expression of Ni-sensitive calcium channels, predominantly found in the distal dendritic compartment (Markram et al., 1995; Williams and Stuart, 2002). Due to the dependency of the excitatory effect on hyperpolarizing chloride gradients and its Ni sensitivity the most likely candidates are (CaV3.2) T-type calcium channels. The facilitated excitability was also observed in the absence of excitatory synaptic transmission in the slice, indicating a direct effect on the pyramidal cell rather than a disinhibition of the network.

Elevated chloride concentrations in the patch pipette led to GABA<sub>A</sub> receptor-mediated decrease in dendritic excitability. The substantial delay with which this effect occurred indicates that the physiological effect of dendritic GABA<sub>A</sub> receptor activation is the initially observed increase in dendritic excitability. This is further

supported by the finding that distal dendrites are depolarized relative to the soma (Larkum et al., 1999 a), which will lead to reduced initial availability of low voltage-activated calcium channels and a larger hyperpolarizing driving force for dendritic compared to somatic GABA<sub>A</sub> receptors.

GABA<sub>A</sub> receptor activation leads inevitably to shunting and often to postsynaptic changes in the membrane potential. While shunting always inhibits spike generation, changes in the membrane potential can be excitatory or inhibitory. As we have shown, both hyper- and depolarizing responses can be excitatory or inhibitory, depending on the voltage-sensitive signaling mechanisms present in the compartment. Strong phasic inhibition has been shown to completely abolish dendritic sodium-calcium spikes (Perez-Garci et al., 2006) most likely due to strong shunting effects. As has been shown previously (Gulledge and Stuart, 2003), shunting is both of shorter duration and more localized than membrane potential changes. Therefore an inhibitory effect due to shunting can be 'surrounded' both spatially and temporally by an excitatory membrane potential change. Our experimental conditions mimicked slow and tonic GABAergic signals; under these conditions the excitatory effects of the membrane potential changes outweigh the inhibitory effects of shunting.

As we show here, changes in the calcium spike threshold can have long lasting effects on cortical networks. Previous reports have shown the strong sensitivity of pairing-induced synaptic plasticity on calcium spike generation. We have similarly found that modest changes in backpropagating AP bursts can alter the long-term consequence of pairing these bursts with incoming EPSPs.

Over the last few years a more and more dynamic picture of GABA<sub>A</sub> receptor signaling has emerged. Their activation may be excitatory or inhibitory depending on the developmental stage of a neuron and its dynamic chloride handling mechanisms. Recent evidence points to compartment-specific chloride homeostasis (Khirug et al., 2008). Here we show that different pyramidal cell compartments can react to the very same GABAergic signal in an opposite manner, adding to the signaling repertoire of these neurons. The highly specific

subcellular targeting by different interneurons thus significantly contributes to the diversity of their functional impact on pyramidal cell signaling.

## 2.6 References

**Birtoli B, Ulrich D** (2004) Firing mode-dependent synaptic plasticity in rat neocortical pyramidal neurons. *J Neurosci* 24:4935-4940.

**Broser P, Grinevich V, Osten P, Sakmann B, Wallace DJ** (2008) Critical period plasticity of axonal arbors of layer 2/3 pyramidal neurons in rat somatosensory cortex: layer-specific reduction of projections into deprived cortical columns. *Cerebral Cortex* 18:1588-1603.

**Cauler LJ, Clancy B, Connors BW** (1998) Backward cortical projections to primary somatosensory cortex in rats extend long horizontal axons in layer I. *J Comp Neurol* 390:297-310.

**Cauler LJ, Connors BW** (1994) Synaptic physiology of horizontal afferents to layer I in slices of rat SI neocortex. *J Neurosci* 14:751-762.

**Destexhe A, Sejnowski TJ** (2002) The initiation of bursts in thalamic neurons and the cortical control of thalamic sensitivity. *Philos Trans R Soc Lond B Biol Sci* 357:1649-1657.

**Feldman M** (1984) Morphology of the neocortical pyramidal neuron. In: *Cerebral Cortex* (Peters, A. and E.G., J., eds), pp 123-200 New York: Plenum Publishing Corporation.

**Fritschy JM, Mohler H** (1995) GABAA-receptor heterogeneity in the adult rat brain: differential regional and cellular distribution of seven major subunits. *J Comp Neurol* 359:154-194.

**Fritschy JM, Weinmann O, Wenzel A, Benke D** (1998) Synapse-specific localization of NMDA and GABA(A) receptor subunits revealed by antigen-retrieval immunohistochemistry. *J Comp Neurol* 390:194-210.

**Glickfeld LL, Roberts JD, Somogyi P, Scanziani M** (2009) Interneurons hyperpolarize pyramidal cells along their entire somatodendritic axis. *Nat Neurosci* 12:21-23.

**Gulledge AT, Stuart GJ** (2003) Excitatory actions of GABA in the cortex. *Neuron* 37:299-309.

**Hausser M, Spruston N, Stuart GJ** (2000) Diversity and dynamics of dendritic signaling. *Science* 290:739-744.

**Huguenard JR, Hamill OP, Prince DA** (1989) Sodium channels in dendrites of rat cortical pyramidal neurons. *Proc Natl Acad Sci U S A* 86:2473-2477.

**Huguenard JR, McCormick DA** (1992) Simulation of the currents involved in rhythmic oscillations in thalamic relay neurons. *J Neurophysiol* 68:1373-1383.

**Johnston D, Magee JC, Colbert CM, Christie BR** (1996) Active properties of neuronal dendrites. *Annu Rev Neurosci* 19:165-186.

**Kang HW, Park JY, Jeong SW, Kim JA, Moon HJ, Perez-Reyes E, Lee JH** (2006) A molecular determinant of nickel inhibition in Cav3.2 T-type calcium channels. *J Biol Chem* 281:4823-4830.

**Khirug S, Yamada J, Afzalov R, Voipio J, Khiroug L, Kaila K** (2008) GABAergic depolarization of the axon initial segment in cortical principal neurons is caused by the Na-K-2Cl cotransporter NKCC1. *J Neurosci* 28:4635-4639.

**Larkum ME, Kaiser KM, Sakmann B** (1999 a) Calcium electrogenesis in distal apical dendrites of layer 5 pyramidal cells at a critical frequency of back-propagating action potentials. *Proc Natl Acad Sci U S A* 96:14600-14604.

**Larkum ME, Zhu JJ, Sakmann B** (1999 b) A new cellular mechanism for coupling inputs arriving at different cortical layers. *Nature* 398:338-341.

**Loup F, Weinmann O, Yonekawa Y, Aguzzi A, Wieser HG, Fritschy JM** (1998) A highly sensitive immunofluorescence procedure for analyzing the subcellular distribution of GABA<sub>A</sub> receptor subunits in the human brain. *J Histochem Cytochem* 46:1129-1139.

**Löw K, Crestani F, Keist R, Benke D, Brünig I, Benson J, Fritschy J, Rülicke T, Bluethmann H, Möhler H, Rudolph U** (2000) Molecular and neuronal substrate for the selective attenuation of anxiety. *Science* 290:131-134.

**Markram H, Helm PJ, Sakmann B** (1995) Dendritic calcium transients evoked by single back-propagating action potentials in rat neocortical pyramidal neurons. *J Physiol* 485:1-20.

**Markram H, Sakmann B** (1994) Calcium transients in dendrites of neocortical neurons evoked by single subthreshold excitatory postsynaptic potentials via low-voltage-activated calcium channels. *Proc Natl Acad Sci U S A* 91:5207-5211.

**Markram H, Toledo-Rodriguez M, Wang Y, Gupta A, Silberberg G, Wu C** (2004) Interneurons of the neocortical inhibitory system. *Nat Rev Neurosci* 5:793-807.

**McBain CJ, Fisahn A** (2001) Interneurons unbound. *Nat Rev Neurosci* 2:11-23.

**McCormick DA** (1989) GABA as an inhibitory neurotransmitter in human cerebral cortex. *J Neurophysiol* 62:1018-1027.



**Nevian T, Sakmann B** (2006) Spine Ca<sup>2+</sup> signaling in spike-timing-dependent plasticity. *J Neurosci* 26:11001-11013.

**Paysan J, Kossel A, Bolz J, Fritschy JM** (1997) Area-specific regulation of gamma-aminobutyric acid type A receptor subtypes by thalamic afferents in developing rat neocortex. *Proc Natl Acad Sci U S A* 94:6995-7000.

**Perez-Garci E, Gassmann M, Bettler B, Larkum ME** (2006) The GABAB1b isoform mediates long-lasting inhibition of dendritic Ca<sup>2+</sup> spikes in layer 5 somatosensory pyramidal neurons. *Neuron* 50:603-616.

**Petilla Interneuron Nomenclature Group**, Ascoli GA, Alonso-Nanclares L, Anderson SA, Barrionuevo G, Benavides-Piccione R, Burkhalter A, Buzs, Buzsaki G, Cauli B, Defelipe J, Fair, n A, Feldmeyer D, Fishell G, Fregnac Y, Freund TF, Gardner D, Gardner EP, Goldberg JH, Helmstaedter M, Hestrin S, Karube F, Kisv, rday ZF, Lambolez B, Lewis DA, Marin O, Markram H, Munoz A, Packer A, Petersen CC, Rockland KS, Rossier J, Rudy B, Somogyi P, Staiger JF, Tamas G, Thomson AM, Toledo-Rodriguez M, Wang Y, West DC, Yuste R (2008) Petilla terminology: nomenclature of features of GABAergic interneurons of the cerebral cortex. *Nat Rev Neurosci* 9:557-568.

**Pouille F, Scanziani M** (2001) Enforcement of temporal fidelity in pyramidal cells by somatic feed-forward inhibition. *Science* 293:1159-1163.

**Schiller J, Schiller Y, Stuart G, Sakmann B** (1997) Calcium action potentials restricted to distal apical dendrites of rat neocortical pyramidal neurons. *J Physiol* 505:605-616.

**Sieghart W, Sperk G** (2002) Subunit composition, distribution and function of GABA(A) receptor subtypes. *Curr Top Med Chem* 2:795-816.

**Spruston N** (2008) Pyramidal neurons: dendritic structure and synaptic integration. *Nat Rev Neurosci* 9:206-221.

**Stuart GJ, Sakmann B** (1994) Active propagation of somatic action potentials into neocortical pyramidal cell dendrites. *Nature* 367:69-72.

**Suzuki S, Rogawski MA** (1989) T-type calcium channels mediate the transition between tonic and phasic firing in thalamic neurons. *Proc Natl Acad Sci U S A* 86:7228-7232.

**Szabadics J, Varga C, Molnar G, Olah S, Barzo F, Tamas G** (2006) Excitatory effect of GABAergic axo-axonic cells in cortical microcircuits. *Science* 311:233-235.

**Williams SR, Stuart GJ** (2002) Dependence of EPSP efficacy on synapse location in neocortical pyramidal neurons. *Science* 295:1907-1910.

**Yuste R, Gutnick MJ, Saar D, Delaney KR, Tank DW** (1994) Ca<sup>2+</sup> accumulations in dendrites of neocortical pyramidal neurons: an apical band and evidence for two functional compartments. *Neuron* 13:23-43.

**Yuste R, Tank DW** (1996) Dendritic integration in mammalian neurons, a century after Cajal. *Neuron* 16:701-716.

### **3 Manuscript II: Imaging Inhibitory Synaptic Potentials Using Voltage Sensitive Dyes**

**Marco Canepari,<sup>†Δ\*</sup> Silvia Willadt,<sup>†Δ</sup> Dejan Zecevic,<sup>‡</sup> and Kaspar E. Vogt<sup>†\*</sup>**

Status of publication: Submitted November 19, 2009, and accepted for publication January 15, 2010, Biophysical Journal.

† Division of Pharmacology and Neurobiology, Biozentrum-University of Basel, Basel, Switzerland; and ‡Department of Cellular and Molecular Physiology, Yale University School of Medicine, New Haven, Connecticut

Marco Canepari's present address is Research Group 3, Calcium Channels, Functions, and Pathologies, Unite´ Inserm 836, Grenoble Institute of Neuroscience, Site Sante´, BP 170, 38042 Grenoble cedex 09, France.

Δ Marco Canepari and Silvia Willadt contributed equally to this work.

\*Correspondence: marco.canepari@unibas.ch or kaspar.vogt@unibas.ch

Editor: Francisco Bezanilla.

My contribution was equally Marco Canepari's work in performing experimental design, procedure and analysis in all shown figures.

### **3.1 Abstract**

Studies of the spatio-temporal distribution of inhibitory postsynaptic potentials (IPSPs) in a neuron have been limited by the spatial information that can be obtained by electrode recordings. We describe a method that overcomes these limitations by imaging IPSPs with voltage-sensitive dyes. CA1 hippocampal pyramidal neurons from brain slices were loaded with the voltage-sensitive dye JPW-1114 from a somatic patch electrode in whole-cell configuration. After removal of the patch electrode, we found that neurons recover their physiological intracellular chloride concentration. Using an improved voltage-imaging technique, dendritic GABAergic IPSPs as small as 1 mV could be resolved optically from multiple sites with spatial averaging. We analyzed the sensitivity of the technique, in relation to its spatial resolution. We monitored the origin and the spread of IPSPs originating in different areas of the apical dendrite and reconstructed their spatial distribution. We achieved a clear discrimination of IPSPs from the dendrites and from the axon. This study indicates that voltage imaging is a uniquely suited approach for the investigation of several fundamental aspects of inhibitory synaptic transmission that require spatial information.

## 3.2 Introduction

Fast inhibitory synapses use chloride ( $\text{Cl}^-$ ) permeable channels to generate inhibitory postsynaptic potentials (IPSPs) in different regions of the postsynaptic neuron (Somogyi and Klausberger, 2005). These signals, from different classes of interneurons, play various functional roles in the brain (Mody and Pearce, 2004). The analysis of the spatial and temporal distribution of IPSPs in neuronal processes is therefore critical to understanding the mechanisms of inhibition.

To carry out this analysis, one must measure IPSP signals from processes of individual neurons at high spatial resolution and under minimal perturbation of the intracellular  $\text{Cl}^-$ -concentration ( $[\text{Cl}^-]_i$ ). Whereas standard electrode measurements do not provide adequate spatial resolution and also interfere with  $[\text{Cl}^-]_i$ , it became possible recently to successfully carry out multisite optical measurements of relatively large subthreshold excitatory synaptic potentials using voltage sensitive dyes and signal averaging (Djurisic et al., 2004).

In recording optically membrane potential signals from processes of individual neurons, the required sensitivity could be achieved only if single cells were stained selectively by diffusion of a voltage-sensitive dye from a patch electrode. The major challenge in extending this approach to the study of synaptic inhibition was to advance the sensitivity of recording to a level that would allow monitoring small amplitude IPSPs at the required spatial resolution. This critical improvement has been achieved by using single wavelength laser excitation at 532 nm in epi-illumination, wide-field microscopy mode.

### **3.3 Materials and Methods**

#### **3.3.1 Slice preparation and electrophysiology**

Experiments, approved by Basel cantonal authorities, were done in 250  $\mu\text{m}$  thick transversal slices of the hippocampus from 24–32 days old mice (C57BL/6), decapitated after isoflurane anesthesia (according to the Swiss regulation). Slices were prepared in ice-cold solution using a HM 650 V vibroslicer (Microm, Volketswil, Switzerland), incubated at 35°C for 40 min and maintained at room temperature. The solution used for slicing was the modified recording extracellular solution with reduced  $\text{CaCl}_2$  concentration (0.5 mM instead of 2 mM). Somatic whole-cell recordings were done using a Multiclamp 700A amplifier (Axon Instruments) and an upright microscope (Olympus BX51-WI). The recording extracellular solution contained (in mM): 125 NaCl, 26  $\text{NaHCO}_3$ , 20 glucose, 3 KCl, 1  $\text{NaH}_2\text{PO}_4$ , 2  $\text{CaCl}_2$ , and 1  $\text{MgCl}_2$ , pH 7.4 when bubbled with a gas mixture containing 95%  $\text{O}_2$ , 5%  $\text{CO}_2$ . The basic intracellular solution contained (in mM): 5 Na-ATP, 0.3 Tris-GTP, 14 Tris-phosphocreatine, 20 HEPES, and either 125  $\text{KMeSO}_4$ , 5 KCl, or 90  $\text{KMeSO}_4$ , 40 KCl. Solutions were adjusted to pH 7.35 with potassium hydroxide. During whole-cell recordings, the real membrane potential was estimated after correcting for the junction potential (-11.0 mV for the 5 mM  $\text{Cl}^-$  and -9.4 mV for the 40 mM  $\text{Cl}^-$  intracellular solution calculated using JPCalc software; Barry, 1994). Local stimulation of presynaptic fibers was carried out with patch pipettes filled with extracellular solution positioned under transmitted light using hydraulic manipulators (Narishige, Tokyo, Japan). Somatic electrode recordings were acquired at 16 kHz and filtered at 4 kHz using the A/D board of the Redshirt imaging system.

#### **3.3.2 Neuronal loading**

Individual neurons were loaded with the voltage sensitive dye JPW-1114 (0.2–0.5 mg/mL) as described previously (Canepari et al., 2007; 2008). The dye was purchased from Molecular Probes-Invitrogen (Carlsbad, CA). Intracellular

staining was accomplished by free diffusion of the dye from a patch-electrode. To avoid extracellular deposition of the dye and the resulting large background fluorescence, the tip of the electrode was filled with dye-free solution and the positive pressure was kept at the minimum before reaching the cell. For this study, we used 4–5 M $\Omega$  electrodes obtained by pulling borosilicate pipettes with 1.5 mm external diameter and 1.17 mm internal diameter without filament to a tip diameter of  $\sim$ 1  $\mu$ m. We back-filled the tip of these electrodes with dye free solution using negative pressure from a 10 mL syringe for 10–20 s and we applied a positive pressure of  $\sim$ 30 mbar for  $\sim$ 10 s as measured with a manometer (Model 840081; Sper Scientific, Scottsdale, AZ) while approaching the cell in the slice. The patch electrode used for dye loading was attached to the neuron in whole-cell configuration for 25–30 min. The amount of staining was determined by measuring the resting fluorescence from the cell body at reduced excitation light intensity ( $\sim$ 0.1 % of the laser light). The staining did not cause pharmacological effects (Antic et al., 1999; Palmer and Stuart, 2006; Canepari et al., 2007; 2008). After loading was completed, the patch electrode was carefully detached from the cell by forming an outside-out patch. In the experiments where we needed to carry out measurements during the loading process the temperature was set to 32–34°C. Otherwise, loading at room temperature (24°C) resulted in better preservation of neurons in experiments that lasted for  $>$ 2 h after loading termination.

### **3.3.3 Optical recording**

Optical recordings were carried out by exciting the voltage-sensitive fluorescence with a 532 nm-300 mW solid state laser (model MLL532; CNI, Changchun, China). The laser beam was directed to a light guide coupled to the microscope via a single-port epifluorescence condenser (TILL Photonics GmbH; Gräfelfing, Germany) designed to overfill the back aperture of the objective. In this way, near uniform illumination of the object plane was attained. The signal-to-noise ratio (S/N) in light intensity measurement is a linear function of the product of the

relative fluorescence change ( $\Delta F/F$ ) in response to membrane potential changes and the square root of the resting fluorescence light intensity. Thus, compared to previous studies using the light from a xenon lamp filtered by a bandpass interference filter ( $525 \pm 25$  nm) (Canepari et al., 2007; 2008), laser excitation improved the sensitivity of recordings, in terms of S/N in two ways. First, the  $\Delta F/F$  for a given change in membrane potential is  $\sim 2.5$  times larger with the laser than with the lamp (see Supporting Material). Second, the excitation light intensity provided by the laser (as measured with a power meter from LaserCheck, Coherent, Santa Clara, CA) was  $>10$  times higher than the excitation light intensity from the arc-lamp. In the shot-noise limited measurements, the higher excitation light intensity improves the S/N but also increases the probability of photodynamic damage. We kept the photodynamic damage under control by limiting the light intensity and the exposure time. We established that 6–12.5 % of the full laser light output was sufficient to resolve  $\text{Cl}^-$ -mediated synaptic potentials at 500 Hz. At this light level, it was possible to obtain 40–80 intermittent recording trials of 100 ms, separated by 30-s dark periods between consecutive exposures. In some measurements, we recorded action potentials and synaptic potentials at the frame rate of 2 kHz, using 25 % full laser light output and 50 ms intermittent exposures separated by 1-min dark periods between consecutive exposures. In imaging action potentials signals in the axon at the frame rate of 10 kHz, we used the full laser light output and 25-ms exposures with 1-min dark periods between consecutive exposures. In experiments using 25–100 % of the laser light, we limited the number of recording trials to the maximum of 10 to avoid possible phototoxic effects. Under these conditions, repetitive light exposures did not cause any detectable change in the kinetics of the action potential recorded electrically from the soma and optically from the dendrite (see Supporting Material). Optical signals were captured with a high-speed, 80 x 80 pixels CCD camera NeuroCCD-SM (RedShirtImaging LLC, Decatur, GA). The excitation light was directed to a water immersion objective, either Olympus 60x/1.1 NA or Nikon 60x/1 NA (Olympus, Tokyo, Japan). The fluorescent image of the cell was projected via a 0.25x or a 0.1x optical coupler onto the CCD camera. Depending



on optical magnification, the imaged field in our measurements was either  $\sim 125 \mu\text{m} \times 125 \mu\text{m}$  or  $\sim 300 \mu\text{m} \times 300 \mu\text{m}$ . The excitation light was directed to the preparation using a 570 nm dichroic mirror and the emission light was filtered with a 610 nm long-pass filter. Optical and electrophysiological recordings were done at 32–34°C. Recordings at frame rates of 0.5–2 kHz were done at full-frame readout (80 x 80 pixels). Recordings at 10 kHz were done at partial readout (80 x 12 pixels). Optical signals corresponding to GABAergic synaptic potentials were typically averages of 4–16 trials. Optical signals corresponding to action potentials were either single recording trials or averages of four trials.

### **3.3.4 Anatomical reconstruction and data analysis**

Anatomical reconstruction of neurons was carried out from a stack of two-photon excitation fluorescence images obtained using a tuneable, mode-locked titan-sapphire laser (MaiTai HP, Spectra Physics, Germany) set to 850 nm and a laser scanning system (FV300, Olympus Switzerland) with a high-aperture 20x water-immersion lens (Olympus LUMPLAN 20x). Images and electrophysiological recordings were analyzed with dedicated software written in MATLAB (The MathWorks, Natick, MA). Optical signals were analyzed as fractional changes of fluorescence ( $\Delta F/F$ ). In this analysis, the  $\Delta F/F$  decrease due to bleach was subtracted using one-exponential fits of trials without electrical stimulation. Results from t-tests were considered significantly different for  $p < 0.01$ . Supporting movies were done using Windows Movie Maker.

## 3.4 Results

### 3.4.1 Staining procedure and IPSP optical recordings

Individual CA1 hippocampal pyramidal neurons from mouse brain slices were loaded with the voltage sensitive dye JPW-1114 by diffusion from a patch-electrode as described previously (Canepari et al., 2007; 2008). IPSPs were evoked by extracellular stimulation (5–20  $\mu$ A, 100 ms duration) of presynaptic axons in the presence of AMPA receptor antagonist NBQX (10  $\mu$ M) and NMDA receptor antagonist D-AP5 (50  $\mu$ M). The polarity of an IPSP is determined by the  $\text{Cl}^-$  reversal potential ( $V_{\text{Cl}}$ ) as described by the Nernst equation:

$$V_{\text{Cl}} = RT \times \log([\text{Cl}^-]_i/[\text{Cl}^-]_o)/F \quad (1)$$

where  $[\text{Cl}^-]_i$  and  $[\text{Cl}^-]_o$  are the intracellular and extracellular  $\text{Cl}^-$ -concentrations,  $R$  is the thermodynamic gas constant,  $T$  is the temperature, and  $F$  is the Faraday constant. Because the whole-cell recording involves dialysis of the cytoplasm with the solution in the patch pipette, the  $[\text{Cl}^-]_i$  shifts toward the  $\text{Cl}^-$ -concentration of the patch pipette. We used intracellular solutions containing either 40 or 5 mM  $\text{Cl}^-$ .

In the experiment shown in Figure 3.1 (A) the cell was loaded with the voltage-sensitive dye from the patch electrode with the intracellular solution containing 40 mM  $\text{Cl}^-$ , leading to  $V_{\text{Cl}} \approx -31$  mV. Thus, the  $\text{Cl}^-$ -mediated synaptic potential evoked at the baseline potential of -84 mV and recorded with the somatic electrode during the loading period had large positive polarity (Figure 3.1 A, top trace). Noticeably, the polarity of the  $\text{Cl}^-$ -mediated synaptic potential was positive within seconds after establishing the whole-cell configuration. After the electrode was removed, the cell was left undisturbed for 30–60 min to allow for the diffusion of the dye into distal dendrites and possible  $[\text{Cl}^-]_i$  re-equilibration.

After this period, we recorded optically from the dendritic branches contained within an area of  $\sim 125 \mu\text{m} \times 125 \mu\text{m}$  (Figure 3.1 A). The  $\text{Cl}^-$ -mediated synaptic potential evoked by a  $\sim 10 \mu\text{A}$  stimulus and recorded optically as the spatial

average from all dendritic branches had negative polarity (Figure 3.1 A, middle left trace), suggesting substantial reduction of the  $[Cl^-]_i$  after resealing of the neuron. To test for the stability of the resting membrane potential and the overall health of the cell, we repatched it with the same 40 mM  $Cl^-$  containing intracellular solution without the dye. Application of the same stimulus evoked a synaptic potential, recorded optically from the dendrites and electrically from the soma, which, again, had positive polarity (Figure 3.1 A, bottom left trace).

To confirm that the electrically and optically recorded synaptic potentials were mediated by  $GABA_A$  receptors, somatic synaptic potentials were recorded with the patch electrode whereas the proximal part of the dendrite was monitored optically. In these recordings, made ~20 min after the start of the staining procedure, both the electrical and the optical synaptic potentials signals were blocked by addition of 20  $\mu$ M of the  $GABA_A$  receptor antagonist bicuculline (Figure 3.1 B, top traces). After electrode removal, bicuculline was washed out and the hyperpolarizing signal was recorded optically and blocked again in bicuculline solution (Figure 3.1 B, bottom traces). The summary result from five experiments (Figure 3.1 B, graph) shows that bicuculline effects were robust and statistically significant ( $p < 0.01$  paired t-test).

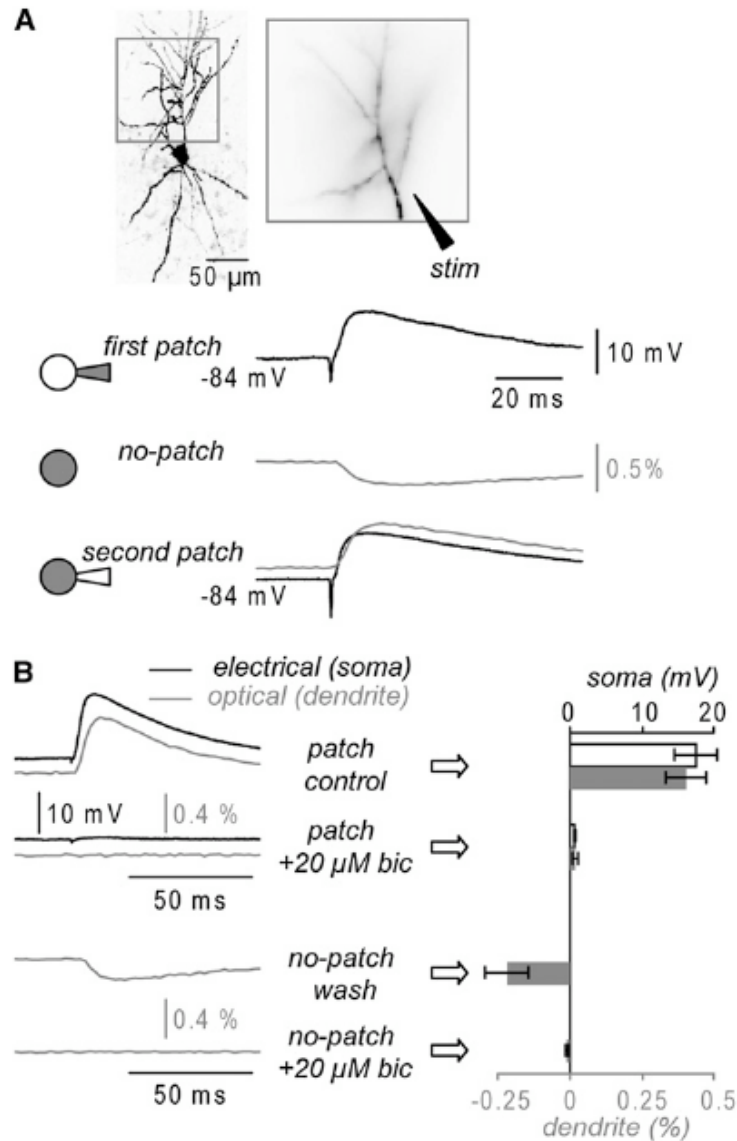


**Figure 3.1 . Optical measurements of GABA-mediated synaptic potentials. (A)** (Top) Fluorescence image of a CA1 hippocampal pyramidal neuron (left). Dendritic region in recording position (right). (Upper trace) Electrical somatic recording (black) of a depolarizing evoked synaptic potential during dye loading with 40 mM  $\text{Cl}^-$  internal solution (first patch). (Middle trace) Hyperpolarizing synaptic potential evoked by the same stimulus and recorded optically as spatial average from all dendrites after electrode removal (no-patch). (Bottom trace) Superimposed electrical somatic (black) and optical dendritic (gray) recordings of the synaptic potential after repatch with an electrode containing 40 mM  $\text{Cl}^-$  (second patch). Synaptic potentials are averages of nine trials. **(B)** (Left/top) Electrical (black) and optical (gray) dendritic synaptic potential recordings during loading (40 mM  $\text{Cl}^-$ ) before and after addition of 20 mM bicuculline. (Left/bottom) optical dendritic recordings 30 min after patch termination and bicuculline washout before (upper trace) and after (lower trace) reapplication of bicuculline. (Right/ top) Synaptic potential peak amplitude (mean  $\pm$  SD; n = 5 cells) for electrical (white) and optical (gray) signals during loading before and after addition of 20 mM bicuculline. (Right/bottom) Optical synaptic potential signal peak amplitude (mean  $\pm$  SD; n = 5 cells) after electrode removal before and after addition of bicuculline. Effects statistically significant ( $p < 0.01$ , paired t-test).

### **3.4.2 Estimate of intracellular Cl<sup>-</sup> concentration ([Cl<sup>-</sup>]<sub>i</sub>) without use of electrodes**

A critical requirement in studying synaptic inhibition is the preservation of the physiological gradient of Cl<sup>-</sup>. The substantial hyperpolarizing shift after resealing observed in experiments with high Cl<sup>-</sup> internal solutions indicates that the cells can restore a physiological Cl<sup>-</sup> homeostasis in a surprisingly short time. Our experiments therefore can provide not only a measurement of GABAergic potentials under physiological conditions, but also the direct measurement of the physiological [Cl<sup>-</sup>]<sub>i</sub> in the neuron. Thus, in a series of experiments, we investigated the effect of the staining protocol on the [Cl<sup>-</sup>]<sub>i</sub> in more detail. The change in the [Cl<sup>-</sup>]<sub>i</sub> after establishing the whole cell is very quick and we could not obtain a reliable estimate of the [Cl<sup>-</sup>]<sub>i</sub> from patch electrode measurements. Instead, we estimated the [Cl<sup>-</sup>]<sub>i</sub> without the use of electrodes with the procedure illustrated in Figure 3.2 In the experiment shown in Figure 3.2 (A), the neuron was loaded with the voltage sensitive dye from an electrode containing 40 mM Cl<sup>-</sup>. After the electrode was removed, the cell was left undisturbed for 30 min to allow the diffusion of the dye into distal dendrites. We then optically recorded dendritic signals in response to extracellular stimulation, in the presence of glutamate receptor antagonists, at two different intensities. The weak stimulus (s1; 10 μA), evoked a hyperpolarizing synaptic potential signal as shown in Figure 3.2 (B; left trace). The strong stimulus (s2; ~100 μA), excited the cell directly eliciting an action potential that was also recorded optically from the same dendritic area (Figure 3.2 B, right traces). The evidence that an action potential could be evoked indicated that the resting membrane potential ( $V_{rest}$ ) was below the firing threshold. Thus, a hyperpolarizing synaptic potential indicated that the corresponding [Cl<sup>-</sup>]<sub>i</sub> after the recovery period was much lower than the [Cl<sup>-</sup>]<sub>i</sub> during dye-loading. After these measurements, the neuron was repatched with the dye-free electrode containing 40 mM Cl<sup>-</sup> and the following sequence of measurements was carried out.

1. We estimated  $V_{Cl}$  for the cell dialyzed with 40 mM  $Cl^-$  solution ( $V_{Cl}(40\text{ mM})$ ) by linearly fitting the amplitude of the synaptic currents measured under voltage clamp at different holding potentials (Figure 3.2 C, left traces, fit not shown).
2. In current clamp configuration, the baseline membrane potential (BP) was set to a desired value, (-84 mV in the experiment shown in Figure 3.2 C) and a synaptic potential was evoked by a weak stimulus (s1) and optically recorded from the dendritic area indicated in Figure 3.2 (A).
3. In current clamp configuration, an action potential, evoked at BP levels using the strong extracellular stimulation (s2) was recorded optically from the same dendritic area. The amplitude of the optically recorded spike varied predictably as a function of BP (Figure 3.2 C; top right traces) and, thus, could be used to estimate  $V_{rest}$  from optical recordings of spike signal amplitude in cells without an intracellular electrode.

The membrane potential transient ( $\Delta V_m$ ) corresponding to  $Cl^-$ -mediated synaptic potential in an intact neuron is proportional to the driving force for  $Cl^-$  and can be expressed as

$$\Delta V_m (1) = \sigma \times (V_{Cl} - V_{rest}), (2)$$

where  $\sigma$  is a constant and  $V_{Cl}$  is unknown. If the neuron is dialyzed from the patch pipette, the  $[Cl^-]_i$  and the  $V_{Cl}$  are known and the expression becomes

$$\Delta V_m (2) = \sigma \times (V_{Cl}(40\text{ mM})-BP), (3)$$

Thus, the estimate of  $V_{Cl}$  and of the corresponding  $[Cl^-]_i$  can be obtained from the ratio of Equation 2 and 3 without a need for intracellular electrode. This estimate

is accurate under the assumption that  $[Cl^-]_i$  is uniform over the part of the neuron where the optical signal is spatially averaged. In the example of Figure 3.2 (A–C) the estimate of  $[Cl^-]_i$  was 30.68 mM with the patch electrode attached and 3.42 mM without patch electrode. In seven cells loaded with an internal solution containing 40 mM  $Cl^-$ , the estimated intracellular  $Cl^-$  concentration was  $32.6 \pm 6.8$  mM (mean  $\pm$  SD) with the patch electrode attached and  $3.90 \pm 1.15$  mM without the patch electrode. To assess whether this value was independent of the  $Cl^-$  concentration in the loading patch pipette, we repeated the same experiment using an internal solution containing 5 mM  $Cl^-$ . The same sequence of measurements, as carried out for internal solution containing 40 mM  $Cl^-$  (Figure 3.2 A–C), is illustrated in Figure 3.2 (D–F). In six cells we found that  $[Cl^-]_i$  was  $5.33 \pm 0.37$  mM with the patch electrode attached and  $4.55 \pm 1.40$  mM without patch electrode (Figure 3.2 G and H). The summary data showed that the values of  $[Cl^-]_i$  in neurons without attached patch electrode, obtained after dye-loading using an internal solution containing either 40 mM or 5 mM  $Cl^-$ , were not different ( $p > 0.1$ , two populations t-test). The results show that neurons restored their physiological  $[Cl^-]_i$  after dye loading from the patch pipette and that voltage imaging can be used to estimate this important biophysical parameter.

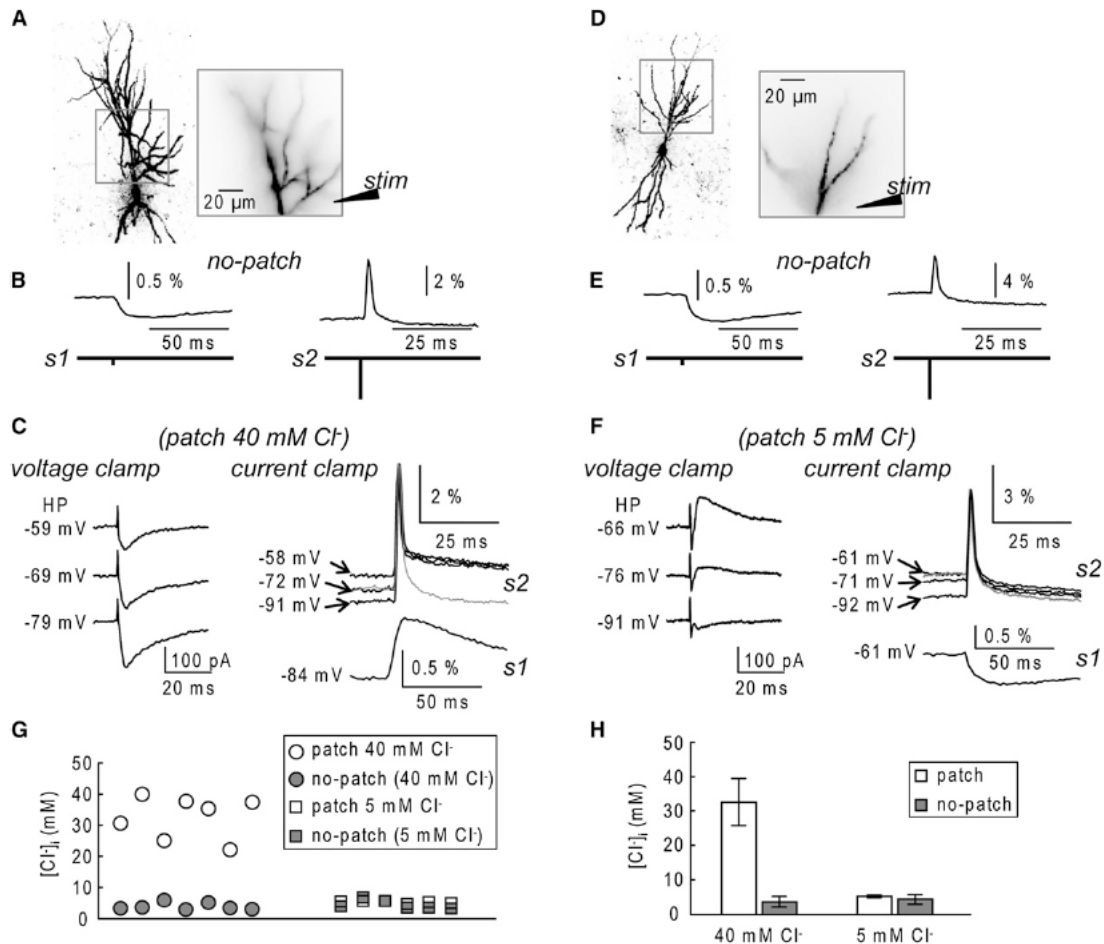


**Figure 3.2 . Optically recorded  $\text{Cl}^-$ -mediated synaptic potentials are independent of the  $\text{Cl}^-$  concentration in the patch pipette used for dye loading.** (A) (Left) Fluorescence image of a CA1 hippocampal pyramidal neuron: intracellular solution for dye loading contained 40 mM  $\text{Cl}^-$ . (Right) Dendritic region in recording position ( $\sim 125 \mu\text{m} \times 125 \mu\text{m}$ , apical dendrite). (B) (Left)  $\text{Cl}^-$ -mediated synaptic potential in response to low-intensity (s1) stimulation recorded optically (average of nine trials) after patch termination and after cell recovery obtained as the spatial average from all dendritic branches. (Right) Action potential signal evoked by high-intensity (s2) stimulation and recorded from the same area as the IPSP signal. (C) (Left) Synaptic currents under voltage-clamp obtained at different holding potentials during second recording with 40 mM  $\text{Cl}^-$  internal solution. (Right) Optical recording of membrane potential signals under current-clamp conditions after s2 and s1 stimulations (second patch-electrode recording). (Upper traces) Action potential signals evoked at different baseline potentials. Gray trace is the action potential signal recorded before the patch-pipette was attached; estimated  $V_{\text{rest}}$  in B = -72 mV. (Lower trace) Response to s1 stimulations evoked at a baseline membrane potential of -84 mV. (D–F) Same as A–C for a cell dialyzed from an electrode with 5 mM  $\text{Cl}^-$  intracellular solution; estimated  $V_{\text{rest}}$  in E = -61 mV. (G) Estimates of  $[\text{Cl}^-]_i$  plotted for neurons dialyzed from patch electrode containing 40 mM  $\text{Cl}^-$  ( $n = 7$ ) and 5 mM  $\text{Cl}^-$  ( $n = 6$ ). The values obtained after recovery period after patch-electrode removal are included. (H) Summary result (mean  $\pm$  SD) for the data shown in G; The  $[\text{Cl}^-]_i$  after recovery period for two groups did not differ significantly ( $p \pm 0.38$ , two-populations t-test).

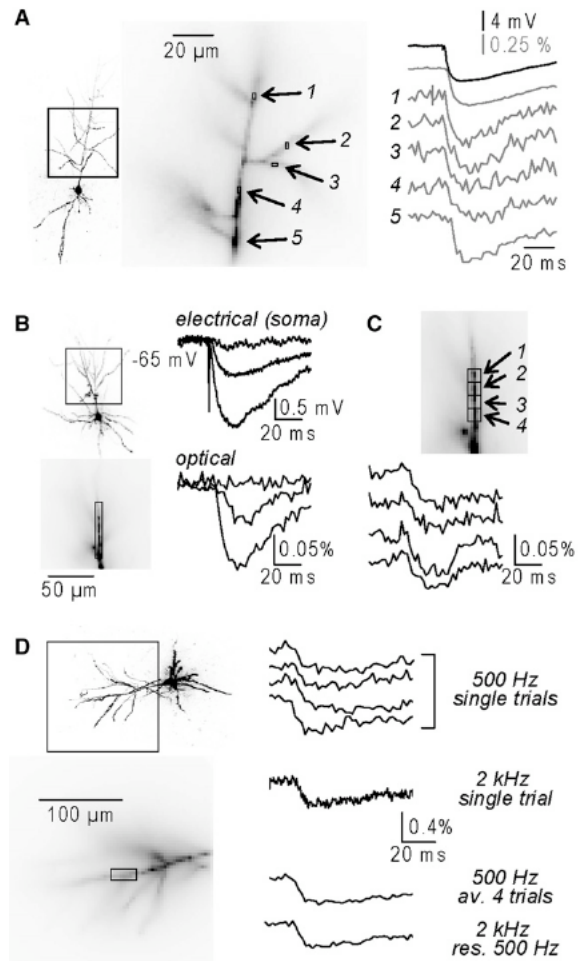


### **3.4.3 Resolution of optical IPSP measurements**

The excellent S/N in the recordings shown in Figure 3.1 and Figure 3.2 is typical for ~10 mV synaptic potential signals averaged spatially over large portions of the dendritic arbor and further improved by temporal averaging of nine trials. For signals of this size, however, it was possible to obtain adequate S/N by averaging signals over 2–4 pixels, with a pixel size of 1.56 x 1.56  $\mu\text{m}$ . In the example shown in Figure 3.3 (A),  $\Delta F/F$  signals from regions 1–5 associated with an IPSP of ~8 mV are reported. Each region is formed by two pixels and the signals were obtained by averaging nine trials. IPSPs of 5–10 mV in amplitude shown above are typically associated with stimulation of more than one interneuron under physiological  $[\text{Cl}]_i$ . IPSPs of smaller amplitude, evoked by the stimulation of a single interneuron (unitary IPSPs), are still resolvable under our experimental conditions, but at a lower spatial resolution. The fluorescence intensity traces in Figure 3.3 (B; bottom traces) are averages of 16 trials from a set of pixels covering a length of ~75  $\mu\text{m}$  of the apical dendrite (Figure 3.3 B, bottom image).

**Figure 3.3 . Spatial resolution and sensitivity.**

**(A)** Fluorescence image of a neuron (left) and dendritic region in recording position (middle); regions 1–5 are  $\sim 1.56 \text{ mm} \times 3.12 \text{ mm}$  (2 pixels). (Right) Electrical somatic recording (black trace) and optical dendritic recordings (gray) of an IPSP  $\sim 8 \text{ mV}$  in amplitude from regions 1–5. Signals are averages of nine trials. **(B)** (Left) Image of a neuron (top) and apical dendrite in recording position (bottom);  $\sim 75 \text{ mm}$  long region of interest outlined. Right: electrical somatic recordings (top) and optical recording from the region of interest (bottom) of IPSPs ( $[\text{Cl}^-]_i \sim 5 \text{ mM}$ ) in response to three stimulus intensities (4  $\mu\text{A}$ , 5  $\mu\text{A}$ , and 10  $\mu\text{A}$ ). Signals are averages of 16 trials. Four  $\mu\text{A}$  stimulation fails to evoke an IPSP. Stimulations of 5  $\mu\text{A}$  and 10  $\mu\text{A}$  evoke IPSPs of  $\sim 800 \text{ }\mu\text{V}$  and  $\sim 2 \text{ mV}$  in amplitude respectively. **(C)** Optical recording of the  $\sim 800 \text{ }\mu\text{V}$  IPSP in B from the  $\sim 6.5 \text{ mm}$  long regions of interest 1–4. **(D)** (Left) Image of a neuron (top) and an apical dendrite in recording position (bottom); one region of interest indicated. (Right) Optical recordings from the region of interest; (top traces) four single trials recorded at 500 Hz at 6 % of the laser power; (middle trace) a single trial recorded at 2 kHz at 25 % of the laser power; (bottom traces) the average of the four trials at 500 Hz and the trial at 2 kHz resampled at 500 Hz.



The neuron was patched with an electrode containing 5 mM  $\text{Cl}^-$  internal solution, approaching the physiological condition, so that the amplitude of the optically recorded IPSP in the very proximal dendrite could be calibrated using the electrical recording from the soma (Figure 3.3 B, top traces). Three different stimulation intensities were tested. The weakest intensity failed to evoke an IPSP. The two higher intensities evoked IPSPs of  $\sim 800 \text{ }\mu\text{V}$  and  $\sim 2 \text{ mV}$  respectively. The results showed clearly that an IPSP of  $< 1 \text{ mV}$  in amplitude can be resolved at this spatial resolution (Figure 3.3 B, bottom traces). The same signal could be still detected, but with a worse S/N, from regions 1–4, covering lengths of  $\sim 6.5 \text{ }\mu\text{m}$  (Figure 3.3 C). In summary, by averaging 9–16 recordings, IPSPs of 1–2 mV and 5–10 mV can be reliably resolved with a spatial resolution of  $\sim 50 \text{ }\mu\text{m}$  and  $\sim 2 \text{ }\mu\text{m}$ , respectively. The experiments shown above were carried

out by illuminating the preparation with 6–12.5 % of the total power of the laser. The S/N can be further improved by increasing the intensity of illumination while increasing the frame rate to avoid saturation of the CCD. In the experiments Figure 3.3 (D), IPSPs at a given stimulation intensity were first recorded at 500 Hz using 6 % of the laser power and at 2 kHz using 25 % of the laser power. Top traces in Figure 3.3 (D) are  $\Delta F/F$  signals, from the dendritic region indicated in the bottom image, corresponding to four trials recorded at a frame rate of 500 Hz and one trial recorded at a frame rate of 2 kHz. The average of four trials at 500 Hz has a S/N comparable to the single trial at 2 kHz resampled at 500 Hz (Figure 3.3 D). The advantage of increasing the S/N by increasing the light is however counterbalanced by the increased photodynamic damage. Thus, fewer recordings can be done at stronger illumination intensity. As shown in the Supporting Material (Manuscript II), the use of moderate illumination intensity (6–12.5 %) allows for >40 recordings with no detectable photodynamic damage. The increased illumination is therefore especially advantageous in applications that require very short recording periods and few recordings.

#### **3.4.4 Spatial distribution of IPSPs from different classes of interneurons**

In the next series of experiments we compared the spatial distribution of IPSP signals evoked by localized electrical stimulation in different areas of the hippocampus. One stimulating electrode was positioned near the proximal part of the apical dendrite in the stratum pyramidale or in the stratum radiatum and another stimulating electrode in the stratum lacunosum-moleculare, at a distance of ~300  $\mu\text{m}$  from the soma. As predicted from morphological data, these two stimulations are likely to excite different subpopulations of interneurons (Vida et al., 1998; Price et al., 2005; Buhl et al., 1994; Fuentealba et al., 2008). Indeed, stimulation in the stratum lacunosum-moleculare is likely to excite a subpopulation of interneurons that target pyramidal neurons distally from the soma whereas stimulation in the stratum pyramidale or in the stratum radiatum may excite cells that form contacts in different areas of the postsynaptic neuron

(Klausberger and Somogyi, 2008). To compare IPSP signals from distal and proximal areas of the dendrite, we recorded from the larger field of view corresponding to the area of  $\sim 300 \mu\text{m} \times 300 \mu\text{m}$  in the object plane.

In the experiment shown in Figure 3.4 A and B, the stimulating electrodes were positioned near the proximal part of the apical dendrite (prox) and distally, in the stratum lacunosum-moleculare (dist). The signals from three subcellular regions (Figure 3.4 A, top right, locations 1–3), generated in response to extracellular stimulation via the two electrodes were analyzed and compared. In region 1 (distal area of the apical dendrite) the IPSP signal associated with distal stimulation was larger and with a faster rise than the IPSP signal associated with proximal stimulation (Figure 3.4 A, traces). In contrast, in region 3 (proximal oblique dendrite) the IPSP signal was larger and with a faster rise for proximal stimulation than for distal stimulation. The two signals were nearly identical in the intermediate region 2. This result identified two distinct spatio-temporal patterns of IPSPs after stimulation of the two different hippocampal areas. This spatio-temporal pattern is shown Figure 3.4 (B) and in Movie S1 (see supplementary material, Manuscript II). The consistent difference in the spatial distribution of the IPSP related optical signal associated with distal and proximal stimulation is shown for three additional neurons as a color-coded map in Figure 3.4 (C). To quantify the spatial patterns of IPSPs after stimulation of the two different hippocampal areas, we analyzed  $\Delta F/F$  signals over large dendritic regions  $>200 \mu\text{m}$  from the soma, mostly in the stratum lacunosum-moleculare (SLM), and within  $100 \mu\text{m}$  from the soma in the stratum radiatum (SR) (Figure 3.4 D, left-drawing). In these two regions (SLM and SR), we calculated the ratio of the peak signals after distal and proximal stimulation (dist/ prox). In six cells tested, the mean  $\pm$  SE of this ratio was  $1.35 \pm 0.12$  for the stimulus applied to SLM region, significantly different ( $p < 0.001$ , two-sample t-test) from the ratio calculated for the measurements after stimulation of the SR region ( $0.75 \pm 0.06$ ). These results show the ability of multisite optical recording to reliably detect specific spatial distribution of relatively small input signals on the dendritic arbor. In addition, they show that the spatial distribution of dendritic inhibition in CA1 hippocampal

pyramidal neurons is different for classes of interneurons that make contacts in the proximal and distal parts of the dendrite.

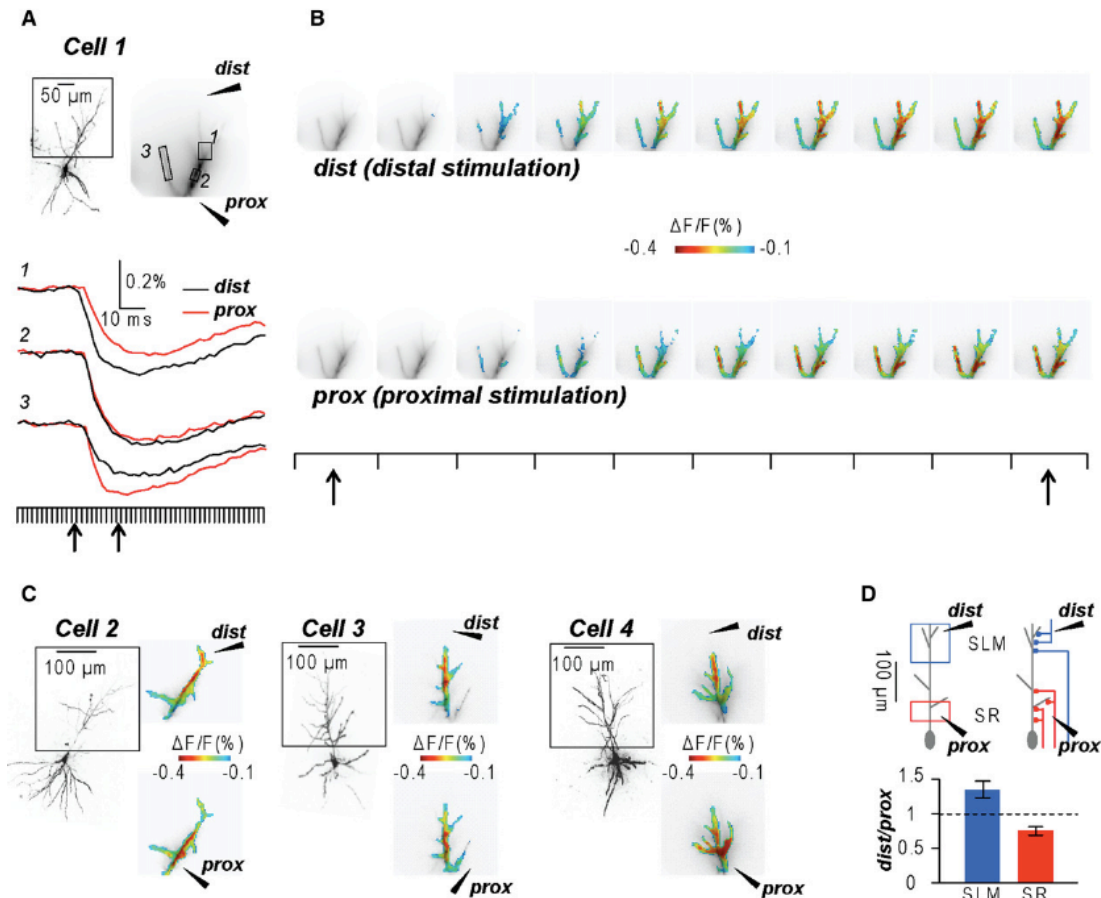


**Figure 3.4 . Spatial distribution of IPSPs along the apical dendrite. (A)** (Top) Image of a neuron with an area of  $\sim 300 \mu\text{m} \times 300 \mu\text{m}$  projected onto the CCD camera outlined; position of a distal (dist) and a proximal (prox) stimulating electrode shown schematically. (Bottom) Optical recordings of IPSPs evoked by dist (black) or prox (red) stimulation. Signals are averages of nine trials from locations 1–3. Frame sequence indicated below. **(B)** Sequence of frames between the two arrows in A showing a color-coded display of the spatio-temporal pattern of IPSP initiation and spread after distal and proximal stimulation. See Movie S1 in supplementary material (Manuscript II). **(C)** (Left) Images of three additional neurons analyzed. (Right) Spatial distribution of the IPSPs in the dendritic tree shown by color-coded representation of signal peak amplitude. The IPSP peak corresponds to red. **(D)** (Top left) Schematic drawing of a CA1 hippocampal pyramidal neuron with dist and prox stimulating electrodes. The location of two separate areas (SLM and SR) indicated by blue and red rectangles, respectively. (Top right) Schematic drawing of interneurons excited by dist and prox electrodes based on anatomical information. (Bottom) Mean  $\pm$  SE of the ratio of peak signals associated with dist and prox stimulation from six cells. Values from SLM and SR regions are significantly different ( $p < 0.001$ , two-sample t-test).

#### **3.4.5 IPSP recordings from axons and basal dendrites**

In another series of experiments we tested if IPSPs can be measured selectively from the axon. We recorded IPSP signals from the axon and from the neighboring basal dendrites, by monitoring regions of  $\sim 125 \mu\text{m} \times 125 \mu\text{m}$  in the stratum oriens. Imaging fluorescence from the initial segment of a CA1 hippocampal pyramidal neuron axon is complicated by the spatial overlap with dendrites. Thus, axonal signals can be contaminated by out-of focus fluorescence from the dendrites and vice versa. A way to discriminate between the two fluorescence sources is to image an action potential that in the axon is characterized by considerably faster kinetics compared to the dendritic action potential (Palmer and Stuart, 2006; Shu et al., 2007).

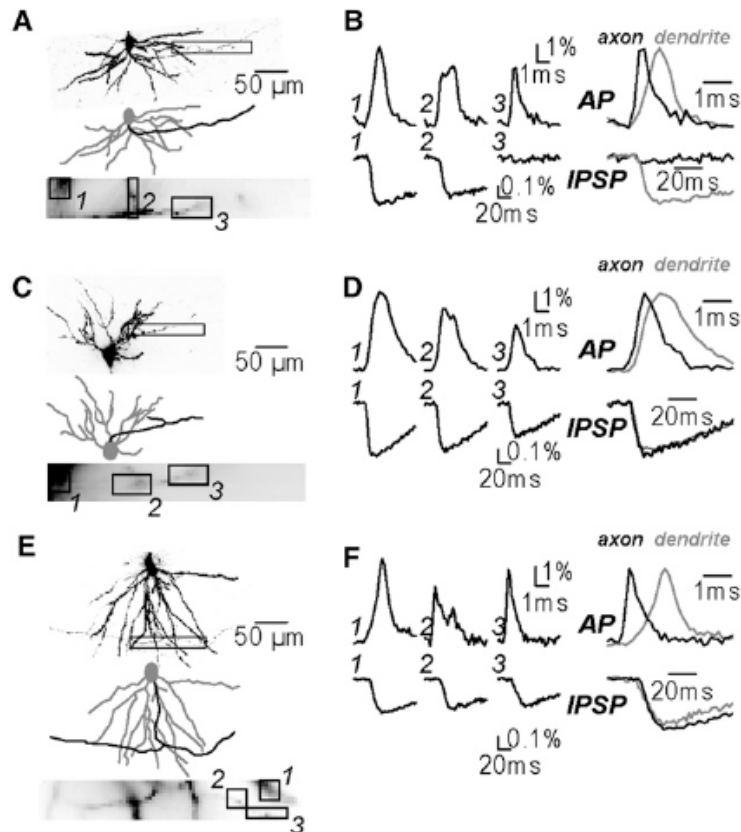


**Figure 3.5 . IPSPs recorded simultaneously in the axon and in the basal dendrite.** (A) Image of a part of a CA1 pyramidal neuron in the stratum oriens with drawing of basal dendrites (gray) and axon (black). Part of a neuron projected onto a subset of pixels of the CCD camera for voltage-imaging (bottom image). Three recording locations are labeled 1–3. (B) (Left traces) Optical signals associated with an evoked action potential (top) and an IPSP (bottom) from locations 1–3 shown in C; location 1: dendritic signal; location 2: mixed signal; location 3: axonal signal. (Right traces) Optical signals from location 1 (dendrite, gray trace) and location 3 (axon, black trace) normalized in amplitude and superimposed. Action potential signal is present in the axon and in the dendrite. IPSP signal is absent in the axon (see also Movie S2 in supplementary material, Manuscript II). (C and E and D and F) Same sequence of measurements as in A and B from two additional neurons; IPSP observed both in the dendrite and in the axon. Action potential and IPSP signals were averages of 4 and 16 trials, respectively.

In the three experiments shown in Figure 3.5 the action potential signals recorded from locations 1 and 3 at a frame rate of 10 kHz had a single peak and kinetics that could be associated with the dendrite and with the axon respectively. In contrast, the action potential signal from location 2, exhibited two peaks suggesting that it was a mixture of axonal and dendritic signals. Similar results were obtained in all cells. Following these measurements, the IPSP signals evoked by stimulation in the stratum pyramidale were recorded from the same

location and different results were obtained from different cells. In the experiment shown in Figure 3.5 A and B,  $\Delta F/F$  signals indicated clearly that the evoked IPSP was present in the dendrite (location 1) but absent in the axon (location 3; see also Movie S2 in supplementary material, Manuscript II). In the other two cells in Figure 3.5 (C–F) and in additional two neurons (not shown) the evoked IPSP was detected both in the dendrite and in the axon. Because it is well established that the charge-shift voltage-sensitive dye used here tracks the membrane potential precisely, different results obtained in different neurons suggest that different types of interneurons were stimulated in different experiments. These recordings unambiguously show the possibility to analyze in detail the spatial segregation of IPSPs from identified functionally different regions of the neuron.



### 3.5 Discussion

The study of GABAergic signals is particularly challenging because these signals are generally small and localized to distinct areas of the neuron. Therefore, a new technique is needed for monitoring small changes of membrane potential with high spatial resolution. Direct patch clamp recordings provide high sensitivity and high temporal resolution, but poor spatial resolution. This limitation is critical in many studies. In addition, the dialysis of neurons with electrode solutions may introduce substantial distortions in the electrical behavior of target structures. These limitations are overcome by the described optical methodology that permits multiple site measurements of voltage signals from relatively small portions of dendrites and axons. We have shown here that illumination with stable solid-state lasers, the use of high numerical aperture lenses, and detection with fast and large well capacity CCD cameras currently provide optimal conditions for these measurements. The ions mediating the response of GABA<sub>A</sub> receptors, Cl<sup>-</sup> and bicarbonate, and therefore the polarity and the size of GABAergic synaptic potentials vary during development (Cherubini et al., 1991; Rivera et al., 2005). The technique of perforated patch recording using gramicidin (Rhee et al., 1994; Kyrozis and Reichling, 1995), that introduces negligible perturbation to the physiological [Cl<sup>-</sup>]<sub>i</sub>, has been used to show the presence of subcellular gradients of Cl<sup>-</sup> resulting in GABAergic synaptic potentials of different polarity (Gulledge and Stuart, 2003; Szabadics et al., 2006; Khirug et al., 2008). This method, however, lacks the spatial resolution necessary to record synaptic potentials at the site of origin. In contrast, voltage imaging seems to be a uniquely suited technique to investigate local inhibitory signals and a tool to provide reliable estimates of physiological [Cl<sup>-</sup>]<sub>i</sub>. The evidence that after termination of patch recordings cells recovered to a low Cl<sup>-</sup> concentration within minutes indicates that functioning transporter systems can restore physiological conditions.

In our experiments, all the responses we measured were hyperpolarizing, regardless of the subcellular location or of the site of stimulation. This important result suggests that  $[Cl^-]_i$  is low in all areas of mature CA1 hippocampal pyramidal neurons confirming the conclusions from another study where noninvasive techniques were used (Glickfeld et al., 2009). In addition, our results show the ability of multisite optical recording to consistently detect specific spatial distribution of IPSP input signals in the dendritic arbors and in the axon. This kind of information, uniquely available from high spatial resolution optical recordings, will likely facilitate further studies of the role of inhibition in determining the input-output transform carried out by individual nerve cells.

In summary, we believe this study shows a significant advance in the sensitivity of voltage imaging allowing detection of  $\sim 1$  mV IPSP signals at multiple subcellular sites. This approach overcomes important limitations of electrode measurements opening the gate to the spatial analysis of synaptic inhibition from individual nerve cells. The spatial distribution of IPSPs at physiological  $[Cl^-]_i$  can be now investigated in many other types of neurons using the experimental protocols presented here. A current limitation is the use of extracellular stimulation that, in general, precludes the precise identification of the stimulated interneurons and of the postsynaptic area where synaptic contacts are formed. Future work must overcome this limitation by coupling voltage imaging with selective presynaptic stimulation.

## **3.6 Supplementary material**

Movie S1: Spread of dendritic IPSPs

Movie S2: Dendritic vs axonal signals

### 3.7 References

**Antic S, Major G, Zecevic D** (1999) Fast Optical Recordings of Membrane Potential Changes From Dendrites of Pyramidal Neurons. *J Neurophysiol* 82:1615-1621.

**Barry PH** (1994) JPCalc, a software package for calculating liquid junction potential corrections in patch-clamp, intracellular, epithelial and bilayer measurements and for correcting junction potential measurements. *J Neurosci Methods* 51:107-116.

**Buhl EH, Han ZS, Lörinczi Z, Stezhka VV, Karnup SV, Somogyi P** (1994) Physiological properties of anatomically identified axo-axonic cells in the rat hippocampus. *J Neurophysiol* 71(4):1289-307.

**Canepari M, Djurisic M, Zecevic D** (2007) Dendritic signals from rat hippocampal CA1 pyramidal neurons during coincident pre- and post-synaptic activity: a combined voltage- and calcium-imaging study. *J Physiol* 580:463-484.

**Canepari M, Vogt K, Zecevic D** (2008) Combining Voltage and Calcium Imaging from Neuronal Dendrites. *Cell Mol Neurobiol* 28:1079-1093.

**Cherubini E, Gaiarsa JL, Ben-Ari Y** (1991) GABA: an excitatory transmitter in early postnatal life. *Trends Neurosci* 14:515-519.

**Djurisic M, Antic S, Chen WR, Zecevic D** (2004) Voltage Imaging from Dendrites of Mitral Cells: EPSP Attenuation and Spike Trigger Zones. *J Neurosci* 24:6703-6714.

**Fuentealba P, Begum R, Capogna M, Jinno S, Márton LF, Csicsvari J, Thomson A, Somogyi P, Klausberger T** (2008) Ivy cells: a population of nitric-oxide-producing, slow-spiking GABAergic neurons and their involvement in hippocampal network activity. *Neuron* 57(6):917-29.

**Glickfeld LL, Roberts JD, Somogyi P, Scanziani M** (2009) Interneurons hyperpolarize pyramidal cells along their entire somatodendritic axis. *Nat Neurosci* 12:21-23.

**Gulledge AT, Stuart GJ** (2003) Excitatory Actions of GABA in the Cortex. *Neuron* 37:299-309.

**Khirug S, Yamada J, Afzalov R, Voipio J, Khiroug L, Kaila K** (2008) GABAergic Depolarization of the Axon Initial Segment in Cortical Principal Neurons Is Caused by the Na-K-2Cl Cotransporter NKCC1. *J Neurosci* 28:4635-4639.

**Klausberger T, Somogyi P** (2008) Neuronal Diversity and Temporal Dynamics: The Unity of Hippocampal Circuit Operations. *Science* 321:53-57.

**Kyrozis A, Reichling DB** (1995) Perforated-patch recording with gramicidin avoids artifactual changes in intracellular chloride concentration. *J Neurosci Methods* 57:27-35.

**Mody I, Pearce RA** (2004) Diversity of inhibitory neurotransmission through GABAA receptors. *Trends Neurosci* 27:569-575.

**Palmer LM, Stuart GJ** (2006) Site of Action Potential Initiation in Layer 5 Pyramidal Neurons. *J Neurosci* 26:1854-1863.

**Price CJ, Cauli B, Kovacs ER, Kulik A, Lambolez B, Shigemoto R, Capogna M** (2005) Neurogliaform neurons form a novel inhibitory network in the hippocampal CA1 area. *J Neurosci* 25(29):6775-86.

**Rhee JS, Ebihara S, Akaike N** (1994) Gramicidin perforated patch-clamp technique reveals glycine-gated outward chloride current in dissociated nucleus solitarii neurons of the rat. *J Neurophysiol* 72:1103-1108.

**Rivera C, Voipio J, Kaila K** (2005) Two developmental switches in GABAergic signalling: the  $K^+$ - $Cl^-$  cotransporter KCC2 and carbonic anhydrase CAVII. *J Physiol* 562:27-36.

**Shu Y, Duque A, Yu Y, Haider B, McCormick DA** (2007) Properties of Action-Potential Initiation in Neocortical Pyramidal Cells: Evidence From Whole Cell Axon Recordings. *J Neurophysiol* 97:746-760.

**Somogyi P, Klausberger T** (2005) Defined types of cortical interneurone structure space and spike timing in the hippocampus. *J Physiol* 562:9-26.

**Szabadics J, Varga C, Molnar G, Olah S, Barzo P, Tamas G** (2006) Excitatory Effect of GABAergic Axo-Axonic Cells in Cortical Microcircuits. *Science* 311:233-235.

**Vida I, Halasy K, Szinyei C, Somogyi P, Buhl EH** (1998) Unitary IPSPs evoked by interneurons at the stratum radiatum-stratum lacunosum-moleculare border in the CA1 area of the rat hippocampus in vitro. *J Physiol* 506:755-773.



## **4 Manuscript III: Feedforward Inhibition Controls The Spread Of Excitation Within The Dendritic Tree Of CA1 Pyramidal Neurons**

Silvia Willadt, Markus Nenniger and Kaspar E. Vogt

Status of publication: Submitted PlosOne

Neurobiology/Pharmacology; Biozentrum; Klingelbergstrasse 50/70; 4056 Basel, Switzerland

Corresponding author:  
Kaspar Vogt  
Neurobiology/Pharmacology  
Biozentrum  
University of Basel  
Klingelbergstrasse 50/70  
4056 Basel

kaspar.vogt@unibas.ch

I have contributed to all aspects of this manuscript. In general, I participated in designing the research and writing the draft of the manuscript; I performed all experiments, collected and analyzed the data, assembled the figures.

## 4.1 Abstract

Signal integration in the central nervous system is critically shaped by inhibitory synaptic transmission. In the hippocampus feedforward inhibition controls the time window of synaptic integration. It is still unclear, however, how exactly inhibition affects dendritic signal integration spatially. Here we demonstrate that feedforward inhibition crucially shapes the integration of synaptic signals in pyramidal cell dendrites. Using voltage-sensitive dye imaging we studied the transmembrane voltage patterns in CA1 pyramidal neurons after Schaffer collateral stimulation. We observed a high degree of variability in the excitation/inhibition ratio between different branches of the dendritic tree. On average the apical dendrite close to the soma and especially the basal dendrites received the most inhibition. Many dendritic segments actually received no excitatory signals at all. Application of the GABA<sub>A</sub> receptor antagonist bicuculline revealed an excitatory signal in all dendritic segments studied, indicating that the original patterns were indeed due to inhibitory synaptic transmission. Application of a tetanic stimulus induced significant alterations in the pattern of excitation/inhibition, indicating that they can be modified by synaptic plasticity. In summary, we show that GABAergic inhibition shapes synaptic integration in a dendrite-specific manner, with a large fraction of the dendritic arborization receiving predominantly or exclusively inhibitory signals after stimulation of CA1 inputs.



## 4.2 Introduction

Under physiological conditions principal cells (PCs) in the central nervous system receive biphasic innervation patterns composed of excitatory postsynaptic potentials (EPSPs) from direct excitatory inputs and inhibitory postsynaptic potentials (IPSPs) from interneurons, activated by collaterals of the excitatory input (Buzsáki, 1984; Freund and Buzsáki, 1996). Experimental data suggests a prominent sharpening role of the inhibitory component at the network level (Katzner et al., 2011); this sharpening can occur in the spatial domain, controlling the number of cells activated or in the temporal domain, controlling the time window for excitation. On one hand, lateral inhibition, which describes the competitive interaction between neighbouring excitatory and inhibitory innervation, sharpens the borders of sensory fields by tuning the excitatory input (Miller et al., 2001; Foeller et al., 2005). On the other hand, in feedforward inhibition (FFI), excitatory and - with a short delay - inhibitory inputs converge onto the same target cell. In the hippocampus, Pouille and Scanziani (Pouille and Scanziani, 2001) have shown that feedforward inhibition controls the time window for synaptic integration in pyramidal neurons, thereby ensuring temporal precision in the CA1 area.

While its role is well investigated at the network level, less is known about the influence of inhibition on signal processing at the cellular and especially subcellular level. The inhibitory system exhibits a high degree of spatial organization. In the hippocampus many different subtypes of interneurons (Klausberger and Somogyi, 2008) can be characterized by their precise targeting of different subcellular compartments (Freund and Buzsáki, 1996). It is therefore plausible that this spatial specificity and diversity translate into functional specialization.

There is a longstanding interest in the influence of dendritic morphology on signal integration. At the most basic level, loss of charge during propagation in dendrites, reduces synaptic potentials on their way towards the soma. Thus, distal synapses will affect the membrane potential at the site of action potential

initiation more weakly. To counteract this dendritic filtering, excitatory synapses in the CA1 area show scaling, with increased synaptic strength at more distant synapses, as shown by Cash and Yuste (Cash and Yuste, 1999). The location of excitatory synapses on the dendritic tree of PCs also determines their rules for spike timing-dependent plasticity (Froemke et al., 2010).

Less information is available on the influence of synapse location for GABAergic inputs. In particular, the rules governing the interaction between excitatory and inhibitory inputs in the spatial domain have not been fully investigated. The study of dendritic signal integration at high resolution with conventional electrode-based techniques is challenging and restricted to a limited number of recording sites. Voltage-sensitive-dye (VSD) imaging, can overcome this restriction, allowing the observation of signal propagation over large sections of the dendritic arborization.

VSD imaging has previously been used in the study of the spatial organization of inhibition, albeit at the network level. In these experiments hyperpolarization was found to form a ring-like shape around a center of more excited cells, so-called center-surround inhibition (Derdikman et al., 2003).

The study of subcellular patterns of excitation and inhibition are more demanding and has so far received less attention. Single cell VSD imaging allows the detection of membrane voltages at high spatial resolution (Zecevic, 1998; Antic et al., 1999); due to recent developments inhibitory postsynaptic potentials can nowadays be resolved in detail (Canepari, 2010).

Here we study the influence of feedforward inhibition on dendritic signal integration using VSD imaging. Different compartments of hippocampal CA1 pyramidal cells in acute brain slices were imaged after Schaffer collateral stimulation. We demonstrate a critical influence of GABA<sub>A</sub>R-mediated inhibition on the subcellular membrane potential patterns in CA1 pyramidal neurons.

## **4.3 Materials and methods**

### **4.3.1 Brain slice preparation**

All experiments were approved by Basel cantonal veterinary authorities. Recordings were performed in 300  $\mu\text{m}$  thick brain slices of heterozygous knock-in mice P21 to 32 expressing GFP from the GAD67 gene locus (Tamamaki et al., 2003). After deep isoflurane anaesthesia mice were decapitated and transversal hippocampal slices were cut using a vibrating microtome (VT1200S, Leica, Switzerland). Slicing was performed in ice-cold solution containing (in mM) NaCl 87, Sucrose 75, Glucose 25,  $\text{NaHCO}_3$  25,  $\text{MgCl}_2$  7, KCl 2.5,  $\text{NaH}_2\text{PO}_4$  1.25,  $\text{CaCl}_2$  0.5, equilibrated with 95%  $\text{O}_2$  and 5%  $\text{CO}_2$ . After cutting, slices were incubated at 35°C for 30 min in artificial cerebrospinal fluid (ACSF), also used as extracellular solution for the experiments. This solution contained (in mM): NaCl 125,  $\text{NaHCO}_3$  26,  $\text{NaH}_2\text{PO}_4 \cdot \text{H}_2\text{O}$  1.25, KCl 2.5,  $\text{MgSO}_4$  1.0, CaCl 2.5; 310 mOsmol and pH 7.4 when bubbled with a gas mixture containing 95%  $\text{O}_2$ , 5%  $\text{CO}_2$ .

### **4.3.2 Neuronal loading**

CA1 pyramidal cells were loaded with the voltage sensitive dye (VSD) JPW-1114 (0.2-0.5 mg/ml, Molecular Probes-Invitrogen) as described previously in detail (Canepari et al., 2010; 2008).

While staining cells with VSD, somatic recordings were performed using a Multiclamp 700A amplifier (Axon Instruments, Germany) and an upright microscope (Olympus BX51-WI, Olympus, Switzerland).

The  $\text{KMeSO}_4$ -based intracellular solution contained (in mM): 5 Na-ATP, 0.3 Tris-GTP, 14 Tris-phosphocreatine, 20 HEPES, and either 125  $\text{KMeSO}_4$ , 5 KCl, or 90  $\text{KMeSO}_4$ , 40 KCl; 285 mOsmol and pH 7.35 adjusted by potassium hydroxide titration. We used borosilicate electrodes for whole cell patch clamp recordings (1.5 mm external diameter, 1.17 mm internal diameter) without filament and an open tip resistance of 5-6 M $\Omega$  for the whole-cell patch-clamp recordings.

Background fluorescence increases due to dye spillage was avoided by tip-filling the electrode with dye-free solution. In addition, before reaching the cells, positive pressure in the pipettes were kept low in the bath and controlled with a manometer at ~ 5 mbar (Model 840081; Sper Scientific, Scottsdale, AZ). Staining time was determined by measuring the resting fluorescence from the cell body at reduced excitation light intensity (~0.1 % of the laser light). Cell loading with VSD did not cause pharmacological effects (Antic et al., 1999; Canepari et al., 2010). After enough dye diffused into the cell, pipettes were gently removed by forming outside-out patches. Optical recordings were performed when dendrites were sufficiently filled with VSD (~ 20-30 min after patch).

### **4.3.3 Electrophysiology**

If relevant for the experiments, electrical signals were detected at the beginning of the experiments simultaneous to optical signal detection.

For paired recordings, potentially connected interneurons of CA1 stratum radiatum were searched, while pyramidal cells were being filled with the dye. To improve the detection of small unitary inhibitory postsynaptic potentials (uIPSPs), pyramidal cells were patched with intracellular solution containing 40 mM Cl<sup>-</sup>. Hence, the driving force for chloride increased, potentials were larger in amplitude and evoked potentials were positive due to a more depolarized reversal potential for Cl<sup>-</sup>.

Somatic electrode recordings were acquired at 16 kHz and filtered at 4 kHz by using the Redshirt imaging system or at 20 kHz and filtered at 2 kHz by a separate A/D board (NI USB-6343, National Instruments, Switzerland).

### **4.3.4 Optical recordings**

Excitation of the VSD was achieved using a 532 nm- 300 mW solid-state laser (model MLL532; CNI, China). Hence, the dye was stimulated at the border of its

absorption spectrum and the largest dynamic range in fluorescence could be reached.

Advantages of laser illumination compared to a conventional xenon arc lamp were described earlier (Canepari et al., 2010).

GABA<sub>A</sub>-receptor-mediated uIPSPs and evoked EPSP/IPSP patterns were detected optically at a frame rate of 500 Hz and 6 % of the full laser intensity. Optical signals were captured with a high-speed, 80 x 80 pixels CCD camera (NeuroCCD-SM, RedShirtImaging LLC, China). The fluorescence image of the cell was projected via a 0.2 optical coupler onto the CCD camera. The imaged field in our measurements was ~125 μm x 125 μm. The excitation light was directed to the preparation using a 570 nm dichroic mirror and a water immersion objective (Olympus 60x/1.1 NA, Olympus, Switzerland). The emission light was filtered with a 610 nm long-pass filter.

Optical signals were averaged over 10-20 pixels along compartments of the stained cells. To improve the signal-to-noise ratio, averages of 3-12 trials were taken.

For analysis, dendritic sub-compartments (20-50 pixels in size) were chosen by comparing VSD fluorescence images with two-photon reconstructions of the neurons.

#### **4.3.5 Stimulation and Pharmacology**

Extracellular stimulation was performed by using borosilicate patch pipettes filled with ACSF. Hydraulic manipulators (Narishige, Japan) were used to place pipettes. Feedforward inhibition was evoked by stimulation of Schaffer collaterals in stratum radiatum between CA3 and CA1 and feedback inhibition by stimulation of projecting pyramidal cell axons in the alveus. Both innervate different types of interneurons located in stratum pyramidale and radiatum (Klausberger and Somogyi, 2008).

Stimulation pulses were 0.1 ms of duration and strength varied between 20 to 60 μA. Pulses were delivered by an IS4 stimulator (SC-Devices, Switzerland) and

triggered by stimulation protocols written in IGOR Pro software (Wave Metrics, USA).

GABA<sub>A</sub>-receptor-mediated potentials were tested by bath application of the competitive receptor antagonist bicuculline (20 μM).

Direct stimulation of interneurons in the stratum radiatum was avoided by low current injection and careful placement of the stimulus electrode. Control experiments to test for feedforward inhibition were performed by applying 2,3-Dioxo-6-nitro-1,2,3,4-tetrahydrobenzo[f]quinoxaline -7-sulfonamide disodium salt (NBQX, 20 μM), a specific α-amino-3-hydroxy-5-methyl-4-isoxazolepropionic acid receptor (AMPA) antagonist, to block signals from Schaffer collaterals to interneurons and pyramidal cells.

#### **4.3.6 Anatomical reconstruction and analysis**

Anatomical reconstruction of neurons was carried out from a stack of two-photon excitation fluorescence images obtained using a tuneable, mode locked titan-sapphire laser (MaiTai HP, Spectra Physics) set to 880 nm and a laser scanning system (FV300, Olympus) with a high-aperture 20x water-immersion lens (Olympus LUMPLAN 20x).

Optical signals were analysed as fractional changes of fluorescence ( $\Delta F/F$ ). Optical and electrophysiological recordings were analysed with dedicated software written in MATLAB (The MathWorks). Optical signals were corrected for the bleach fraction.

Statistics were calculated in Excel (Microsoft Office 2010) and averages are presented as the mean  $\pm$  standard error of the mean (SEM) or median  $\pm$  median absolute deviation (MAD), as indicated.

## 4.4 Results

We first tested the suitability of voltage-sensitive dye imaging to study feedforward inhibition by comparing classical electrode recordings with VSD imaging.

Membrane potentials over the entire dendrite were detected by VSD imaging. The staining procedure was described in more detail in an earlier publication (Canepari et al., 2010) and is schematically shown in Figure 4.1 A. First, we performed whole-cell patch recordings to load hippocampal CA1 pyramidal cells with the dye JPW1114. After cells were filled adequately, pipettes were slowly removed from the cell somata. We recorded optically the distribution patterns of evoked potentials in several regions of apical and basal dendrites (rectangles, Figure 4.1 A).

Feedforward inhibition could be initiated in CA1 pyramidal cells by extracellular stimulation of projecting Schaffer collaterals (SC) in stratum radiatum of the hippocampus (Figure 4.1 B, left). Excitatory potentials initiated by SC synapses projecting to the CA1 neuron were followed by a disynaptically-induced hyperpolarisation. In further experiments (see Figure 4.2), we also evoked feedback inhibition by placing the stimulation electrode in the alveus (ALV) between CA1 and subiculum (Figure 4.1 B, left). As shown in Figure 4.1 C, both the somatic electrode recording and the average VSD imaging trace show the same familiar de- and hyperpolarizing pattern, indicating that feedforward inhibition can be recorded and is undisturbed by VSD imaging.

The smallest unit of a feedforward signal originates from a single interneuron; we therefore also recorded unitary inhibitory postsynaptic potentials in CA1 neurons. To investigate the impact of a single interneuron on its target pyramidal cell we produced paired recordings between neighbouring GABAergic neurons and dye-filled principal cells (N=7; Figure 4.1 B, right). The ability to detect small voltage transients has been previously demonstrated (Canepari et al., 2010).

We used mice expressing GFP at the GAD67 gene locus to distinguish inhibitory and excitatory neurons. We focused on interneurons located in the stratum radiatum – which have a high probability to receive input from Schaffer collaterals and thus to contribute to feedforward inhibition (Buzsáki, 1984).

Interneurons were stimulated by eliciting action potentials (Lagostena et al., 2010; Figure 4.1 D, black trace,) through somatic current injection, while pyramidal cells were recorded with an intracellular solution containing 40 mM Cl<sup>-</sup> to increase its driving force at resting membrane potential. Hence, evoked responses were depolarizing due to the elevated GABA<sub>A</sub>R-reversal potential (Figure 4.1 D). Still, amplitudes of uIPSPs were small, which made optical recordings challenging. In simultaneous electrical and optical recordings an uIPSP of 3 mV amplitude resulted in a relative change in fluorescence of around 0.2 % (Figure 4.1 D). The optical average signal was taken at the apical dendrite over ~ 300 pixels with a size 1.56 x 1.56 μm per pixel.

After removing the patch pipette, we measured the distribution of the uIPSP along the apical (regions 2-3) and basal (regions 5-6) dendrite in smaller subcompartments of ~ 20 pixels in size (Figure 4.1 F, left). Regions 1 and 4 are averages over the full extent (~ 100 pixels) of apical (bottom) and basal (top) dendrite. Optically measured GABA<sub>A</sub>R-mediated potentials were hyperpolarizing (Figure 4.1 F, right side), which indicates that the pyramidal cell was able to recover from the high amount of Cl<sup>-</sup> loading during the patch recording (Canepari et al., 2010). The signal distribution showed a relatively homogeneous pattern of the evoked uIPSP along the whole apical-basal axis. Except for a short delay in the response in the apical dendrite, which might be caused by the anatomical location of the connected synapses, no significant difference between dendritic subcompartments could be detected. In the seven pairs imaged, all imaged apical dendritic compartments showed hyperpolarizing responses without obvious heterogeneity, indicating a spread of the GABAergic signal throughout the target pyramidal cell.



Given the relative homogeneity of the responses to the stimulation of a single interneuron, how do feedforward signals composed of multiple excitatory and inhibitory inputs look like at higher spatial resolution?

Optical recordings showed pronounced inhomogeneity of EPSP/IPSP patterns (right side) along the imaged apical dendrite (Figure 4.1 E). Regions of interest (regions 1-6) on the apical dendrite (left, top) are indicated in the fluorescence image of the cell (left, bottom). Note that in region 1 close to the soma we were only detecting inhibition, while other parts of the dendritic arborization show biphasic excitatory/inhibitory transients.

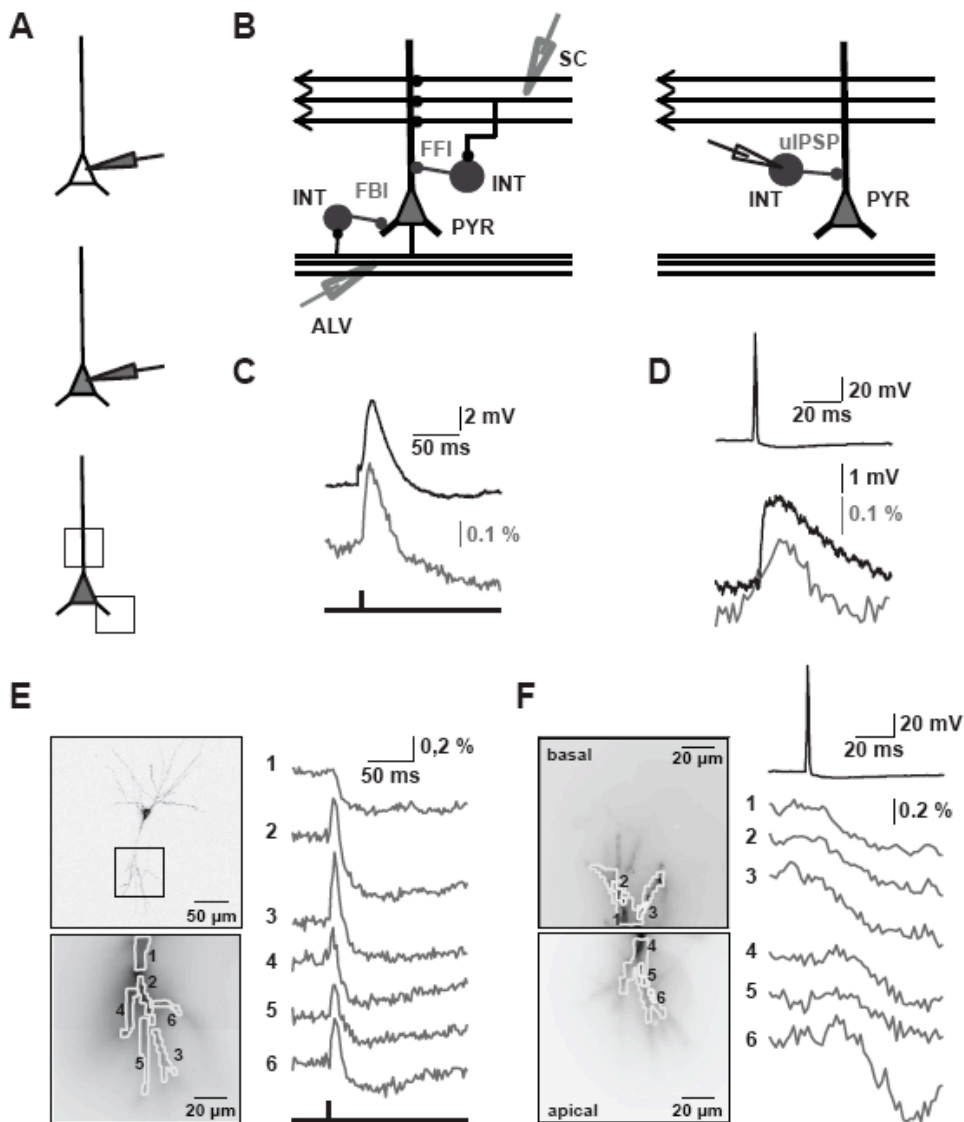


**Figure 4.1 . Measuring inhibitory IPSPs by VSD.** **A.** Schematic configuration of staining procedure. Top: whole-cell patch configuration. Middle, filling of CA1 pyramidal cell during patch stage. Bottom: optically recordings in non-patch stage. Rectangles represent recording sites in filled cell. **B.** Schematic illustration of stimulation location. Left: Schaffer collaterals (SC) and alveus (ALV) stimulation to activate feedforward (FFI), respectively feedback inhibition (FBI). ALV stimulation, see Fig. 2 experiments. INT, interneuron; PYR, CA1 pyramidal cell. Right: synaptically connected cell pair recording between INT of stratum radiatum and PYR to measure uIPSPs. **C.** and **D.** Simultaneous electrical (black trace) and optical  $\Delta F/F$  (grey trace) recordings. **C.** SC activated monosynaptic EPSP followed by disynaptic IPSP. Signals are averages of 6 trials. **D.** uIPSP in response to a spike in presynaptic interneuron (top trace). Signals are averages of 3 trials. **E.** Optical recording example for SC stimulation. Left top: two-photon reconstruction of imaged cell; rectangle shows imaged region at the apical dendrite. Left bottom: regions of interest (1-6). Right, optical dendritic recordings of EPSPs, IPSPs in regions of interest (average of 10 trials). **F.** Optical recording example for uIPSP recording. Left top: fluorescence image of basal dendrite of CA1 pyramidal cell. Left bottom: fluorescence image of apical dendrite in same cell. Regions of interest (1-6, 1 and 4 are spatial averages over all measured compartments).

Right: top trace spike in presynaptic interneuron, optical traces of evoked uIPSP in regions of interest (average of 3 trials).

To analyse this phenomenon in detail we imaged apical and basal dendrites of CA1 pyramidal neurons and subdivided the apical dendrites into the main trunk and its side branches (Figure 4.2). We carefully placed stimulus electrodes in both the SC and the ALV to compare the spatial distribution patterns of feedforward and feedback circuits (Buzsáki, 1984), avoiding direct activation of the recorded cells. Optical measurements were taken in the apical (bottom, left) and basal (bottom, right) dendrite of the pyramidal cell (Figure 4.2) in several dendritic regions of interest (Figure 4.2 A, bottom; apical: region 1-4; basal: region 5-8). See also supplemental material for animated data.

Stimulation in SC to activate feedforward inhibition produced the familiar inhomogeneous EPSP/IPSP sequence in the apical dendrite (Figure 4.2 B, left, regions 1-4); interestingly the basal dendrites exhibited much more pronounced inhibition with most of the regions showing only hyperpolarizing responses (Figure 4.2 B, left, regions 5-8).

Activation of the feedback circuitry through ALV stimulation produced relatively homogeneous inhibition throughout the imaged apical and basal dendritic compartments (Figure 4.2 B, right, apical: region 1-4; basal: region 5-8). Such evoked feedback patterns were recorded in five more cells (data not shown).

Quantitative analysis of the feedforward patterns (Figure 4.2 C-E) in 12 cells revealed, a significant difference between apical (Figure 4.2 C, blue and green) and basal (Figure 4.2 C, red) dendritic compartments. The majority of basal dendritic compartments (13 out of 17 imaged) showed only an inhibitory response, while only a minority (16 out of 65 imaged) apical compartments exhibited only an IPSP (Fischer test  $p < 0.01$ ). For the compartments with EPSP/IPSP sequences we observed a large variability in their relative strength. The EPSP/IPSP ratio was  $0.76 \pm 0.36$  for ad,  $0.9 \pm 0.38$  for sd and  $0.77 \pm 0.04$  for bd (median  $\pm$  MAD).

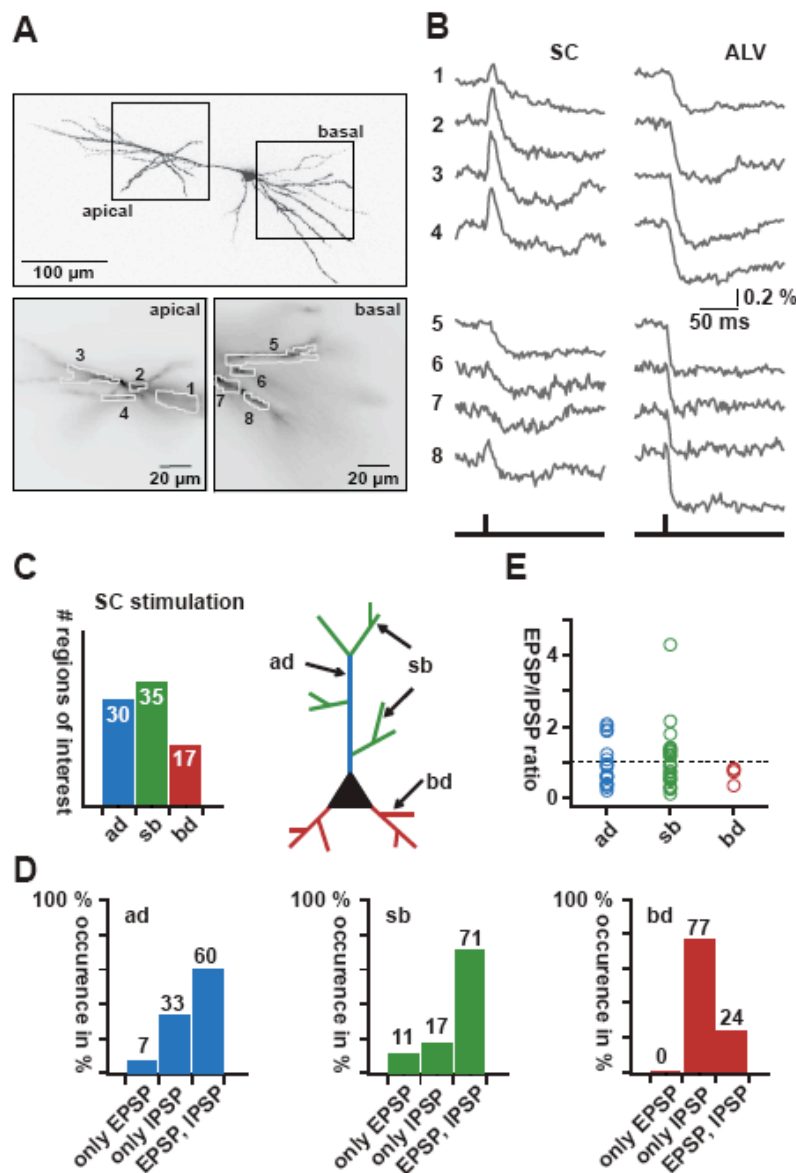


**Figure 4.2 . Title: EPSPs, IPSPs in distinct dendritic branches.** **A.** Top: two-photon reconstruction of imaged cell. Rectangles show recording site at the apical and basal dendrite. Bottom: regions of interest in apical (1-4, left) and basal (5-8, right). Total amount of averaged pixels per region ~20-50. **B.** Optical recordings in apical and basal dendrite. Regions of interest as in A. Left: EPSP, IPSP patterns evoked of stimulation in SC in apical (region 1-4) and basal dendrite (region 5-8). Right: Recordings of the same regions in apical and basal dendrite, stimulation of ALV. (recordings were averages of 4-10 trials). See also supplementary movie S1. **C.** Assignment of measured dendritic subcompartments (20-50 pixels) in SC experiments. ap = apical dendrite (blue), sb = side branch (Devonshire et al.), bd = basal dendrites (red). Total of cells N = 12 (thereof 5 for experiments in the basal dendrites). Left: plot of total analysed subcompartments; Right: schematic illustration of CA1 pyramidal cell, colour code shows subdivision of the dendrites in ap, sb and bd. **D.** Frequency of occurrence plots for only EPSPs, only IPSPs or both in ad, sb or bd subcompartments. 100 % represents the total amount of regions measured for ad, sb or bd. **E.** Distribution of EPSP/IPSPs in ap, sb and bd. Dotted line represents balance between excitatory and inhibitory response.

In conclusion, excitation seems to occur to a variable degree and only in a subset of dendritic compartments. It is notably absent from basal dendrites after SC stimulation. Is this variability intrinsic to the neuron and its connectivity, or is it actively shaped by inhibition? To study the role of inhibition, we used the GABA<sub>A</sub> receptor blocker bicuculline (20  $\mu$ M) and compared the membrane potential patterns before and after its application.

We performed SC activation experiments in which we analysed EPSP/IPSP distribution patterns by imaging small dendritic subcompartments (~20 pixels/region of interest; Figure 4.3 A).

Optical recordings in dendritic subregions (regions 1-8) along the apical dendrite revealed the typical inhomogeneous EPSP/IPSP distribution under control conditions (Figure 4.3 B, left). Note the decrease in EPSP size within the apical trunk towards the soma (region 1) and the complete absence of EPSPs in two side branches (regions 7 and 8). Bath application of bicuculline (20  $\mu$ M) completely suppressed the IPSPs in all regions imaged (Figure 4.3 B, right). Moreover it revealed robust depolarizing potentials throughout the dendrite – notably in areas in which no EPSP was visible before (regions 7 and 8). Animated data is available in the supplemental material. In accordance with previous electrode recordings (Pouille and Scanziani, 2001) the excitatory transients also lasted substantially longer. This was particularly visible in average scans from the apical and basal dendrites (Figure 4.3 C). We quantified the effect of bicuculline by subtracting the hyperpolarization under control conditions from the peak depolarization under bicuculline (see Figure 4.3 C) and normalized it by the hyperpolarization amplitude; values above 1 indicate a net depolarization under bicuculline. In the seven cells tested the median (+/- MAD) of this value was 3.07 +/- 1.26; individual values are shown in Figure 4.3 E (left).

All synaptic signals were sensitive to the addition of the AMPA receptor antagonist NBQX (10  $\mu$ M; Figure 4.3 D) to the perfusate. EPSPs were all blocked below the level of detectability (N=6 cells), while IPSPs were blocked by  $79 \pm 27$  % (mean +/- SEM; N=6 cells; Figure 4.3 E, right). This demonstrates that

inhibitory synaptic signals were originating from interneurons indirectly activated by SC stimulation and thus represented feedforward inhibition.

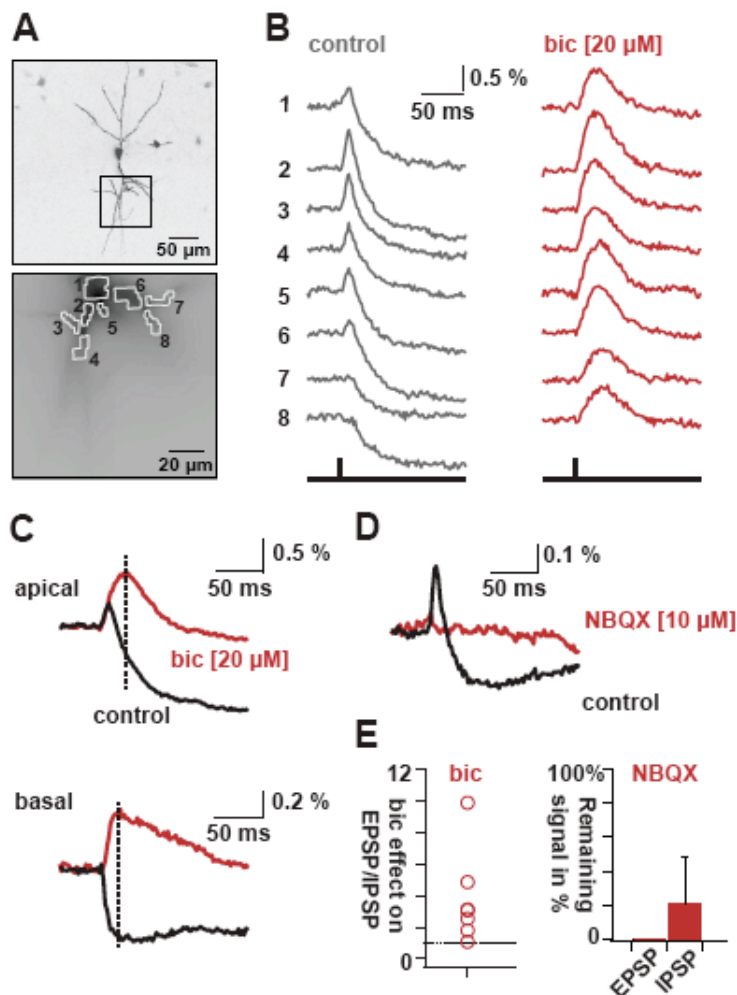


**Figure 4.3 . Center-surround inhibition.** **A.** Top: two-photon reconstruction of imaged cell. Rectangle indicates recording site in apical dendrite. Bottom: regions of interest (1-8). Averaged pixels per region ~20. **B.** Bicuculline (bic, 20  $\mu$ M) effect on SC evoked potentials in apical dendritic subcompartments. Region assignment as in A. Traces are averages of 6 trials. Left: control conditions. Right: bic conditions. See also supplementary movie S2. **C.** Trace-overlay of control (black) and under bicuculline (red). Dotted line represents taken values for calculation in E, left. Top: responses in apical dendrite (average of 6 trials). Bottom: responses in basal dendrite (average of 5 trials). **D.** Test for disynaptic inhibition with bath-application of NBQX (10  $\mu$ M) to block Glutamate-mediated receptors; control (black) and NBQX (red), traces are averages of 11 trials for control, respectively 7 trials for NBQX. **E.** Quantitative analysis of bic and NBQX effect. Left: plot shows the reduction effect of GABAergic inhibition on excitatory innervation (calculation:  $EPSP(bic) - IPSP(control) / |IPSP(control)|$ ); N=7). Right: NBQX reduced EPSPs (N=5) by 100 %. IPSPs (N=6) were reduced to  $21 \pm 26.9$  % (N=5 cells).

Our data demonstrate that GABA<sub>A</sub>R mediated inhibition is shaping excitatory propagation CA1 pyramidal cell dendrites. Are these patterns static or can they be altered by synaptic plasticity?

To study this issue, we applied simple tetanic stimuli in SC (100 pulses by 100 Hz; Figure 4.4 B), known to induce plasticity in the SC pathway. Optical recordings were taken shortly before and after the tetanic stimulus in several apical subcompartments of four different neurons (N=29 subcompartments). The size of the imaged subregions ranged between 20-50 pixels. In Figure 4.4 A regions of interest (right side) for one example neuron (left side) are illustrated. An overlay of pre (grey traces) and post (black traces) tetanic optical recordings (Figure 4.4 C) showed a change in the EPSP/IPSP pattern in several subcompartments. The changes were more pronounced in distal compared to proximal compartments and resulted in an increase in the EPSP/IPSP ratio. Such patterns were found in all four cells tested (Figure 4.4 D) – with the red line indicating the result from the most proximal compartment imaged in each cell. Overall the tetanic stimulation resulted in a highly significant alteration in the EPSP/IPSP patterns ( $p=0.0003$ ; Rank-Sum-Test).



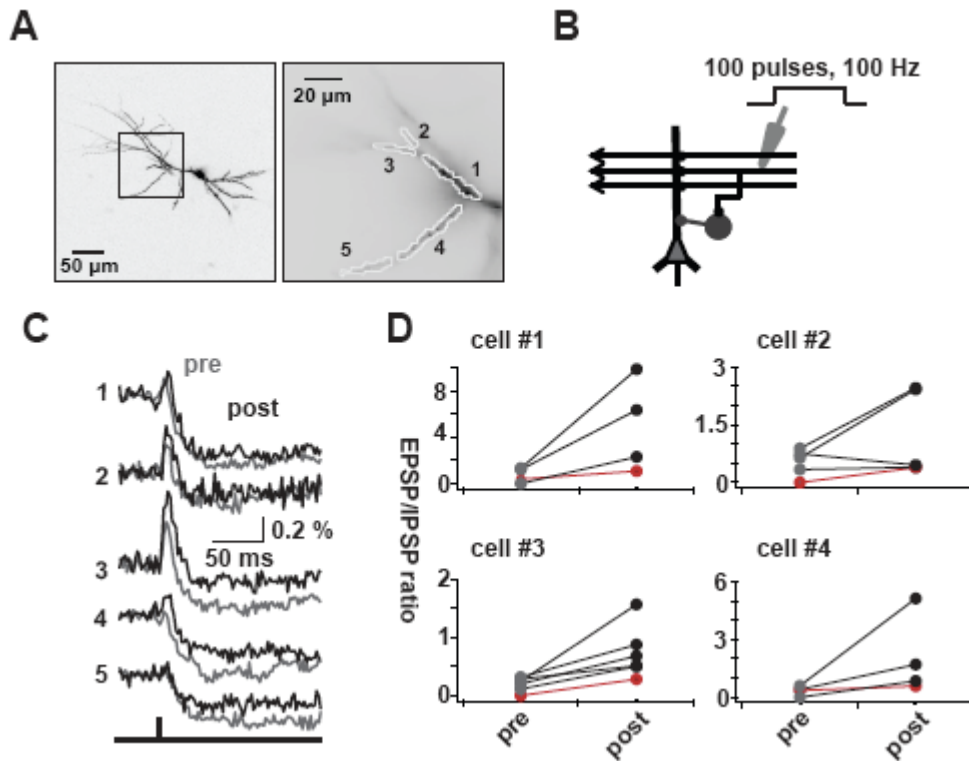


**Figure 4.4 . Plastic changes of EPSP, IPSP patterns.** **A.** Left: two-photon reconstruction of pyramidal cell. Rectangle represents recording site. Right: regions of interest in apical dendrite (1-5). Averaged pixels per region ~20-50. **B.** Schematic illustration of plasticity protocol. Tetanus application in SC (100 pulses, 100 Hz). **C.** Trace-overlay of pre (grey) and post (black) tetanic evoked potentials for one cell example. Region assignment as in A. Signals are averages of 8 for pre, respectively 4 for post tetanic trials. **D.** Plots of EPSP/IPSP ratios versus pre and post tetanus for 4 cells. Red traces indicates the most proximal dendritic compartment. Size of subcompartments ~20-50 pixels.

## 4.5 Discussion

We have revealed a significant degree of inhomogeneity in dendritic membrane potential transients in CA1 pyramidal cells after SC stimulation. While NBQX-sensitive feedforward hyperpolarization was detected in all dendritic subregions, many dendritic segments, particularly in basal dendrites showed no discernible excitatory response. In the absence of GABA<sub>A</sub>R mediated feedforward inhibition, excitation did spread throughout the dendritic arborization, indicating that these patterns are actively shaped by the network of interneurons surrounding CA1 pyramidal cells (Buzsáki, 1984; Liu, 2004).

Paired recordings between individual interneurons and CA1 pyramidal cells showed more uniform hyperpolarization in both basal and apical dendrites. The shaping effect of GABA<sub>A</sub>Rs on dendritic EPSPs is therefore most likely due to shunting, which is significantly more localized than the hyperpolarization they cause (Gulledge and Stuart, 2003). Thus, to understand the subcellular effects of different interneuron subclasses in the hippocampus it is useful to design experiments that reveal shunting inhibition; ideally by combining GABA<sub>A</sub>R activation with signals, which are susceptible to shunting, such as EPSPs or backpropagating action potentials.

The control of excitation in time and space by GABAergic inhibition is crucial in shaping the propagation of information in the central nervous system. This is particularly evident in sensory processes. In the spatial domain, active GABAergic neurons reduce the activity of nearby pyramidal cells, sharpening and controlling their excitatory profiles. Such activity has been observed in several sensory brain areas, e.g. the whisker barrel cortex or the visual system (Hartline et al., 1956; Brumberg et al., 1996; Derdikman et al., 2003). Blocking GABA<sub>A</sub>R mediated inhibition broadens the tuning curves of pyramidal neurons in olfactory (Poo and Isaacson, 2009) auditory (Wehr and Zador, 2003) and visual cortex (Katzner et al., 2011). While lateral inhibition was generally assumed to shape cortical receptive fields, recent data also suggests other forms of GABAergic

synaptic transmission (Katzner et al., 2011). In the temporal domain feedforward inhibition in the hippocampus (Pouille and Scanziani, 2001) and cortex (Gabernet et al., 2005) was shown to shorten and thus control the integration time window for excitatory synaptic input. These network effects are reflected at the individual neuron level where excitatory and inhibitory signals are integrated. Recent evidence shows that this is accomplished at the level of dendritic compartments and controlled by their properties (London and Häusser, 2005). The result of this spatial interaction between multiple inputs finally determines neuronal output (Rall, 1964; Liu, 2004). Here we describe a sharpening feature of GABAergic synaptic transmission at this subcellular level - the focusing of dendritic depolarization by feedforward inhibition.

Parallel to earlier findings (Pouille and Scanziani, 2001), we have found more prominent feedforward signals closer to the soma in the apical dendrite. In addition we were able to observe more fine-grained effects on dendritic signal integration - many branches actually do not 'see' any excitatory signal at all and basal dendrites in particular are mainly silenced by SC stimulation. Both excitatory and inhibitory inputs to CA1 pyramidal cells show a layer-specific topographic organization and this provides a likely explanation for the patterns we have observed. SCs axons from CA3 neurons close to the hilus contact chiefly apical dendrites and their branches, while CA3 pyramidal cells close to CA2 send their axons mostly to basal dendrites (Ishizuka et al., 1990). Extracellular stimulation of the classical SC pathway at the border of CA3 to CA1 preferentially activates fibres, which terminate in the apical stratum radiatum (Wittner et al., 2007). As we show, this selective innervation leads to focused dendritic depolarization only in the presence of feedforward inhibition. By preventing the spread of excitation to large fractions of CA1 pyramidal cell dendrites, feedforward inhibition ensures that processes such as synaptic plasticity are spatially restricted to the site of innervation in these cells. The observed propagation of excitatory responses throughout these neurons after blocking GABAergic synaptic transmission shows the consequence of losing this important function of the inhibitory network.

The exact nature of the interneurons involved is unclear, however the strong evidence of layer-specific innervation by different subtypes of interneurons makes the selective silencing of dendritic subcompartments possible. We thus postulate a network of excitatory and inhibitory connections that innervate pyramidal neurons such that the excitatory input is surrounded by inhibitory synapses. Certainly basket cells, which innervate the soma and have been shown to participate in feedforward inhibition (Freund and Buzsáki, 1996; Gullledge and Stuart, 2003) are likely to contribute to preventing the spread of apical EPSPs to basal dendrites.

VSD imaging is particularly suited to the study of dendritic signals in the extremely thin basal dendrites. To date, their integrative properties remain largely unknown due to the difficulties in recording from their thin branches with classical electrode techniques. Recently, it has been shown in layer V pyramidal neurons that they exhibit strong synaptic scaling and can generate active signals (Nevian et al., 2007). Given their high input resistance they are particularly susceptible to GABAergic shunting, which may control these active properties.

Dendritic membrane potential patterns by themselves are not fixed, but can be altered by stimuli that induce synaptic plasticity. Interestingly, this plasticity is non-uniform in itself – proximal portions of the apical dendrite showed small changes in the EPSP/IPSP ratio, while distal portions showed a pronounced increase. The exact locations of the synaptic changes will need further investigation.

To conclude, feedforward inhibition restricts synaptic integration to specific subcellular regions of pyramidal cells, thus sharpening excitatory input both in time and space.

## **4.6 Supplementary material**

Movie S1: Distribution pattern in apical and basal dendrites (SR stimulation)

Movie S2: Effect of bicuculline (SR stimulation)

## 4.7 References

**Antic S, Major G, Zecevic D** (1999) Fast Optical Recordings of Membrane Potential Changes From Dendrites of Pyramidal Neurons. *J Neurophysiol* 82:1615-1621.

**Brumberg JC, Pinto DJ, Simons DJ** (1996) Spatial gradients and inhibitory summation in the rat whisker barrel system. *J Neurophysiol* 76:130-140.

**Buzsáki G** (1984) Feed-forward inhibition in the hippocampal formation. *Prog Neurobiol* 22:131-153.

**Canepari M, Vogt K, Zecevic D** (2008) Combining Voltage and Calcium Imaging from Neuronal Dendrites. *Cell Mol Neurobiol* 28:1079-1093.

**Canepari M, Willadt S, Zecevic D, Vogt KE** (2010) Imaging Inhibitory Synaptic Potentials Using Voltage Sensitive Dyes. *Biophysical Journal* 98:2032-2040.

**Cash S, Yuste R** (1999) Linear Summation of Excitatory Inputs by CA1 Pyramidal Neurons. *Neuron* 22:383-394.

**Derdikman D, Hildesheim R, Ahissar E, Arieli A, Grinvald A** (2003) Imaging Spatiotemporal Dynamics of Surround Inhibition in the Barrels Somatosensory Cortex. *J Neurosci* 23:3100-3105.

**Devonshire IM, Dommert EJ, Grandy TH, Halliday AC, Greenfield SA** (2010) Environmental enrichment differentially modifies specific components of sensory-evoked activity in rat barrel cortex as revealed by simultaneous electrophysiological recordings and optical imaging in vivo. *Neuroscience* 170:662-669.

**Foeller E, Celikel T, Feldman DE** (2005) Inhibitory Sharpening of Receptive Fields Contributes to Whisker Map Plasticity in Rat Somatosensory Cortex. *J Neurophysiol* 94:4387-4400.

**Freund TF, Buzsáki G** (1996) Interneurons of the hippocampus. *Hippocampus* 6:347-470.

**Froemke RC, Letzkus JJ, Kampa B, Hang GB, Stuart G** (2010) Dendritic synapse location and neocortical spike-timing-dependent plasticity. *Front Synaptic Neurosci* 2(29).

**Gabernet L, Jadhav SP, Feldman DE, Carandini M, Scanziani M** (2005) Somatosensory Integration Controlled by Dynamic Thalamocortical Feed-Forward Inhibition. *Neuron* 48:315-327.

**Gulledge AT, Stuart GJ** (2003) Excitatory Actions of GABA in the Cortex. *Neuron* 37:299-309.

**Hartline HK, Wagner HG, Ratliff F** (1956) Inhibition in the eye of limulus. *J Gen Physiol* 39:651-673.

**Ishizuka N, Weber J, Amaral DG** (1990) Organization of intrahippocampal projections originating from CA3 pyramidal cells in the rat. *J Comp Neurol* 295:580-623.

**Katzner S, Busse L, Carandini M** (2011) GABA<sub>A</sub> Inhibition Controls Response Gain in Visual Cortex. *J Neurosci* 31:5931-5941.

**Klausberger T, Somogyi P** (2008) Neuronal Diversity and Temporal Dynamics: The Unity of Hippocampal Circuit Operations. *Science* 321:53-57.

**Lagostena L, Rosato-Siri M, D'Onofrio M, Brandi R, Arisi I, Capsoni S, Franzot J, Cattaneo A, Cherubini E** (2010) In the Adult Hippocampus, Chronic Nerve Growth Factor Deprivation Shifts GABAergic Signaling from the Hyperpolarizing to the Depolarizing Direction. *J Neurosci* 30:885-893.

**Liu G** (2004) Local structural balance and functional interaction of excitatory and inhibitory synapses in hippocampal dendrites. *Nat Neurosci* 7:373-379.

**London M, Häusser M** (2005) Dendritic computation. *Annu Rev Neurosci* 28:503-532.

**Miller KD, Pinto DJ, Simons DJ** (2001) Processing in layer 4 of the neocortical circuit: new insights from visual and somatosensory cortex. *Curr Opin Neurobiol* 11:488-497.

**Nevian T, Larkum ME, Polsky A, Schiller J** (2007) Properties of basal dendrites of layer 5 pyramidal neurons: a direct patch-clamp recording study. *Nat Neurosci* 10:206-214.

**Poo C, Isaacson JS** (2009) Odor Representations in Olfactory Cortex: "Sparse" Coding, Global Inhibition, and Oscillations. *Neuron* 62:850-861.

**Pouille F, Scanziani M** (2001) Enforcement of Temporal Fidelity in Pyramidal Cells by Somatic Feed-Forward Inhibition. *Science* 293:1159-1163.

**Rall W** (1964) *In neural theory and modeling*. Stanford University Press, Stanford, Calif 73-97.

**Tamamaki N, Yanagawa Y, Tomioka R, Miyazaki J-I, Obata K, Kaneko T** (2003) Green fluorescent protein expression and colocalization with calretinin, parvalbumin, and somatostatin in the GAD67-GFP knock-in mouse. *J Comp Neurol* 467:60-79.

**Wehr M, Zador AM** (2003) Balanced inhibition underlies tuning and sharpens spike timing in auditory cortex. *Nature* 426:442-446.

**Wittner L, Henze D, Záborszky L, Buzsáki G** (2007) Three-dimensional reconstruction of the axon arbor of a CA3 pyramidal cell recorded and filled in vivo. *Brain Structure and Function* 212:75-83.

**Zecevic D, Antic, S.** (1998) Fast optical measurement of membrane potential changes at multiple sites on an individual nerve cell. *Histochemical Journal* 30:197-216.



## 5 Discussion

My thesis demonstrates that there exists a high dependency of dendritic integration properties on focal GABA<sub>A</sub> receptor activation.

Numerous excitatory and inhibitory synaptic contacts are found over the entire somato-dendritic axis of pyramidal neurons, whose signaling repertoire is enhanced by the underlying morphological and functional compartmentalization (Spruston, 2008). Such a compartmentalized structure of pyramidal cells allows the spatially segregated integration of excitatory and inhibitory signaling. In the case of inhibitory signaling, distinct populations of a rich diversity GABAergic interneurons target specific cellular domains on pyramidal neurons to provide focal inhibition and regulation of the cell activity (Somogyi and Klausberger, 2005; Klausberger and Somogyi, 2008; Spruston, 2008). It has been shown that these different interneuron types are active at precise instances during specific brain states, e.g. basket cell fire during up phase of hippocampal theta oscillations (Klausberger and Somogyi, 2008).

It is obvious that such a sophisticated structure cannot occur as the result of a random process, but has to follow a highly regulated developmental plan. As we have seen, the connectivity of the involved neurons shows a remarkably selective arrangement, nevertheless a highly adaptable design of basic cell circuits emerges. Comparing different cortical areas, we e.g. find the relatively homogeneous arrangement in the hippocampus or the repetitive circuits in each layer of the isocortex (Somogyi et al., 1998).

It is useful to analyze different circuits and cellular assemblies, to study the diverse effects of GABAergic activation on dendritic integration. To begin, we studied a novel compartment-specific effect of GABA<sub>A</sub> receptor activation in cortical layer 5 pyramidal cells. In this study measurements were restricted to somatic whole-cell patch-clamp recordings and spatial information had to be obtained indirectly. It was therefore clear that subsequent studies would profit

from more direct spatial information. We therefore investigated the suitability of voltage-sensitive dye recording of GABAergic signals in a second study.

In the third set of experiments in CA1 pyramidal cells we could subsequently reveal a significant degree of inhomogeneity in dendritic membrane potential transients, shaped by GABAergic signals, after SC stimulation.

A first indication that GABAergic effects could depend on the subcellular site of activation was obtained in the first project of this thesis. We showed, by using classic somatic whole-cell patch clamp recordings compartment-specific effects of GABA<sub>A</sub> receptor activation in layer 5 pyramidal cells (Manuscript I). Limitation of GABA<sub>A</sub> receptor activation to somatic and dendritic compartments by iontophoretically applied GABA showed either a decrease in dendritic excitability after somatic application or respectively an increase in the excitability after dendritic application. Cortical layer 5 pyramidal neurons have a strong morphological and functional compartmentalization (Branco and Häusser, 2010) that enables apical distal dendrites to function independently of the soma; apical dendrites are able to perform local synaptic signal integration and produce distinctive sodium-calcium APs (Spruston et al., 1995, Larkum et al., 1999 a).

We have found that the observed opposite effects of GABA<sub>A</sub> receptor activation are indirectly due to the presence of low-voltage activated Ca<sup>2+</sup>-channels that are found in dendrites (Johnston et al., 1996). Hyperpolarization of the distal dendrite activates the channels and facilitates the excitability of the membranes. We suggested that the observed differential effect in the distal dendrites is due to the expression of Ni-sensitive calcium channels that are found predominantly in the distal dendritic compartment (Markram et al., 1995; Williams and Stuart, 2002). Due to the dependency of the excitatory effect on hyperpolarizing chloride gradients and its Ni sensitivity the most likely candidates are (CaV3.2) T-type calcium channels.

Due to their depolarized state, dendrites possess a reduced initial availability of low voltage-activated calcium channels and a larger hyperpolarizing driving force for dendritic compared to somatic GABA<sub>A</sub> receptors. This then explains how

intrinsic voltage-sensitive signaling mechanisms present in specific compartments are responsible for excitatory or inhibitory effects. In addition, we show that changes in the calcium spike threshold can have long lasting effects on cortical networks. Previous reports have shown the strong sensitivity of pairing-induced synaptic plasticity on calcium spike generation (Dan and Poo, 2004; Letzkus et al., 2006). We have similarly found that modest changes in backpropagating AP bursts can alter the long-term consequences of pairing these bursts with incoming EPSPs.

In the first part of my thesis we show that different pyramidal cell compartments can react to the very same GABAergic signals in an opposite manner, adding the signaling repertoire of these neurons.

Consequently, the diversity of the functional impact on pyramidal cell integration by GABAergic signals is significantly depending on the highly specific subcellular targeting by different interneurons.

Studying those GABAergic signals is particularly challenging because their size is generally small and conventional techniques also do not provide the possibility to detect these signals in different areas of the neuron simultaneously. In addition, direct patch clamp recordings in the soma as well in the dendrite may dialyze the neurons with electrode solutions, which can introduce substantial distortions in the electrical behavior of target structures. Therefore, we developed a novel approach to monitor small changes of membrane potentials induced by GABA with a high spatial resolution (Manuscript II). The described optical method permits multisite measurements of voltage signals from relatively small portions of dendrites and axons. Optimal conditions for those measurements were achieved by using illumination with a stable solid-state laser, a high numerical aperture lenses, and detection with fast and large well capacity CCD cameras.

In response to GABA<sub>A</sub> receptor activation, ions such as Cl<sup>-</sup> and bicarbonate flow across the membrane and determine polarity and size of GABAergic synaptic potentials.

There are several reports in the literature that the relevant gradients are not stable over time (Ben-Ari, 2002) and might even be different in subcellular compartments (Szabadics et al., 2006). Alternative techniques, such as perforated-patch recordings can have some shortcomings to the cells. Breakage of the perforated patch can go unnoticed and will dialyze the cell with a potentially unphysiological chloride concentration. Further, the recordings provide only limited spatial resolution and cannot reach small dendrites. However, voltage-sensitive dye imaging provides an unparalleled level of spatial resolution, but comes with its own drawbacks. First, without a calibration signal the changes in fluorescence cannot be directly translated into voltages, however de- or hyperpolarization are easily distinguished. Second, great care must be taken to avoid phototoxic effects of the currently available dyes; this can mostly be achieved by keeping the amount of dye loaded and its exposure to a minimum. Thus, in weighting all these options, voltage sensitive dye imaging can provide useful information on GABAergic signals that no other method can.

In all performed experiments, measured responses were hyperpolarizing, regardless of the subcellular location or of the site of stimulation suggesting that  $[Cl^-]_i$  is low in all areas of mature CA1 hippocampal pyramidal neurons.

Interestingly, the results show the ability of multisite optical recording to consistently detect specific spatial distribution of IPSP input signals in the dendritic arbor and in the axon.

In summary, this kind of high spatial resolution optical recordings provides the opportunity to detect small physiological GABAergic signals focally. Hence, a further step was achieved to measure impact of GABAergic signals on dendritic integration processes. The only limitation performing the experiments was in the use of extracellular stimulation because, in general, it precludes the precise identification of stimulated interneurons and of the postsynaptic area where synaptic contacts are formed.

Thus, to understand GABAergic effects on subcellular integration processes it was advantageous to design experiments in which the basics of underlying

circuits processes are mostly known and the activation of GABA<sub>A</sub> receptors show clear effects as shunting effects on EPSPs or backpropagating action potentials. We performed voltage-sensitive dye imaging in CA1 pyramidal cells to study the effects of feedforward inhibition on dendritic integration processes (Manuscript III). The results revealed a significant degree of inhomogeneity in dendritic membrane potential transients in CA1 pyramidal cells after SC stimulation. While NBQX-sensitive feedforward hyperpolarization was detected in all dendritic subregions, some dendritic segments, particularly in basal dendrites showed no discernible excitatory response. By blocking GABA<sub>A</sub> receptor mediated feedforward inhibition, excitation did spread throughout the dendritic arborization, indicating that these patterns are actively shaped by the network of interneurons surrounding CA1 pyramidal cells (Buzsáki, 1984; Liu, 2004). Interestingly, less pronounced patterns with uniform hyperpolarization in both basal and apical dendrites we detected in paired recordings between individual interneurons and CA1 pyramidal cells. The pronounced shaping effects of GABA<sub>A</sub> receptors on dendritic EPSPs we have shown are therefore most likely due to shunting whose occurrence is significantly more localized than hyperpolarization changes of the membrane (Gulledge and Stuart, 2003). Hence, the experiment we designed, which mixed excitatory and inhibitory signals, was ideal to study GABAergic effects on a subcellular level.

Especially in sensory processes, the control of excitation in time and space by GABAergic inhibition is crucial in shaping the propagation of information. Pouille and Scanziani (2001) have shown that the cell is not dependent on the membrane time constant to control synaptic integration in time – feedforward inhibition can shorten the integration time window and thus make information transfer much more precise. We have now shown the same mechanism in space – cells are not dependent on the dendritic length constant to determine spatial synaptic integration, but can and do control this process through feedforward inhibition.

In this study we describe a sharpening feature of GABAergic synaptic transmission at the subcellular level in a determined circuit – the focusing of dendritic depolarization by feedforward inhibition.

The exact nature of the interneurons involved in the chosen cell circuit is unclear; however the strong evidence of layer-specific innervation by certain subtypes of interneurons we have in the feedforward circuit makes the selective silencing of dendritic subcompartments possible. We thus postulate a network of excitatory and inhibitory connections that innervate pyramidal neurons such that the excitatory input is surrounded by inhibitory synapses. Types of interneurons participating in feedforward inhibition are the so-called basket cells, which are also innervating the soma (Freund and Buzsáki, 1996, Glickfeld and Scanziani, 2006). Their activity suggests a contribution in preventing the spread of apical EPSPs to basal dendrites.

In addition, by using VSD imaging the study of dendritic signals in the extremely thin basal dendrites was possible. To date, their integrative properties remain largely unknown due to the difficulties in recording from these thin branches with classical electrode techniques. Recently, it has been shown in layer V pyramidal neurons that they exhibit strong synaptic scaling and can generate active signals (Nevian et al., 2007). Given their high input resistance they are particularly susceptible to GABAergic shunting, which may keep these active properties under control.

The dendritic membrane potentials patterns we have observed were not fixed; they could be altered by stimuli that induce synaptic plasticity. Interestingly, this plasticity is non-uniform in itself – proximal portions of the apical dendrite showed small changes in the EPSP/IPSP ratio, while distal portions showed a pronounced increase. The exact locations of the synaptic changes will need further investigation.

Overall, my thesis demonstrates the relevance of location-specific GABA<sub>A</sub> receptor activation in neuronal integration. GABA signaling influences either directly the membrane potential integration in the innervated compartment by

shaping excitatory inputs or indirectly by activating or blocking voltage-dependent channels in this area. The results provide a major step to understand GABAergic effects on subcellular signaling.

To learn more about influences of specific interneurons on subcellular dendritic levels further investigations are necessary. Paired recordings in combination with VSD imaging are difficult to perform and the success rate in the hippocampus is quite rare. Changing the brain region to perform those experiments would be one option; possibly are areas in the cortex since their connectivity rate is higher. Another possibility of selective interneuron stimulation would be photostimulation of interneurons labeled with the light-sensitive protein channelrhodopsin (ChR2). Simultaneous VSD imaging in connected pyramidal cells would need a different voltage-sensitive dye since absorption spectra of JPW1114 and channelrhodopsin are overlapping.

Furthermore, it would be interesting to investigate the integration of backpropagating action potentials by GABAergic signals in subcellular compartments. Backpropagating action potential plays a role in plasticity processes in the neuron. Paired with excitatory signals, long-lasting changes in the synaptic composition in dendritic compartments can occur. In this context, it would be interesting to know how GABA<sub>A</sub> receptor activation on a subcellular level is contributing in the integration processes.

Conclusively, fundamental knowledge of GABA<sub>A</sub> signaling of specific interneurons on dendritic subcellular integration could be gained.

## 6 References

**Alger BE, Nicoll RA** (1979) GABA-mediated biphasic inhibitory responses in hippocampus. *Nature* 281:315-317.

**Bazemore A, Elliott KAC, Florey E** (1956) Factor I and [gamma]-Aminobutyric Acid. *Nature* 178:1052-1053.

**Ben-Ari Y** (2002) Excitatory actions of gaba during development: the nature of the nurture. *Nat Rev Neurosci* 3:728-739.

**Ben-Ari Y, Cherubini E, Corradetti R, Gaiarsa JL** (1989) Giant synaptic potentials in immature rat CA3 hippocampal neurones. *J Physiol* 416:303-325.

**Ben-Ari Y, Gaiarsa J-L, Tyzio R, Khazipov R** (2007) GABA: A Pioneer Transmitter That Excites Immature Neurons and Generates Primitive Oscillations. *Physiol Rev* 87:1215-1284.

**Ben-Ari Y, Gaiarsa J-L, Tyzio R, Khazipov R** (2007) GABA: A Pioneer Transmitter That Excites Immature Neurons and Generates Primitive Oscillations. *Physiol Rev* 87:(4) 1215-1284;

**Blaesse P, Airaksinen MS, Rivera C, Kaila K** (2009) Cation-Chloride Cotransporters and Neuronal Function. *Neuron* 61:820-838.

**Branco T, Häusser M** (2010) The single dendritic branch as a fundamental functional unit in the nervous system. *Curr Opin Neurobiol* 20:494-502.

**Buhl EH, Halasy K, Somogyi P** (1994) Diverse sources of hippocampal unitary inhibitory postsynaptic potentials and the number of synaptic release sites. *Nature* 368:823-828.

**Buzsáki G** (1984) Feed-forward inhibition in the hippocampal formation. *Prog Neurobiol* 22:131-153.

**Cash S, Yuste R** (1999) Linear Summation of Excitatory Inputs by CA1 Pyramidal Neurons. *Neuron* 22:383-394.

**Cherubini E, Ben-Ari Y** (2011) The immature brain needs GABA to be excited and hyper-excited. *J Physiol* 589:2655-2656.

**Dan Y, Poo M-m** (2004) Spike Timing-Dependent Plasticity of Neural Circuits. *Neuron* 44:23-30.



**Douglas RJ, Martin KA** (1990) Control of neuronal output by inhibition at the axon initial segment. *Neural Comp* 2:283-292.

**Eccles JC** (1994) *The physiology of synapses*. Springer-Verlag Berlin

**Enna SJ, Möhler H** (2007) *The GABA receptors*. Humana-Press, New Jersey  
Third edition.

**Florey E** (1954) An inhibitory and an excitatory factor of mammalian central nervous system, and their action of a single sensory neuron. *Arch Int Physiol* 62:33-53.

**Florey E** (1991) GABA: history and perspectives. *Can J Physiol Pharmacol* 69(7):1049-1056.

**Freund TF, Buzsáki G** (1996) Interneurons of the hippocampus. *Hippocampus* 6:347-470.

**Galzi J-L, Cangeux J-P** (1994) Neurotransmitter-gated ion channels as unconventional allosteric proteins. *Curr Opin Struct Biol* 4(4):554-565.

**Ganter P, Szücs P, Paulsen O, Somogyi P** (2004) Properties of horizontal axo-axonic cells in stratum oriens of the hippocampal CA1 area of rats in vitro. *Hippocampus* 14:232-243.

**Glickfeld LL, Roberts JD, Somogyi P, Scanziani M** (2009) Interneurons hyperpolarize pyramidal cells along their entire somatodendritic axis. *Nat Neurosci* 12:21-23.

**Glickfeld LL, Scanziani M** (2006) Distinct timing in the activity of cannabinoid-sensitive and cannabinoid-insensitive basket cells. *Nat Neurosci* 9:807-815.

**Gulledge AT, Stuart GJ** (2003) Excitatory Actions of GABA in the Cortex. *Neuron* 37:299-309.

**Halasy KS, Somogyi P** (1993) Distribution of GABAergic synapses and their targets in the dentate gyrus of rat: a quantitative immunoelectron microscopic analysis. *J Hirnforsch* 34:299-308.

**Hevers W, Lüddens H** (1998) The diversity of GABA<sub>A</sub> receptors. *Mol Neurobiol* 18:35-86.

**Holmgren, CD, Mukhtarov M, Malkov AE, Popova IY, Bregestovski P, Zilberter Y** (2009) Energy substrate availability as a determinant of neuronal resting potential, GABA signaling and spontaneous network activity in the neonatal cortex 'in vitro'. *J Neurochem* 112(4):900-912.

**Howard A, Tamas G, Soltesz I** (2005) Lighting the chandelier: new vistas for axo-axonic cells. *Trends Neurosci* 28:310-316.

**Johnston D, Magee JC, Colbert CM, Christie BR** (1996) Active Properties of Neuronal Dendrites. *Ann Rev Neurosci* 19:165-186.

**Kandel ER, Schwartz JH, Jessell TM** (2000) Principles of neural science. The McGraw-Hill Companies Fourth edition.

**Klausberger T, Somogyi P** (2008) Neuronal Diversity and Temporal Dynamics: The Unity of Hippocampal Circuit Operations. *Science* 321:53-57.

**Koch C, Segev I** (2000) The role of single neurons in information processing. *Nat Neurosci Suppl*:1171-1177.

**Kravitz EA, Kuffler SW, Potter DD** (1963 a) Gamma-aminobutyric acid and other blocking compounds in crustacea: III. Their relative concentrations in separated motor and inhibitory axons. *J Neurophysiol* 26:739-751.

**Kravitz EA, Kuffler SW, Potter DD, van Gelder NM** (1963b) Gamma-aminobutyric acid and other blocking compounds in crustacea: II. Peripheral nervous system. *J Neurophysiol* 26:729-738.

**Krnjevic K, Schwartz S** (1966) Is [gamma]-Aminobutyric Acid an Inhibitory Transmitter? *Nature* 211(5056):1372-1374.

**Larkum ME, Kaiser KMM, Sakmann B** (1999 a) Calcium electrogenesis in distal apical dendrites of layer 5 pyramidal cells at a critical frequency of back-propagating action potentials. *Proc Natl Acad Sci U S A* 96:14600-14604.

**Larkum ME, Zhu JJ, Sakmann B** (1999 b) A new cellular mechanism for coupling inputs arriving at different cortical layers. *Nature* 398:338-341.

**Letzkus JJ, Kampa BM, Stuart GJ** (2006) Learning Rules for Spike Timing-Dependent Plasticity Depend on Dendritic Synapse Location. *J Neurosci* 26:10420-10429.

**Liu G** (2004) Local structural balance and functional interaction of excitatory and inhibitory synapses in hippocampal dendrites. *Nat Neurosci* 7:373-379.

**Harvey LF** (1999) Molecular cell biology. New York: Scientific American Books Fourth edition.

**London M, Häusser M** (2005) Dendritic computation. *Ann Rev Neurosci* 28:503-532.

**Mann EO, Paulsen O** (2007) Role of GABAergic inhibition in hippocampal network oscillations. *Trends Neurosci* 30:343-349.

**Markram H, Helm PJ, Sakmann B** (1995) Dendritic calcium transients evoked by single back-propagating action potentials in rat neocortical pyramidal neurons. *J Physiol* 485:1-20.

**Markram H, Toledo-Rodriguez M, Wang Y, Gupta A, Silberberg G, Wu C** (2004) Interneurons of the neocortical inhibitory system. *Nat Rev Neurosci* 5:793-807.

**McBain CJ, Fisahn A** (2001) Interneurons unbound. *Nat Rev Neurosci* 2:11-23.

**Megias M, Emri Z, Freund TF, Gulyás AI** (2001) Total number and distribution of inhibitory and excitatory synapses on hippocampal CA1 pyramidal cells. *Neurosci* 102:527-540.

**Möhler H** (2001) *Pharmacology of GABA and Glycine Neurotransmission*. Springer-Verlag Berlin Heidelberg.

**Nevian T, Larkum ME, Polsky A, Schiller J** (2007) Properties of basal dendrites of layer 5 pyramidal neurons: a direct patch-clamp recording study. *Nat Neurosci* 10:206-214.

**Olsen R, Tobin A** (1990) Molecular biology of GABA<sub>A</sub> receptors. *The FASEB Journal* 4:1469-1480.

**Owens DF, Kriegstein AR** (2002) Is there more to gaba than synaptic inhibition? *Nat Rev Neurosci* 3:715-727.

**Petilla Interneuron Nomenclature Group**, Ascoli GA, Alonso-Nanclares L, Anderson SA, Barrionuevo G, Benavides-Piccione R, Burkhalter A, Buzsáki G, Cauli B, Defelipe J, Fairman A, Feldmeyer D, Fishell G, Fregnac Y, Freund TF, Gardner D, Gardner EP, Goldberg JH, Helmstaedter M, Hestrin S, Karube F, Kisvárdy ZF, Lambolez B, Lewis DA, Marin O, Markram H, Mozrzymas F, Ozols A, Packer A, Petersen CC, Rockland KS, Rossier J, Rudy B, Somogyi P, Staiger JF, Tamas G, Thomson AM, Toledo-Rodriguez M, Wang Y, West DC, Yuste R (2008) Petilla terminology: nomenclature of features of GABAergic interneurons of the cerebral cortex. *Nat Rev Neurosci* 9:557-568.

**Pouille F, Scanziani M** (2001) Enforcement of Temporal Fidelity in Pyramidal Cells by Somatic Feed-Forward Inhibition. *Science* 293:1159-1163.

**Pouille F, Scanziani M** (2004) Routing of spike series by dynamic circuits in the hippocampus. *Nature* 429:717-723.

**Rall W** (1964) Theoretical significance of dendritic trees for neuronal input-output relations. In neural theory and modeling, ed R.F.Reiss Stanford Univ Press.

**Rall W** (1967) Distinguishing theoretical synaptic potentials computed for different soma-dendritic distributions of synaptic input. *J Neurophysiol* 30:1138-1168.

**Rall W** (1969) Time Constants and Electrotonic Length of Membrane Cylinders and Neurons. *Biophys J* 9:1483-1508.

**Rall W, Burke RE, Smith TG, Nelson PG, Frank K** (1967) Dendritic location of synapses and possible mechanisms for the monosynaptic EPSP in motoneurons. *J Neurophysiol* 30:1169-1193.

**Rheims S, Holmgren CD, Chazal G, Mulder J, Harkany T, Zilberter T, Zilberter Y** (2009) GABA action in immature neocortical neurons directly depends on the availability of ketone bodies. *J Neurochem* 110(4):1330-1338.

**Rivera C, Voipio J, Payne JA, Ruusuvuori E, Lahtinen H, Lamsa K, Pirvola U, Saarma M, Kaila K** (1999) The K<sup>+</sup>/Cl<sup>-</sup> co-transporter KCC2 renders GABA hyperpolarizing during neuronal maturation. *Nature* 397:251-255.

**Roberts E, Frankel S** (1950)  $\gamma$ -aminobutyric acid in brain: its formation from glutamic acid. *J Biol Chem* 187:55-63.

**Rudolph U, Crestani F, Benke D, Brunig I, Benson JA, Fritschy J-M, Martin JR, Bluethmann H, Mohler H** (1999) Benzodiazepine actions mediated by specific  $[\gamma]$ -aminobutyric acidA receptor subtypes. *Nature* 401:796-800.

**Schiller J, Schiller Y, Stuart G, Sakmann B** (1997) Calcium action potentials restricted to distal apical dendrites of rat neocortical pyramidal neurons. *J Physiol* 505:605-616.

**Segev I** (2006) What do dendrites and their synapses tell the neuron? *J Neurophysiology* 95(3):1295-1297.

**Sherrington C** (1947) *The Integrative Action of the Nervous System*. New Haven: Yale Univ Press. Second edition.

**Smith GB, Olsen RW** (1995) Functional domains of GABA<sub>A</sub> receptors. *Trends Pharmacol Sciences* 16:162-168.

**Somogyi P, Klausberger T** (2005) Defined types of cortical interneurone structure space and spike timing in the hippocampus. *J Physiol* 562:9-26.

**Somogyi P, Tamás G, Lujan R, Buhl EH** (1998) Salient features of synaptic organisation in the cerebral cortex. *Brain Research Rev* 26:113-135.

**Spruston N** (2008) Pyramidal neurons: dendritic structure and synaptic integration. *Nat Rev Neurosci* 9:206-221.

**Spruston N, Schiller Y, Stuart G, Sakmann B** (1995) Activity-dependent action potential invasion and calcium influx into hippocampal CA1 dendrites. *Science* 268:297-300.

**Staley KJ, Mody I** (1992) Shunting of excitatory input to dentate gyrus granule cells by a depolarizing GABAA receptor-mediated postsynaptic conductance. *J Neurophysiol* 68:197-212.

**Stuart G, Spruston N, Häusser M** (2008) *Dendrites*. Oxford University Press First edition.

**Stuart G, Spruston N, Sakmann B, Hausser M** (1997 a) Action potential initiation and backpropagation in neurons of the mammalian CNS. *Trends Neurosci* 20:125-131.

**Stuart G, Schiller J, Sakmann B** (1997 b) Action potential initiation and propagation in rat neocortical pyramidal neurons. *J Physiol* 15(505):617-632.

**Szabadics J, Varga C, Molnar G, Olah S, Barzo P, Tamas G** (2006) Excitatory Effect of GABAergic Axo-Axonic Cells in Cortical Microcircuits. *Science* 311:233-235.

**Tyzio R, Allene C, Nardou R, Picardo MA, Yamamoto S, Sivakumaran S, Caiati MD, Rheims S, Minlebaev M, Milh M, Ferre P, Khazipov R, Romette J-L, Lorquin J, Cossart R, Khalilov I, Nehlig A, Cherubini E, Ben-Ari Y** (2011) Depolarizing Actions of GABA in Immature Neurons Depend Neither on Ketone Bodies Nor on Pyruvate. *J Neurosci* 31:34-45.

**Williams SR and Stuart GJ** (2002) Dependence of EPSP efficacy on synapse location in neocortical pyramidal neurons. *Science* 295(5561):1907-1910

**y Cajal SR** (1911) *Histologie du Systeme Nerveux de l'Homme et des Vertebres*. Maloine, Paris chap. II.

## **7 Supplementary Material**

Movies for Manuscript II and Manuscript III (see CD-R):

### Manuscript II: Imaging Inhibitory Synaptic Potentials Using Voltage Sensitive Dyes

- 1) Movie S1: Spread of dendritic IPSPs
- 2) Movie S2: Dendritic vs axonal signals

### Manuscript III: Feedforward inhibition controls the spread of excitation within the dendritic tree of CA1 pyramidal neurons

- 1) Movie S1: Distribution pattern in apical and basal dendrites (SR stimulation)
- 2) Movie S2: Effect of bicuculline (SR stimulation)

## 8 List of Abbreviations

AAC = axo-axonic-cell	IPSPs = inhibitory postsynaptic potentials
ad = apical dendrite	KCC2 = K-Cl cotransporter
ACSF = artificial cerebrospinal fluid	MAD = median absolute deviation
ADP = afterdepolarisation potential	NBQX = 2,3-Dioxo-6-nitro-1,2,3,4-tetrahydrobenzo[f]quinoxaline-7-sulfonamide disodium salt
ALV = alveus	Ni = nickel
AP = action potential	NKCC1 = Na-K-2Cl cotransporter
bd = basal dendrite	O-LM = oriens-lacunosum moleculare
BP = baseline membrane potential	p/P = postnatal
BPAP = backpropagating action potential	PC = principal cell
CCC = cation-chloride cotransporters	prox = proximal
Cl <sup>-</sup> = chloride	PSPs = postsynaptic potentials
[Cl <sup>-</sup> ] <sub>i</sub> = internal chloride concentration	PV = Parvalbumin
[Cl <sup>-</sup> ] <sub>o</sub> = external chloride concentration	PYR = CA1 pyramidal neuron
C <sub>m</sub> = specific membrane capacitance	R <sub>i</sub> = intracellular resistivity
CNA = central nervous system	R <sub>m</sub> = membrane resistivity
D-AP5 = D-(-)-2-Amino-5-phosphonopentanoic acid	S/N = signal-to-noise ratio
dist = distal	sb = side branch
E <sub>Cl<sup>-</sup></sub> = electrochemical equilibrium potential for chloride	SC = Schaffer collaterals
EPSPs = excitatory postsynaptic potentials	SEM = standard error of the mean
ΔF/F = fractional changes of fluorescence	SLM = stratum lacunosum-moleculare
F <sub>c</sub> = critical frequency	SR = stratum radiatum
FBI = feedback inhibition	τ <sub>m</sub> = time constant
FFI = feedforward inhibition	TM = transmembrane domains
GABA = γ-aminobutyric acid	uIPSP = unitary inhibitory postsynaptic potential
GABA <sub>A</sub> R/GABA <sub>B</sub> R = GABA <sub>A</sub> /GABA <sub>B</sub> receptor	V <sub>Cl<sup>-</sup></sub> = chloride reversal potential
GAD65/67 = L-glutamic acid decarboxylase	V <sub>m</sub> = V <sub>rest</sub> = resting membrane potential
GDPs = giant depolarizing potentials	ΔV <sub>m</sub> = membrane potential transient
GFP = green-fluorescence protein	VSD = voltage-sensitive dye
HCO <sub>3</sub> <sup>-</sup> = hydrogen carbonate	WT = wild type
INT = interneuron	

## 9 Acknowledgements

First of all, I would like to thank Prof. Kaspar Vogt for the opportunity to do my PhD in his lab and for his great guidance and support. I really appreciated the last years in his lab and to work together with him.

I want to thank Dr. Marco Canepari for teaching me the voltage-sensitive dye imaging method and his excellent advice in many parts during my thesis.

Many thanks to Lydia Barth (for the friendship and remembering all the coffee breaks), Julien Gaudias (for his friendship; with who I should discuss now about good and bad music?) and Markus Nenniger (many extra thanks for his help with programming and the nice discussions and being a good friend), also Rosmarie Suetterlin (for being our “om” in the lab) I really enjoyed working together with all of them and I will miss the time. Also I would like to thank H el ene Pierre, our former colleague, for helping at the beginning of my PhD in many parts and her friendship.

I also would like to mention Stephan Gerharz who unfortunately died this year. I think it was a great privilege for us to have met him and to have had him as a colleague.

I also would like to thank Marco Capogna for the opportunity to spend some time in his lab in Oxford during my PdD thesis.

Many many thanks to all my friends to have had and hopefully to still will have a great time; especially Eva Oswald (I will miss our Saturday coffees), Nadine Schmidt (for her support and the nice travelling every day), Rebekka Goetz and Michaela Friedrich (for being good friends of mine now for so long), Mellanie Vollmer and Jennifer Labin (for the nice time in the kitchen) and for sure, all the rest.

And finally, I also would like to thank my mom, my sister, Marlene, Amelie and Philipp for supporting me and always believing in me. Also, I would like to thank my cousin Werner Franzel for helping my family a lot in every situation in the last month.

THANK YOU ALL!



## **10 Curriculum vitae**

### **PERSONAL DATA**

---

**Date of birth:** 08.April.1980  
**Place of birth** Augsburg (Germany, Bavaria)  
**Nationality:** German  
**Marital status:** Unmarried

### **WORK EXPERIENCES**

---

**Current:** Postdoctoral fellow at the Biozentrum,  
University of Basel, Switzerland

**April – June 2012:** Scientific stay at the MRC in Oxford, England

**August 2007 - December 2011:** Scientific assitant at the Biozentrum,  
University of Basel, Switzerland

**February – Mai 2007:** Assistant for behaviour tests to Dr. Ball,  
Neurocenter Freiburg (University Freiburg,  
Germany)

**October 2006 – January 2007:** Assistant for electrophysiological  
investigations to Prof. Behrends (University  
Freiburg, Germany)

**2004 – 2005:** Secretary activities at the workgroup of Prof.  
Driever (University Freiburg, Germany,  
Baden-Württemberg)

## **EDUCATION**

---

- December 2012:** Obtaining a **PhD** (*magna cum laude*) in Neuroscience (Title: "*The influence of GABAergic signalling on dendritic progressing*")
- October – December 2009:** Scientific stay at the MRC in Oxford, England
- August 2007 - December 2011:** PhD studies at "Philosophisch-Naturwissenschaftlichen Fakultät", Biozentrum, University of Basel, Switzerland
- June 2006:** Final degree as „**Diplom-Biologin**“
- June 2005 - June 2006:** Diploma-Thesis (Title: "*Elektrophysiologische Analyse synchroner und asynchroner Transmission an Syt-I defizienten, inhibitorischen GABAergen Synapsen*") at the Physiologial Institut II at the Albert-Ludwigs-University Freiburg, Germany
- April 2002 - June 2006:** Main studies of biology (Major subject: Neurobiology/Animalphysiology) at the Albert-Ludwigs- University Freiburg, Germany
- October 1999 -March 2002:** Primary studies of biology at the University of Regensburg, Germany

## **PUBLICATIONS**

---

**Willadt, S.**, Nenniger, M., Vogt, K.E. (2012) **Feedforward inhibition focuses excitatory signals into distinct dendritic compartments.** *Submitted*

Muhia, M., **Willadt, S.**, Yee, B.K., Feldon, J., Paterna, J.C., Schwendener, S., Vogt, K., Kennedy, M.B., & Knuesel, J. (2012) **Molecular and behavioral changes associated with adult hippocampus specific SynGAP1 knockout.** *Learning&Memory*

**Willadt, S.\***, Canepari, M.\*, Zecevic, D. & Vogt, K. (2010) **Imaging inhibitory synaptic potentials using voltage sensitive dyes.** *Biophysical Journal*

Prut, L., Prenosil, G., **Willadt, S.**, Vogt, K., Fritschy, J.-M. & Crestani, F. (2010) **A reduction in hippocampal GABA<sub>A</sub> receptor  $\alpha 5$  subunits disrupts the memory for location of objects in mice.** *Genes, Brain and Behavior*

**Willadt, S.**, Nenniger, M., Stalbovskiy, A., Canepari, M. & Vogt, K. **Combined voltage-sensitive dye imaging and ChR2-VGAT stimulation.** *In preparation*